NASA CR 135220

(NASA-CR-135220) AN INVESTIGATION OF COMBUSTION AND ENTROPY NOISE Final Report, 15 Jul. 1974 - 14 Jul. 1977 (Georgia Inst. of Tech.) 97 p HC A05/MF A01 CSCL 21E

N77-27118

Unclas
G3/07 36765

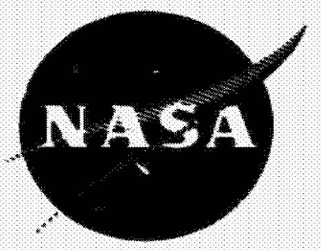


# AN INVESTIGATION OF COMBUSTION AND ENTROPY NOISE

by

W. C. Strahle
M. Muthukrishnan
D. H. Neale
M. K. Ramachandra

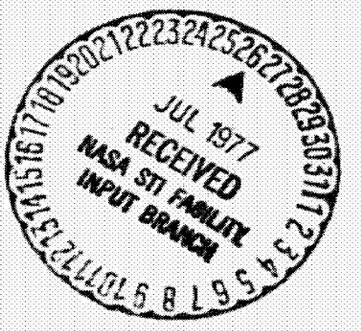


GEORGIA INSTITUTE OF TECHNOLOGY
ATLANTA, GEORGIA 30332

prepared for
NATIONAL AERONAUTICS AND SPACE ADMINISTRATION

NASA Lewis Research Center
Grant NSG 3015
Ronald G. Huff, Technical Monitor

| 1 Report No | 2. Government Accession No. | 3. Recipient's Catalog No. |
|---|---|---|
| NASA CR 135220 | - | - |

| 4 Title and Subtitle | 5. Report Date |
|---|---|
| AN INVESTIGATION OF COMBUSTION AND ENTROPY NOISE | July 15, 1977 |
| | 6. Performing Organization Code: - |

| 7. Author(s) | 8. Performing Organization Report No |
|---|---|
| W. C. Strahle, M. Muthukrishnan, D. H. Neale, M. K. Ramachandra | - |
| | 10. Work Unit No.: - |

| 9. Performing Organization Name and Address | 11. Contract or Grant No |
|---|---|
| School of Aerospace Engineering<br>Georgia Institute of Technology<br>Atlanta, GA 30332 | NSG 3015 |
| | 13. Type of Report and Period Covered: Final Report 7/15/74 - 7/14/77 |

| 12 Sponsoring Agency Name and Address | 14. Sponsoring Agency Code |
|---|---|
| National Aeronautics and Space Administration<br>Washington, D. C. 20546 | |

15 Supplementary Notes

16 Abstract

The program was conducted to determine the relative importance of entropy and direct combustion noise in turbopropulsion systems and to determine the parameters upon which these noise sources depend. Theory and experiment were employed to determine that, at least with the apparatus used here, entropy noise can dominate combustion noise if there is a sufficient pressure gradient terminating the combustor. Measurements included combustor interior fluctuating pressure, near and far field fluctuating pressure, and combustor exit plane fluctuating temperatures, as well as mean pressures and temperatures. Analysis techniques included spectral, cross-correlation, cross power spectra, and ordinary and partial coherence analysis. Also conducted were combustor liner modification experiments to investigate the origin of the frequency content of combustion noise. Techniques were developed to extract non-propagational pseudo-sound and the heat release fluctuation spectra from the data.

| 17 Key Words (Suggested by Author(s)) | 18 Distribution Statement |
|---|---|
| Noise<br>Propulsion<br>Combustion<br>Aeroacoustics<br>Gas Turbine | Unclassified - unlimited |

| 19 Security Classif (of this report) | 20. Security Classif. (of this page) | 21 No of Pages | 22 Price* |
|---|---|---|---|
| Unclassified | Unclassified | 93 | |

* For sale by the National Technical Information Service Springfield Virginia 22161

NASA CR 135220

# An Investigation of Combustion and Entropy Noise

Final Report

National Aeronautics and Space Administration

Grant No. NSG 3015

7/15/74 - 7/14/77

by

School of Aerospace Engineering
Georgia Institute of Technology
Atlanta, Georgia

Warren C. Strahle
Principal Investigator

M. Muthukrishnan
Graduate Research Assistant

Douglas H. Neale
Research Engineer

Manjanatha K. Ramachandra
Graduate Research Assistant

## Table of Contents

## Abstract

The program was conducted to determine the relative importance of entropy and direct combustion noise in turbopropulsion systems and to determine the parameters upon which these noise sources depend. Theory and experiment were employed to determine that, at least with the apparatus used here, entropy noise can dominate combustion noise if there is a sufficient pressure gradient terminating the combustor. Measurements included combustor interior fluctuating pressure, near and far field fluctuating pressure, and combustor exit plane fluctuating temperatures, as well as mean pressures and temperatures. Analysis techniques included spectral, cross-correlation, cross power spectra, and ordinary and partial coherence analysis. Also conducted were combustor liner modification experiments to investigate the origin of the frequency content of combustion noise. Techniques were developed to extract non-propagational pseudo-sound and the heat release fluctuation spectra from the data.

## Introduction

The purpose of this program was to investigate the fundamental causes of core noise in turbopropulsion systems. The program was initiated as NASA Contract NAS3-17861 for which Ref. (1) was issued as a final report. The past three years of effort have been carried out under NASA Grant No. NSG 3015, and this report summarizes those efforts.

It was known at the program outset that there were at least two probable causes for core noise - entropy or indirect noise and direct combustion noise.[2] There had been no prior program aimed at isolating the two suspected causes and determining their relative importance to the core noise problem. Moreover, there were some fundamental difficulties in understanding of the frequency content of direct combustion noise, as discussed in Ref. (1). This report contains experimental and theoretical information aimed at separation of the effect of entropy and direct combustion noise and resolution of the cause of the frequency content of direct combustion noise.

The issue of the importance of core noise to the aircraft noise problem is not addressed here. It is clear that core noise represents a noise floor in current turbopropulsion systems but there is controversy concerning the strength of core noise relative to other sources.[3],[4],[5] It is sufficient to remark here that core noise exists and is measurable. This report will also add to current controversy because a major finding has been that entropy noise is dominant in the apparatus used here, under conditions simulating those that would be found in engine installed configurations. Such a noise source has been rejected in Ref. (4) and correlation of engine noise results based upon a direct combustion noise theory has been claimed. While the experimental results reported here may be apparatus dependent, the theory suggests that both entropy and combustion noise must be contended with in actual engines; moreover, the two sources

are currently linked and, hence, are not independent.

This report is written in summary form with the details contained in appendices. The conclusions contain recommendations for further work, because other noise sources were found in the course of the work which may be important to the core noise problem.

## Summary

The basic combustor unit used in the experimental work was taken from a Boeing 502-7D gas turbine unit. The unit is described in Ref. (1) and in Appendix A. It is a can type combustor with head end and side slots and is operated by discharging directly to the atmosphere (1 atm tests) or through a nozzle to the atmosphere ($\leq$ 2 atm tests). In Appendix A the operating characteristics,such as efficiency and split between bypass and core flow, are discussed. Two can liners, other than the production liner, were manufactured to vary the mean hydraulic diameter of the liner holes over a range of 4:1. These liners are also described in Appendix A. The hole size variation was introduced to test the hypothesis that the integral (macro) scale of the turbulence should play a role in the frequency of combustion generated noise.

Types of measurements made on the combustor unit were far field noise, near field noise, interior pressure fluctuations, and exit plane temperature fluctuations and mean temperature. The types of analysis applied to the recorded signals were spectral, cross spectral, cross correlation, ordinary coherence and partial coherence analysis.(6)

A theory of the noise behavior of combustors is developed in Appendices B and C. The theory is based upon the linearized vorticity-acoustic field equations(7) and several noise sources are recognized for the current experimental situation. Two of these which were not desired in the program were jet noise from the exhaust and the second was turbulence (or hydrodynamic or scrubbing) noise measured by the interior pressure transducer. These sources were not treated in the theory but were experimentally investigated. Another noise source which was eliminated from the theory was lateral vorticity - nozzle interaction noise.(8) This source, caused by velocity fluctuations entering a nozzle pressure gradient, must be investigated in a future program because

of the findings of the current program. However, study of the source was beyond the scope of the current program. The major emphasis in the theory was on direct combustion noise, a dilatation of the flow caused by fluctuations in the aggregate heat release, and entropy noise, pressure waves generated when hot (or cold) spots are convected through a nozzle pressure gradient.

Entropy noise (as well as nozzle-vorticity noise) is absent if the combustor is exhausted directly to the atmosphere. Hence, the direct discharge tests were direct combustion noise studies. Appendix B is concerned with these tests and the investigation of hydrodynamic noise contamination of interior pressure measurements. The primary cause of entropy fluctuations is temperature fluctuations entering a region of pressure gradient, such as a nozzle. The theory indicates that for the apparatus used ($\approx$ 12% rms temperature fluctuations entering the nozzle and correlation length scales of the order of a centimeter) one should expect entropy noise to be seen experimentally. This is especially true if a choked nozzle is attached to the combustor, as it was in the experiments of Appendix D.

The techniques of ordinary and partial coherence analysis were used to make the determination of the relative dominance of combustion of entropy noise. Both techniques show the conclusion of entropy noise dominance at sufficiently high nozzle contraction. Partial coherence was, however, to have been the more sensitive indicator of signal contamination by some other cause, such as vorticity-nozzle interaction noise. Unfortunately, partial coherence analysis is highly sensitive to errors in experimental determination of spatial correlation of temperature fluctuations. Since these correlations were not obtained with high accuracy, the accuracy of the partial coherence analysis suffered. The result was inconclusive determination of the existence of non-considered noise sources.

The connection between entropy noise and combustion noise is investigated in Appendix E. It is shown there, both theoretically and experimentally, that the two noise sources can be either directly correlated or uncorrelated, depending upon the frequency range. For frequencies above the frequency defined by the inverse of a fluid particle stay time the two noise sources are incoherent. Below this frequency there is a high correlation between them. The root cause, of course, is that both noise sources are related to the same heat release fluctuations. There is also evidence presented in Appendix D that a resonance feedback oscillation takes place at a frequency equal to the inverse of a particle stay time. This is a feedback oscillation which links pressure fluctuations to entropy generation. While it takes place at a unique frequency and is of fundamental interest, it is of little interest in noise generation because of the small amount of acoustic power generated.

Of interest from the data reduction standpoint is a novel method which was developed for measurement of thermocouple response time in situ. This method is described in Appendix F.

Substantial early work on this program was expended in development of an entropy pulse facility to measure the entropy admittance coefficient of various nozzles under various flow conditions. Results are only now forthcoming from this work and will be reported later in the archive literature.

Finally, Appendix G addresses the issue of the frequency content of combustion noise. The liner hole size variations were found to have virtually no effect upon the frequency content of the noise when exhausting directly to the atmosphere. Both raw spectra of the interior microphone and derived spectra of the heat release fluctuations were used in the determination. This result was surprising, since it had been suspected that the mean length scale of turbulence, which should have been varied in these tests, was a strong factor in the frequency content.[1] The frequency content issue bears further examination.

## Conclusions

It must be borne in mind that some of the experimental conclusions here may be dependent upon the apparatus and conditions investigated. Most important among these were a) operation at 2 atm or below, b) use of a combustor with temperature fluctuations of about 12% of the mean absolute temperature and c) length scales of the temperature fluctuations of about 1 cm.

1. Theoretically, using experimental input, entropy noise will overtake and dominate combustion generated noise as a) the contraction ratio of a terminating nozzle is increased at fixed mass flow and fuel/air ratio or b) the mass flow at fixed fuel/air ratio is increased for a fixed contraction ratio. This takeover and dominance should be seen first at the higher frequencies (in the range investigated).
2. Experimentally, conclusion # 1 is borne out.
3. At frequencies below roughly 200 Hz, entropy and combustion noise are highly correlated, since they have the same physical origin.
4. Both interior and exterior pressure measurements are contaminated by one or more noise sources, other than entropy or combustion noise. It was inconclusive whether or not vorticity-nozzle interaction noise was a dominant contaminant, and further work is needed to investigate this source.
5. Measurement of the time-space cross power spectra of the temperature fluctuations must be performed with high accuracy if used in partial coherence analysis. In future work it is recommended that a net of many thermocouples be used instead of the two thermocouple traverses used here.
6. Hydrodynamic noise, which is non propagational pseudo-sound, dominates flush mounted interior microphones below about 150 Hz. This may be largely eliminated by use of the infinite tube method with the micro-

phone displaced from the flow field.

7. The frequency content of combustion noise is virtually unaltered by a change in the hydraulic diameter of the combustor liner holes. Past programs have found no combustor or flow variable that significantly alters the frequency content; however, fuel reactivity has not been varied over a wide range and deserves investigation in a future program.

## References


1. Strahle, W. C. and Shivashankara, B. N., "Combustion Generated Noise in Gas Turbine Combustors," NASA CR-134843, August 1974.
2. Strahle, W. C., "A Review of Combustion Generated Noise," Aeroacoustics: Jet and Combustion Noise; Duct Acoustics (Nagamatsu, ed.) AIAA, New York (1974) pp. 229-248.
3. Stone, J. R. "On the Effects of Flight on Jet Engine Exhaust Noise," NASA TM X-71819.
4. Mathews, D. C., Rehos, N. F. and Nagel, R. T., "Combustion Noise Investigation," Report No. FAA RD-77-3, 1977.
5. Reshotho, M., "Core Engine Measurement on a YF-102 Engine," AIAA Paper No. 77-21 (1977).
6. Bendat, J. S. and Piersol, A. G., Random Data: and Measurement Procedures, Wiley, New York (1971).
7. Goldstein, M. E., Aeroacoustics, Chapt. 5, McGraw-Hill, New York (1976).
8. Pickett, G. F., "Core Engine Noise due to Temperature Fluctuations Convecting through Turbine Blade Rows," AIAA Paper No. 75-528 (1977).

## Appendix A

## COMBUSTOR CHARACTERIZATION STUDIES

The combustor used for the present noise measurement program was removed from a Boeing 502-7D gas turbine engine. This unit was designed to perform efficiently at the three-atmosphere, 410°K discharge of a single stage centrifugal compressor. The current burning apparatus supplies air at near ambient pressure and temperature to the combustor. In addition, fuel nozzle flows are, at most, 40% of specified design values. Since off-design operation can significantly reduce burning efficiency, a performance evaluation of the combustor was judged necessary. As a first step, the air and fuel metering systems were checked for accuracy. In the present blow-down facility, air is supplied from a 28 $M^3$ storage vessel initially at 690 kPa (gage). Flow rates are determined at a regulated pressure with an orifice meter using mercury manometers to read upstream pressure and $\Delta P$. An orifice coefficient was computed from Ref. (A1) for the range of flows to be employed in the proposed noise test program. A check on computed air flows was made later in the program during cold-flow pitot surveys at the combustor exhaust plane. Agreement between the two methods was found to be good.

Fuel flows are determined with a Potter turbine meter and readout device. The unit was calibrated in water flow tests and was found to yield a linear output over its useful range. Maximum measured flow agreed within 0.5% of the manufacturer's stated value. The combustor unit was then mounted on the water flow test stand for fuel nozzle evaluation. The spray pattern was observed to consist of a barely discernable central plume, roughly 2 Cm in maximum diameter by 2.5 Cm long, surrounded by an evenly distributed cone of fog-sized droplets. The outer spray cone intersected the liner wall about midway between the inlet and exhaust planes. No significant alteration in spray pattern was seen over the range of flows used in the current test program. In all cases, the nozzle spray

observations were made with no air flow.

A series of cold flow tests were next completed to determine the portion of air which completely bypasses the liner and exhausts through the annulus (Figure A1). Pitot surveys of the exit plane at the locations shown in Figure A1 for flows of 14.2 and 19.8 $M^3$/Min. revealed that 25% $\pm$ 1% of the total air mass flow was bypassed. For both cases the sum of the pitot-measured liner and annulus flows agrees with the orifice-measured flow within $\pm$ 2%. Typical dynamic pressure profiles are shown in Figure A2 for the 14.2 $M^3$/Min. case. Profiles for 19.8 $M^3$/Min. exhibit the expected higher pressure magnitudes but closely resemble those for 14.2 $M^3$/Min. in distribution indicating no significant alteration for changing flow rate.

Two cases with combustion reflecting a change in overall fuel/air ratio were selected for initial study: 14.2 $M^3$/Min. air, $(F/A)_{OA}$ = 0.016; 19.8 $M^3$/Min. air, $(F/A)_{OA}$ = 0.008. As in the cold flow tests, pitot measurements were performed at the stations shown in Figure A1. In addition, temperature measurements were made with a chromel-alumel thermocouple at the same locations. Mass flow calculations from these measurements using mean values of temperature and dynamic pressure showed that the by-pass flow was not altered appreciably when combustion was present. By-pass for both cases was 26% $\pm$ 1% of the total initial air flow. Total mass flow computed from the sum of measured liner and annulus flows in both cases was about 2.5% lower than that calculated from orifice measurements. This slight discrepancy probably reflects the difficulties in obtaining accurate dynamic pressure measurements in a reacting flow. Figures A2 and A3 present dynamic pressure and temperature profiles for the 14.2 $M^3$/Min. case with combustion. As in the cold flow tests, the dynamic pressure profiles with combustion for 19.8 $M^3$/Min. are quite similar in shape to those for 14.2 $M^3$/Min. and differ only in magnitude. The previous statement is also true when temperature profiles for the two cases are compared.

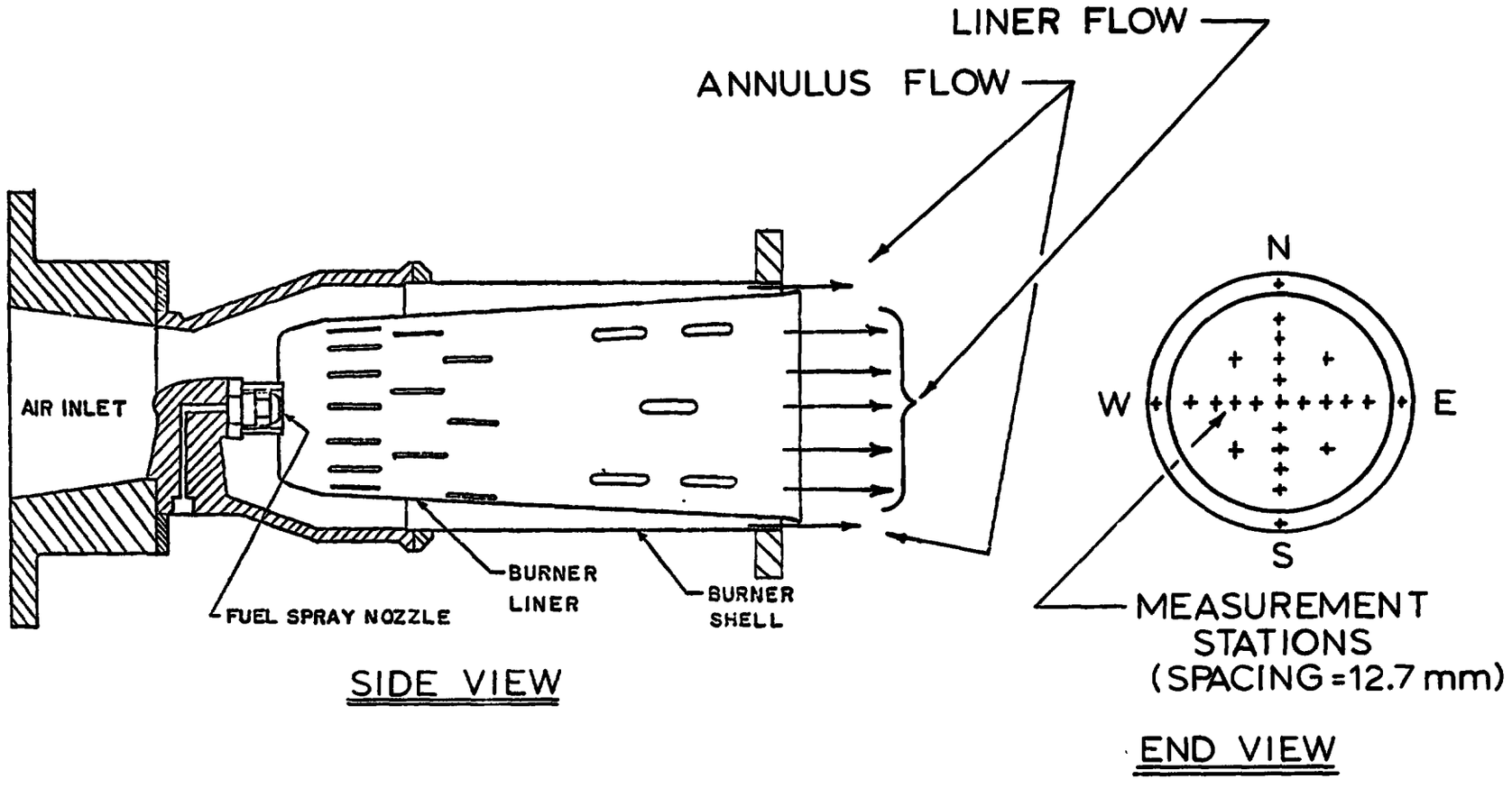


Figure A1. Combustor Test Apparatus.

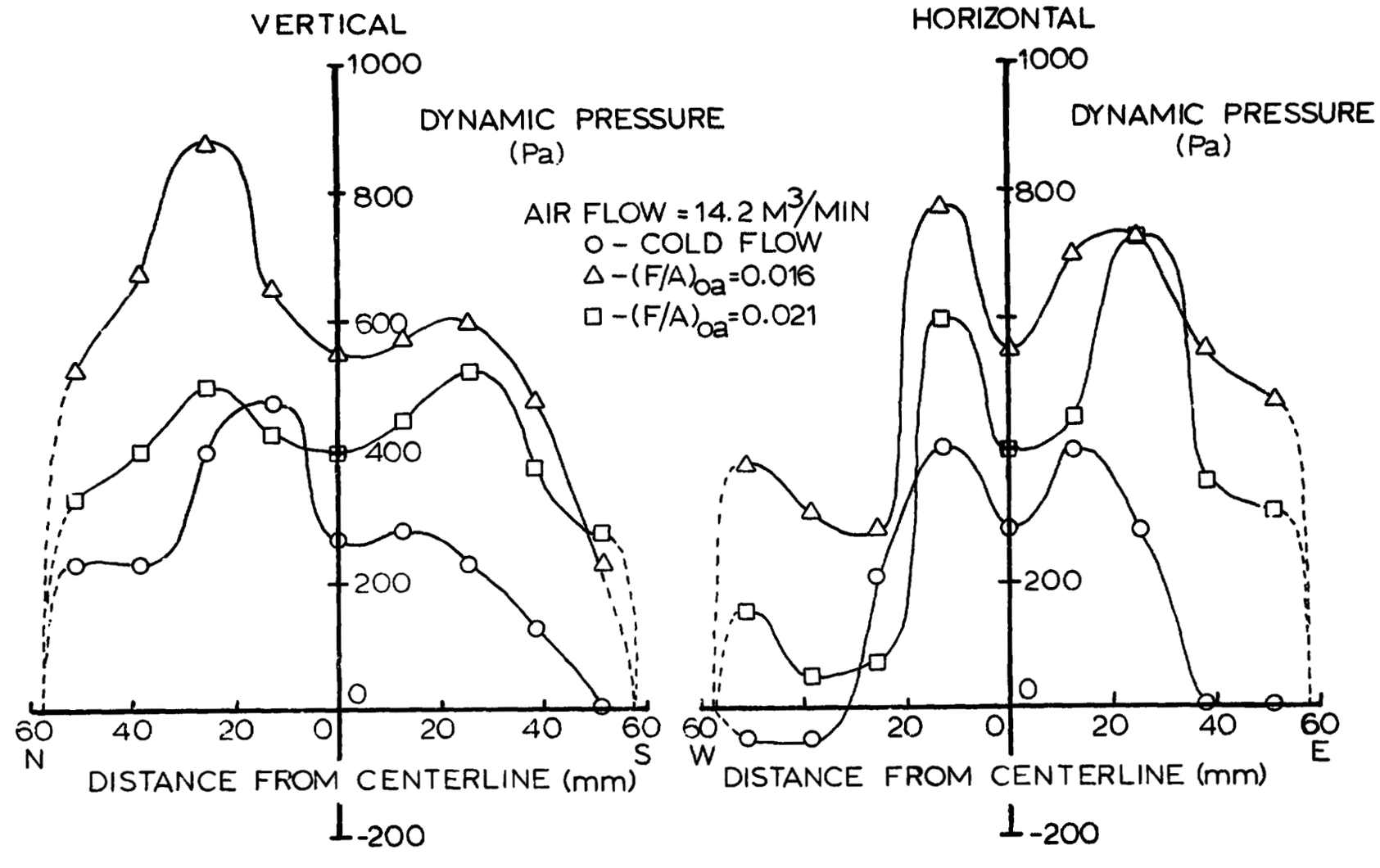


Figure A2. Combustor Exhaust Plane Dynamic Pressure Profiles.

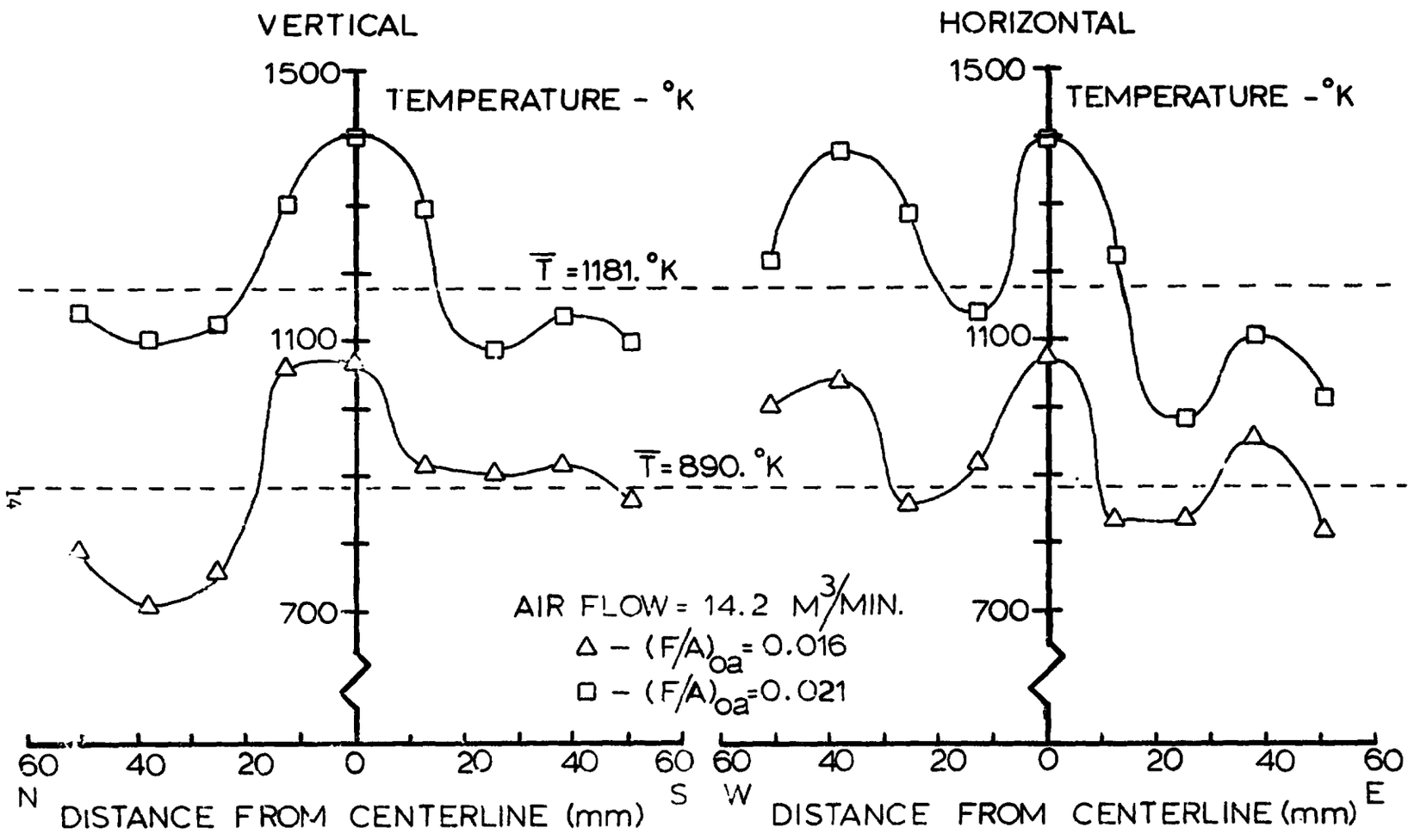


Figure A3. Combustor Exhaust Plane Temperatures Profiles.

It should be noted that the temperature profiles reflect the earlier described fuel spray pattern in which a central plume is enclosed in a conical skirt.

Burner efficiencies were computed for the 14.2 $M^3$/Min. and 19.8 $M^3$/Min. cases with combustion. In each case, efficiency was calculated both with a thermodynamic heat balance and with an expected temperature rise based on the adiabatic flame temperature. Each method ignored the 26% annular flow in accordance with test results showing only minor heating. Figure A4 presents the computed efficiency values and shows that the combustor performance was poor. It was observed from these results, however, that efficiency significantly improved with increased over-all fuel to air ratio. On this basis, it was decided to investigate combustor performance with increasing fuel flow for a given selected air flow.

Figure A5 shows the increase in measured combustor centerline exit temperatures for increased fuel rates at an air flow of 14.2 $M^3$/Min. Lines of constant efficiency based on a thermodynamic heat balance are also plotted for comparison. It should be noted that the mean exhaust temperature rise for these tests is about 80% of the centerline temperature rise so that comparison of experimental data with the efficiency curves is useful for determining trends only. Figure A5 clearly indicates improved performance as fuel flow increases with diminishing returns for $(F/A)_{OA}$ values greater than 0.016. From these results it was decided to select an over-all fuel-air ratio of 0.021 for a more detailed exit plane velocity-temperature scan.

The dynamic pressure and temperature profiles for $(F/A)_{OA}$ = 0.021 are shown in Figs. A2 and A3. Figure A2 indicates that dynamic pressure values decreased significantly from the $(F/A)_{OA}$ = 0.016 case. It was observed during the $(F/A)_{OA}$ = 0.021 tests that the flame routinely approaches and intermittently extends beyond the combustor can exit, indicating that combustion is not yet complete at the plane of measurement. As suggested earlier, measured dynamic pressure magnitudes

| FLOW CONDITIONS | | | $\bar{T}$ - $^{o}K$ | $\eta_b^*$ | $\eta_c^*$ |
|---|---|---|---|---|---|
| Air Flow - $M^3$/Min | $(F/A)_{OA}$ | % Bypass | | | |
| 19.8 | 0.008 | 26.0 | 463. | 0.401 | 0.326 |
| 14.2 | 0.016 | 26.0 | 890. | 0.675 | 0.693 |
| 14.2 | 0.021 | 21.6 | 1181. | 0.853 | 0.898 |

* Based on Liner Flow only

$$\eta_b = \frac{\dot{m}_{air}\, \bar{C}_p\, (\bar{T} - T_{amb})}{Q_R\, \dot{m}_{fuel}}$$

$$\eta_c = \frac{\bar{T} - T_{amb}}{T_{adiabatic\ flame} - T_{amb}}$$

Figure A4. Combustor Performance Summary

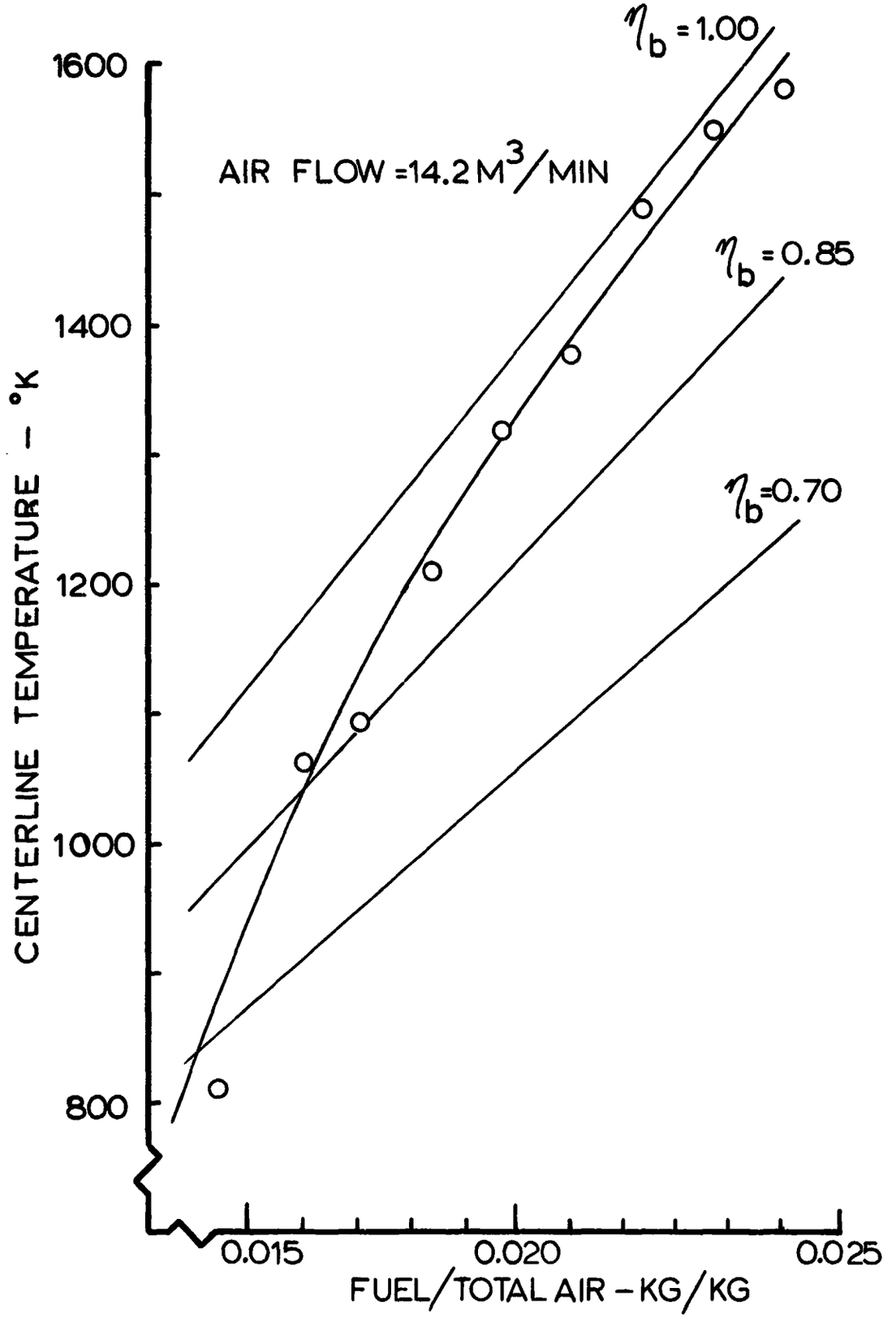


Figure A5. Combustor Exhaust Plane Centerline Temperature.

in reacting gases are unreliable, especially in this particularly severe case. The resulting calculated liner mass flows were, as expected, considerably low. A second test was performed to check the initial measurements. Extra care was taken in obtaining the annular data since liner measurements were not considered reliable. Results of the second test verified the initial findings. By-pass flow was found to be about 22% of the initial total air flow for this case. This small change from previous tests may indicate an actual alteration of the combustor flow pattern, but probably reflects the physical difficulties involved in making measurements in the annular flow with a flame extending past the exit plane. As predicted by the centerline temperature measurements of Fig. A5, the efficiency values for this condition were significantly improved. The performance is tabulated in Fig. A4.

The test program described above reveals that the present combustor unit must be operated at over-all fuel-air ratios on the order of 0.016 or greater to approach design efficiency. Accordingly, all subsequent measurements were performed at "high efficiency" flow ratios so that conclusions about combustor acoustics would not be subject to question from off-design operation.

Two alternate combustion liners were manufactured to study the effects of primary and secondary bleed hole width on combustor noise generation. In each unit axial slot area distribution and slot length was held equal to that of the original liner. With this constraint, machining and symmetry considerations dictated a minimum slot width equal to one-half that of the original ("S.W. x ½") and a maximum slot width equal to twice that of the original ("S.W. x 2"). Area distribution was maintained by doubling the number of narrow slots and halving the number of wide slots (including primary air inlet slots surrounding the fuel nozzle on the liner dome). The new units were fabricated from duplicate liners obtained from the manufacturer. Each liner was modified by filling existing

slots where necessary and milling new slots where required. The original and alternate liners are shown schematically in Fig. A6. Bleed hold area distribution is plotted for the three liners in Fig. A7.

Operating characteristics of both liners were checked prior to the initiation of noise tests. It was observed that the S.W. x 2 liner behaved much like the original liner in starting and steady state operation. Combustion appeared to be less complete than with the original liner as evidenced by larger areas of yellow flame at the liner exit plane. Flame distribution also was observed not to be as uniform as with the original liner. This observation was confirmed in a post-test investigation when areas of discoloration on the liner surface where found. A check of exit plane temperatures at five locations for $(F/A)_{OA}$ = 0.016 (air flow = 14.2 $M^3$/Min) showed only a slightly lower mean temperature than for the original liner.

Exploratory tests with the S.W. x ½ liner revealed that starting or maintaining a flame was impossible for over-all fuel to air ratios less than 0.0145 at an air flow of 14.2 $M^3$/Min. In contrast, the original and S.W x 2 liners could routinely operate at $(F/A)_{OA}$ = 0.008 and lower. Improved distribution of air flow in the primary combustion zone for this liner apparently dilutes the fuel-air mixture uniformly below the flamability limits for the lower fuel flows. Unlike the original and S.W. x 2 liners, the S.W. x ½ liner showed no evidence of yellow flame in the combustion zone. The light-blue flame was well distributed at the exit plane and no discoloration was observed on the liner surface even after repeated runs. A check of exit temperatures at five locations in the exhaust for $(F/A)_{OA}$ = 0.016 (air flow = 14.2 $M^3$/Min) showed the centerline temperature to be about 500°K above that for the original liner. Exhaust temperatures dropped quickly, however, with distance from the centerline and the resulting mean temperature was not significantly higher than that for the original liner.

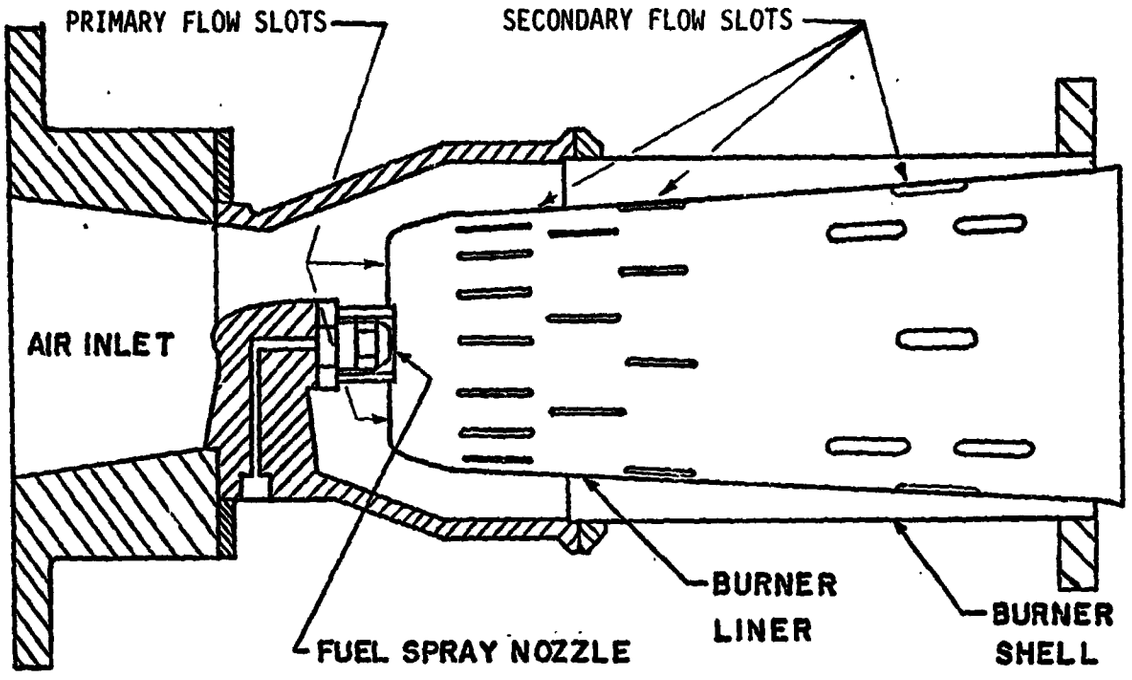


ORIGINAL COMBUSTOR CONFIGURATION

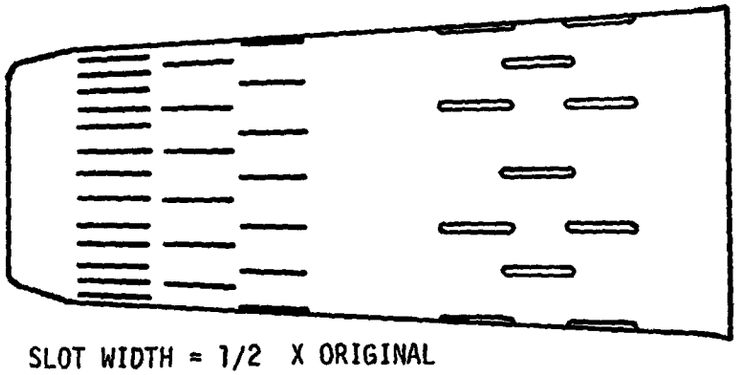

ALTERNATE LINER

SLOT WIDTH = 1/2 X ORIGINAL

SLOT NUMBER = 2 X ORIGINAL

NOTE: ALL LINERS HAVE SAME AXIAL BLEED HOLE AREA DISTRIBUTION (INCLUDING PRIMARY AIR INLET SLOTS)

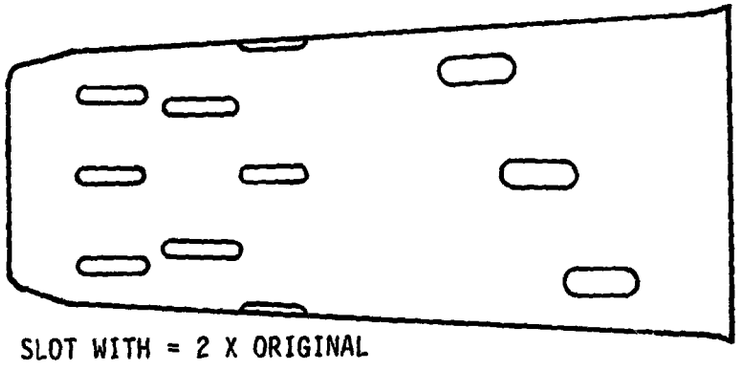

ALTERNATE LINER

SLOT WITH = 2 X ORIGINAL

SLOT NUMBER = 1/2 X ORIGINAL

Figure A6. Combustor Liner Slot Modification.

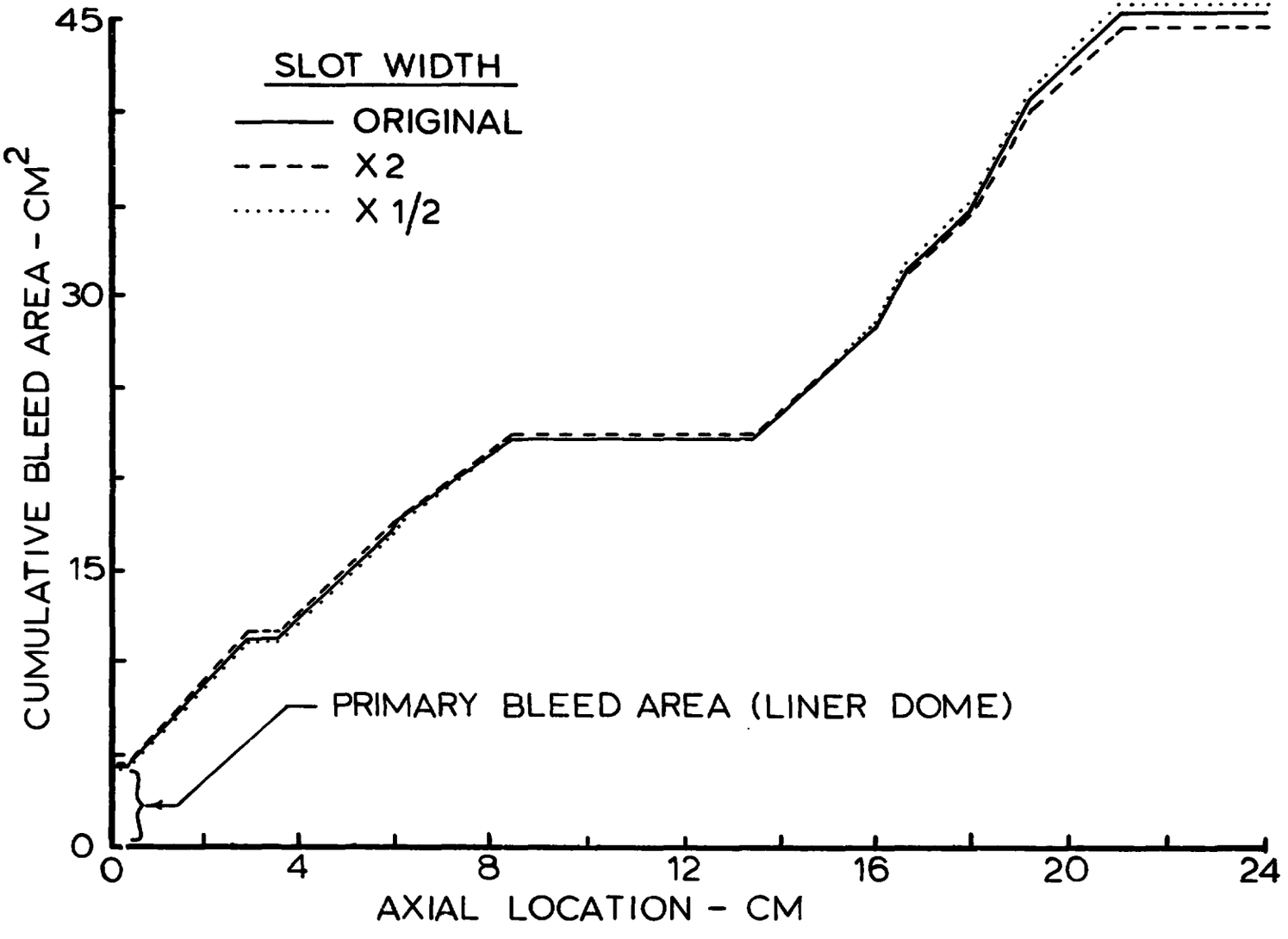


Figure A7. Axial Bleed Hole Distribution.

## Reference

A1 "Shell Flow Meter Engineering Handbook," Edited by T. S. Preston, Royal Dutch/Shell Group, Delft, Waltman, 1968.

## Appendix B

## Coherence between Internal and External Noise Generated by a Gac Turbine Combustor

# COHERENCE BETWEEN INTERNAL AND EXTERNAL NOISE GENERATED BY GAS TURBINE COMBUSTORS

Warren C. Strahle*
M. Muthukrishnan**
Douglas H. Neale***

School of Aerospace Engineering
Georgia Institute of Technology
Atlanta, Georgia 30332

## Abstract

Experiments and analysis on a gas turbine combustor unit are reported with a view in mind to separate propagated acoustic power from non-propagating "pseudo-sound". Analytically, it is suggested that a transition frequency will exist below which the interior pressure fluctuations are non-propagating, whereas above this frequency, of the order of 100 Hz, the noise is dominated by propagating acoustic waves. Coherence measurements are reported which show this concept to be borne out experimentally. Coherence between interior and exterior microphones is measured over a wide range of experimental conditions for a gas turbine combustor exhausting directly to the atmosphere. The purpose is to show that below a certain frequency, measurements of interior noise are not indicative of combustion noise ultimately propagating from an engine.

## Nomenclature

| | |
|---|---|
| $a$ | combustor radius |
| $c$ | speed of sound |
| $D$ | denominator defined by Eq. (15) |
| $e$ | specific sensible internal energy |
| $F$ | transverse tail of series defined by Eq. (17) |
| $f$ | defined by Eq. (11) |
| $G_{ij}$ | cross power spectrum between signals i and j. |
| $i$ | $(-1)^{1/2}$ |
| $J_m$ | Bessel function of $m^{th}$ order |
| $k$ | wavenumber defined by Eqs. (15) |
| $l$ | length of combustor |
| $M$ | Mach number |
| $p$ | pressure |
| $\dot{Q}$ | heat release rate per unit volume |
| $r$ | radial coordinate |
| $S$ | cross-section area |
| $t$ | time |
| $u$ | axial velocity component |
| $V$ | can volume |
| $\underline{v}$ | vector velocity |
| $x$ | axial coordinate measured from the upstream end of the combustor |
| $\beta$ | specific acoustic admittance |
| $\chi$ | eigenvalue defined by Eqs. (15) |
| $\varepsilon$ | constant defined by Eqs. (15) |
| $\gamma$ | ratio of specific heats |
| $\Lambda$ | constant defined by Eqs. (15) |
| $\Psi$ | transverse eigenfunction defined by Eqs. (15) |
| $\eta$ | defined by Eqs. (15) |
| $\rho$ | density |
| $\theta$ | angular coordinate |
| $\omega$ | frequency |
| $\mathcal{O}[\,]$ | of the order of |

**Subscripts**

| | |
|---|---|
| $a$ | acoustic (dilatational) quantity |
| $e$ | combustor exit plane |
| $mn$ | summation indices for transverse modes |
| $o$ | dummy integration variable |
| $v$ | vortical (turbulent) quantity |
| $w$ | side walls of the combustor |
| $\omega$ | Fourier transform |

**Superscripts**

| | |
|---|---|
| $\sim$ | dimensional quantity |
| $-$ | time mean quantities or ensemble average of statistical quantities |
| $\sigma$ | summation index for transverse modes |
| $'$ | perturbation quantities |

## Introduction

It is reasonably well understood that in order for noise generated interior to a turbopropulsion system to propagate to the surroundings a dilatation wave must accompany this noise. That is, in order for a propagational wave to be present, which carries acoustic energy, the divergence of the velocity vector must be non-zero. Alternatively, some of the interior noise is caused by vortical motions of the turbulence which are local in nature, not propagational. This problem of "pseudo-sound" coexisting with propagational noise causes difficulties in interpreting interior microphone measurements insofar as their connection with the ultimately radiated sound is concerned. Nevertheless, one of the primary techniques used to investigate the existence of "core engine noise" or "excess noise" has been the comparison of interior and exterior microphone measurements[1-3]

A technique used previously[1,3] to detect a causal relationship between an interior and exterior microphone has been the cross-correlation function. The use of this function in interpretation of the results requires exact specification of the two functions which are directly proportional to each other. So, for example, the interior pressure and the time derivative of the pressure were cross-correlated with the far field pressure in Ref. (3) to determine which of the two functions was related in direct proportion to the far field pressure. A less specific but powerful function to investigate a linear, causal relation between two variables is the coherence function.[4] It has the property that if two variables are related by a linear transform operation it will be unity, regardless of the transform operation. It will be zero if there is no causal relationship. This behavior occurs regardless of the transform operation. For example, in Ref. 3 the coherence function between either the time derivative of the interior pressure or the pressure itself and the far field pressure would be unity if either of the two quantities were perfectly correlated with the far field pressure because

---

* Regents' Professor, Associate Fellow AIAA
** Graduate Research Assistant
*** Research Engineer, Member AIAA
This work was supported by NASA under grant number NSG 3015

Copyright © American Institute of Aeronautics and Astronautics, Inc., 1977. All rights reserved.

differentiation is a linear transform operation. The coherence function will be used in this paper to determine the frequency regimes, if any, in which there is a linear causal relation between interior and exterior pressure fluctuations.

The purposes of this paper are two-fold. First, it will be analytically established that below a certain frequency (apparatus dependent) the hydrodynamic noise generated by turbulence within a combustor is non-propagational and consequently incoherent with exterior sound measurements. Secondly, for a particular experimental set-up, this fact will be demonstrated.

## Analysis

The theory of combustion noise for the gas turbine combustor will assume that the fluid mechanics process is one of the gas phase alone. Therefore, the complications of fuel evaporation and mass, momentum and energy transfer between liquid and gas phases are avoided. Consideration of these processes is not necessary for an adequate understanding of combustion noise generation, since the dominant noise generation process is a gas phase one - the unsteady heat release in the turbulent gas phase. Although mass release fluctuations in space and time by evaporation from the spray droplets would indeed cause some noise, order of magnitude arguments support the contention that the extreme heat release involved causes greater local fluctuations in gas velocity, the primary source of noise. The approach will be to study the behavior of the fluctuating components of various field quantities about their time-mean values. These fluctuations will contain both the turbulence and acoustic fluctuations, and a split into vortical turbulent motions and acoustic quantities is found possible by the method below.

Molecular transport processes are neglected in comparison with turbulent transport. Although it would be necessary to consider these to recover exact flame structure (since the actual combustion process must take place in the microscale of the turbulence), the flame structure is basically left as an unknown in the following treatment, to be determined by knowledge of both the time-mean field quantities and the fluctuation quantities.

The equations of continuity, momentum, energy and state for an inviscid perfect gas are

$$\frac{\partial \tilde{\rho}}{\partial \tilde{t}} + \tilde{\nabla}\cdot(\tilde{\rho}\tilde{\underline{v}}) = 0, \quad \frac{\partial \tilde{\underline{v}}}{\partial \tilde{t}} + \tilde{\underline{v}}\cdot\nabla\tilde{\underline{v}} = -\frac{\tilde{\nabla p}}{\tilde{\rho}},$$

$$\frac{\tilde{D}\tilde{e}}{\tilde{D}\tilde{t}} + \tilde{p}\,\frac{\tilde{D}(1/\tilde{\rho})}{\tilde{D}\tilde{t}} = \frac{\tilde{\dot{Q}}}{\tilde{\rho}}, \quad \frac{\tilde{p}}{\tilde{\rho}} = (\gamma-1)\tilde{e} \qquad (1)$$

Nondimensionalizing Eqs. (1) by the can length, the exit plane mean speed of sound, density, and pressure, the conservation equations become

$$\frac{\partial \rho}{\partial t} + \nabla\cdot(\rho\,\underline{v}) = 0 \qquad (2)$$

$$\frac{\partial \underline{v}}{\partial t} + \underline{v}\cdot\nabla\underline{v} = -\frac{\nabla p}{\gamma\rho} \qquad (3)$$

$$\frac{Dp}{Dt} - \gamma\,\frac{p}{\rho}\,\frac{D\rho}{Dt} = (\gamma-1)\dot{Q} \qquad (4)$$

Constructing the time mean equation the usual results are found. That is, the pressure gradient is of the order of the square of the Mach number so that if $\bar{M}^2 << 1$, $\bar{p} \approx 1$; furthermore, the primary effect of $\bar{\dot{Q}}$ is to cause a dilation of the velocity vector, not a strong pressure change. These remarks presume well distributed combustion throughout the combustor so that $\nabla\cdot\bar{\underline{v}}$ is of the order of unity throughout the combustor. This is generally true for a spray type diffusion flame.

Now consider the linearized fluctuation equations. By linearization all processes in the turbulence relying on nonlinearities such as generation, spectral transfer and decay (which is not considered because viscosity is not considered) are omitted. Consideration is therefore focused on the energy containing eddies over the can length which is presumed short compared with a length required for a substantial alteration of the turbulence structures. Combining Eqs. (2) and (4), Eqs. (3) and (4) become after linearization

$$\frac{\partial \underline{v}'}{\partial t} + \nabla(\bar{\underline{v}}\cdot\underline{v}') + \nabla\times\bar{\underline{v}}\times\underline{v}' + \nabla\times\underline{v}'\times\bar{\underline{v}} = -\frac{\nabla p'}{\gamma\bar{\rho}} \qquad (5)$$

$$\frac{\partial p'}{\partial t} + \underline{v}'\cdot\nabla\bar{p} + \bar{\underline{v}}\cdot\nabla p' + \gamma p'\nabla\cdot\bar{\underline{v}} + \gamma\bar{p}\,\nabla\cdot\underline{v}' = (\gamma-1)\dot{Q}' \qquad (6)$$

In Eq. (6) the second term may be dropped because $\nabla\bar{p}$ is $\mathcal{O}(M^2)$ and in the fifth term $\bar{p} = 1$ may be used, correct to terms of $\mathcal{O}(M^2)$ compared to unity. Now let the perturbation velocity vector be split into its lamellar and solenoidal components.

$$\underline{v}' = \underline{v}_a' + \underline{v}_v'$$

where $\nabla\cdot\underline{v}_v' = \nabla\times\underline{v}_a' = 0$. Here $\underline{v}_a'$ is associated with a dilatational acoustic motion and $\underline{v}_v'$ is associated with vortical turbulent motions convected by the mean fluid motion. Because of the linearity of Eqs. (5) and (6) the pressure may be considered as split into two components $p_a'$ and $p_v'$ and Eqs. (5) and (6) may be split as follows:

$$\frac{\partial \underline{v}_a'}{\partial t} + \nabla(\bar{\underline{v}}\cdot\underline{v}_a') + \nabla\times\bar{\underline{v}}\times\underline{v}_a' = -\frac{\nabla p_a'}{\gamma\bar{\rho}} \qquad (7)$$

$$\frac{\partial p_a'}{\partial t} + \bar{\underline{v}}\cdot\nabla p_a' + \gamma p_a'\nabla\cdot\bar{\underline{v}} + \gamma\bar{p}\nabla\cdot\underline{v}_a' = (\gamma-1)\dot{Q}' \qquad (8)$$

$$\frac{\partial p_v'}{\partial t} + \bar{\underline{v}}\cdot\nabla p_v' = \frac{\bar{D}}{Dt}p_v' = -\gamma p_v'\nabla\cdot\bar{\underline{v}} \qquad (9)$$

$$\frac{\partial \underline{v}_v'}{\partial t} + \nabla(\bar{\underline{v}}\cdot\underline{v}_v') + \nabla\times\bar{\underline{v}}\times\underline{v}_v' + \nabla\times\underline{v}_v'\times\bar{\underline{v}} = -\frac{\nabla p_v'}{\gamma\bar{\rho}} \qquad (10)$$

In Eq. (8) $\dot{Q}'$ has been associated with the acoustic problem since heat release per unit volume can produce no torque, only dilatation. In Eq. (9) the expected result is present that the pressure fluctuations produced by the vortical motion are convected by the mean flow, modified only by the right hand side of Eq. (9). If terms of the order of the Mach number are neglected, compared with unity, the second and third terms of Eqs. (7) and (8) may be neglected if $\frac{\partial}{\partial t}$ is $\mathcal{O}(1)$ so that wavelengths are of the order of the combustor length. This assures that the $\nabla$ operator is of order unity. In this case, taking the Fourier transform of Eqs. (7) and (8) and combining

$$\nabla^2 p_{a_\omega} + \omega^2 p_{a_\omega} = -\left.\frac{\partial \dot{Q}}{\partial t}\right)_\omega (\gamma-1) \equiv -f_\omega \qquad (11)$$

Equation (11) is an inhomogeneous Helmholtz equation

driven by the fluctuating heat release. Furthermore, the source term is the local Eulerian time derivative of the heat release as has occurred previously,[5] not the total time derivative as in the formulation of Ref. (6).

At low values of the frequency Eq. (11) is not accurate and the primary information comes from Eq. (8) as

$$\gamma \nabla \cdot v_a' = (\gamma-1)\,\dot{Q}' \qquad (12)$$

neglecting terms of $\mathcal{O}(M)$ compared to unity. The pressure is then determined by Eq. (7) without the time derivative term. Equations (11) and (12) are limiting forms of Eqs. (7) and (8) at $\omega$ of $\mathcal{O}(1)$ and $\omega \to 0$, respectively. Integrating Eq. (12) over the combustor volume and assuming a high impedance head end and walls of the combustor, the Fourier transform of the result yields

$$\int_{S_e} v_{a_{\omega_n}}\, dS = \frac{\gamma-1}{\gamma} \int_V \dot{Q}_\omega\, dV \qquad (13)$$

Eq. (13) states that the average normal velocity fluctuation at the can exit plane is directly caused by the sum of the heat release fluctuations interior to the can. The average velocity fluctuation at the can exit will radiate sound in accordance with the impedance relation of Ref. (7). In the limit of low frequency and just outside the can

$$p_\omega \propto \int_{S_e} v_{\omega_n}\, dS \propto \omega \int_V \dot{Q}_\omega\, dV$$

$$p_\omega \to 0 \text{ as } \omega \to 0$$

Consequently, since $\dot{Q}_\omega$ must also go to zero if $\omega \to 0$ (by definition of a fluctuating quantity) an observed experimental fact of very low exterior pressure fluctuations at low frequency is recovered analytically. However, it will be seen experimentally that at low frequency the interior pressure fluctuations remain high while the exit plane fluctuations disappear. An interior microphone will see both $p_v'$ and $p_a'$ whereas exterior microphones will only see the effects of $p_a'$, it being a propagational wave containing fluid dilatation. One can therefore expect a possibility that below a certain frequency, if $p_v'$ dominates $p_v'$ at higher frequency, $p_v'$ may dominate $p_a'$. This is only a possibility analytically because both $p_v'$ and $p_a'$ must go to zero as $\omega \to 0$ but the end plane impedance relation might drive $p_a'$ to zero faster than $p_v'$. Any dominance of $p_a'$ at any frequency must come from the source $\dot{Q}'$ and at $\omega$ of $\mathcal{O}(1)$ Eq. (11) is the dominant equation if the source is strong enough. Experimentally it is known that propagational sound, called combustion noise, is heard from combustors, and, consequently, there is a frequency regime where Eq. (11) is valid. The point is that <u>in the limit of low frequency there is no reason to expect a correlation between an interior pressure measurement and the pressure measurement outside the can</u>. At sufficiently low frequency there is the possibility that non-propagating "pseudo-sound" will dominate interior pressure measurements.

Because the exact nature of the turbulence field is not known, it is impossible to state the exact value of $\omega$ at which a transition will occur from Eqs. (9) and (10) to Eqs. (7) and (8) as the governing system. This will have to be determined experimentally. The transition will be called the hydrodynamic to acoustic transition since Eq. (11) has wave phenomena clearly associated with it while Eqs. (9) and (10) are controlled by the turbulence field. Consider, then, the solution of Eq. (11). To solve Eq. (11) the acoustic behavior of the liner walls and exit plane must be known. From the work of Ref. (7) it is known that the acoustic impedance of the exit plane should differ little from that of an unflanged pipe, open to the infinite surroundings. From the work of Ref. (8) the head end should behave basically as a hard wall. The side walls present a complex acoustic picture, however. It is known experimentally that only weak can resonances appear, so that the side walls must be reasonably absorbent, acoustically. An acoustic admittance, $\beta_w$, will be assigned to the side walls which will be left as a free parameter. The magnitude of $\beta_w$ can be deduced approximately by a comparison of the theoretical and experimental resonance peak heights in the pressure. Under the approximations leading to Eq. (11), therefore, the boundary conditions on $p_\omega$ are (assuming a cylindrical combustor)

$$x = 0 \quad \frac{\partial p_\omega}{\partial x} = 0$$

$$r = a \quad \frac{\partial p_\omega}{\partial r} + i\omega\beta_w p_\omega = 0$$

$$x = 1 \quad \frac{\partial p_\omega}{\partial x} + i\omega\beta_e p_\omega = 0 \qquad (14)$$

where a is the can radius and $\beta_e = \tilde{u}_{\omega_e} \tilde{\rho}_e \tilde{c}_e / \tilde{p}_{\omega_e}$ is the specific acoustic admittance of the exit plane.

The solution to Eq. (11) subject to Eqs. (14) may be worked out by standard methods, by expansion in terms of normal modes of the combustor. Since $\dot{Q}_\omega$ is a random function of position in the combustor can there are no symmetries that may be invoked to simplify the solution and the solution will contain both symmetric and anti-symmetric modes. Since interest is ultimately in comparing a wall-measured pressure against the exterior radiated pressure, the solution is here given for a wall pressure. The solution is

$$p_\omega(x,a,\theta) = \sum_{\substack{m,\,n=0 \\ \sigma=+1,\,-1}}^{\infty} \left(p^{\sigma}_{\omega_{mn,1}} + p^{\sigma}_{\omega_{mn,2}}\right) = p_{\omega_1} + p_{\omega_2}$$

$$p^{\sigma}_{\omega_{mn,1}} = \frac{\Psi^{\sigma}_{mn}(a,\theta)\left[e^{ik_{mn}(1-x)} + \Gamma_{mn} e^{-ik_{mn}(1-x)}\right]}{i S k_{mn} \Lambda_{mn} D_{mn}} \cdot$$

$$\int_0^x dx_o \cos k_{mn} x_o \int_S dS_o\, f_\omega(x_o, r_o, \theta_o)\, \Psi^{\sigma}_{mn}(r_o, \theta_o)$$

$$p^{\sigma}_{\omega_{mn,2}} = \frac{\Psi^{\sigma}_{mn}(a,\theta)\cos k_{mn} x}{i S k_{mn} \Lambda_{mn} D_{mn}} \cdot$$

$$\int_x^1 dx_o \left[e^{ik_{mn}(1-x_o)} + \Gamma_{mn} e^{-ik_{mn}(1-x_o)}\right] \int_S dS_o\, f_\omega \Psi^{\sigma}_{mn}$$

$$k_{mn}^2 = \omega^2 - \kappa_{mn}^2$$

$$\kappa_{mn} J_m'(\kappa_{mn} a) = -i \omega \beta_w J_m(\kappa_{mn} a)$$

$$\psi_{mn}^{\sigma} = J_m(\kappa_{mn} r) \begin{cases} \cos m\theta \\ \sin m\theta \end{cases} \begin{matrix} \sigma = +1 \\ \sigma = -1 \end{matrix}$$

$$D_{mn} = e^{ik_{mn}} - \eta_{mn} e^{-ik_{mn}}$$

$$S = \pi a^2$$

$$\eta_{mn} = \left(1 - \frac{\omega \beta_{e_{mn}}}{k_{mn}}\right) / \left(1 + \frac{\omega \beta_{e_{mn}}}{k_{mn}}\right)$$

$$\Lambda_{mn} = \varepsilon_m \left[1 - \frac{m^2 + (\beta_w \omega a)^2}{(\kappa_{mn} a)^2}\right] J_m^2(\kappa_{mn} a)$$

$$\varepsilon = 1 \; m = 0 \; , \; \varepsilon = 1/2 \; m > 0 \qquad (15)$$

The $p_{\omega 1}$ part of the solution contains the contribution of $f_\omega$ from x = 0 to x and $p_{\omega 2}$ contains the contributions from x (the measuring point) to 1. The first term in the overall sum (m=n=0 , $\sigma$ = +1) is the (nearly) plane wave mode. It is not absolutely plane because $\kappa_{oo} \neq 0$, but is calculated for small $|\kappa_{oo} a|$ from the Bessel function equation to be

$$\kappa_{oo} = \left(\frac{2 i \omega \beta_{w_{oo}}}{a}\right)^{1/2} \qquad [|\kappa_{oo} a| << 1] \qquad (16)$$

For practical purposes, however, little error is made in the use of Eq. (16) for $|\kappa_{oo} a|$ as large as unity. The finite magnitude of $\kappa_{oo}$ means that

$$\psi_{oo}^1 = J_o(\kappa_{oo} r) \neq 1$$

has a radial dependence, and, consequently, $p_{\omega_{oo}}^1$ has a radial dependence which keeps it from purely plane behavior.

For $\beta_e$ large, as it is at low $\omega$, $\eta_{oo} \approx -1$, and $D_{oo}$ has a minimum near $\omega = \pi/2$, the quarter wave resonance point. Thus, a maximum occurs in $p_{\omega_{oo}}^1$ at the quarter wave frequency, as expected. Because each term in the sum contains a different functional weighting of $f_\omega$ in the integrations, each term in the sum is partially incoherent in phase with the other, unless, of course, $f_\omega$ is not random in position, which is not to be expected. $p_\omega$ may also be represented by

$$p_\omega = p_{\omega_{oo,1}} + p_{\omega_{oo,2}} + F \qquad (17)$$

where all three quantities are incoherent with each other and F is the entire transverse mode tail of the doubly infinite series. It would be nice if it could be shown that some of the terms of Eq. (17) could be neglected. Clearly, if $f_\omega = 0$ between x and 1, $p_{\omega_{oo,2}} = 0$. Additionally, if $f_\omega$ is nonzero for only a short axial distance near x = 0 and $\omega$ is low, a careful inspection of Eqs. (15) shows the anticipated behavior that all transverse modes are cutoff ($F \approx 0$) if the measuring point is sufficiently far downstream. This latter case cannot be expected to occur in practice since at best one half of the can length must contain active combustion. On the other hand, there is a reasonable expectation that near the quarter wave resonance point the plane wave mode, $p_{\omega_{oo,1}}$ and 2, will dominate F. Furthermore, in the limit of small $\omega$ ($\omega \to 0$) the plane wave mode will dominate F if $\beta_w$ is small because of the appearance of $k_{oo} \approx \omega$ in the denominator. On the other hand, it should be recalled that at sufficiently low $\omega$ Eq. (11) ceases to be valid. Consequently, numerical calculations are in order to determine the actual magnitudes of various terms.

In order to experimentally determine whether or not any terms may be neglected in Eq. (17), however, the coherence function may be used.[4] Consider a measurement of the pressure at two combustor position, x and 1. The cross power spectrum of these two pressures is

$$G_{x1} = p_\omega(x)\, p_\omega^*(1)$$

where the * denotes a complex conjugate. Here

$$p_\omega(1) = p_{\omega_{oo,1}}^1(1) + F(1)$$

$$p_\omega(x) = p_{\omega_{oo,1}}^1(x) + p_{\omega_{oo,2}}^1(x) + F(x)$$

Now note that part of $p_{\omega_{oo,1}}^1(1)$ contains $p_{\omega_{oo,1}}(x)$ in the integration of Eqs. (15). In fact $p_{\omega_{oo,1}}^1(1) = H(\omega) p_{\omega_{oo,1}}^1(x)$ + J where $H(\omega)$ is a linear determined transfer function and J is a frequency dependent random function which is incoherent with any other term. Consequently, let $p_{\omega_{oo,1}}^1(x) \equiv b$ and the pressures take the form

$$p_\omega(1) = Hb + K$$

$$p_\omega(x) = b + L$$

where K and L are incoherent with b. If a many sample average is taken of $G_{x1}$ to yield $\bar{G}_{x1}$ there results

$$\bar{G}_{x1} = \overline{b\, b^*\, H^*}$$

The auto spectra after averaging are

$$\bar{G}_{xx} = \overline{b\, b^*} + \overline{L\, L^*}$$

$$\bar{G}_{11} = \overline{b\, b^*}\, H\, H^* + \overline{K\, K^*}$$

The coherence function is defined by

$$\gamma^2 = \frac{\bar{G}_{x1}\, \bar{G}_{x1}^*}{\bar{G}_{xx}\, \bar{G}_{11}}$$

and there results

$$\gamma^2 = \frac{\overline{b\,b^*}^2 \; H\,H^*}{(\overline{b\,b^*} + \overline{L\,L^*})(\overline{b\,b^*}\,H\,H^* + \overline{K\,K^*})} \qquad (18)$$

If either a) events between x and 1 dominate $p_w$ behavior (J and L are large so that K and L are large compared with b , or b) F is dominant and F(1) is incoherent with F(x) , $\gamma^2$ is small. On the other hand if b is the dominant term $\gamma^2 \to 1$. A coherence function of unity (or near unity) in a given frequency range will therefore show that a single term dominates the solution of Eqs. (15) and that events between x and 1 are unimportant ($f_w \approx 0$). Furthermore, the coherence function will also show where Eqs. (7) and (8) take over from Eqs. (9) and (10). This can be seen if the microphone at x is dominated by $p'_w$ and the x = 1 microphone is placed slightly outside of the combustor end plane to sense only propagational sound, $p'_a$.

If a frequency band is found where $\gamma^2 \approx 1$, it is assumed that $f_w \approx 0$ between x and 1. Any deviation from $\gamma^2 \approx 1$ at higher frequencies must then indicate the transverse modes competing with the plane wave mode. Calculations have been performed on Eqs. (15) to compare the magnitudes of $p^1_{w_{00}}(x)$ and $p^{11}_{w_{10}}(x)$. A $\beta_w$ magnitude has been chosen to give roughly the quarter wave resonance peak magnitude which is experimentally observed. $\beta_w$ has been assumed real, on the basis of no other information. In the calculation, $\gamma^1_{oo}(a,\theta) = 1$ and $K_{10}$ real ($\beta_{w_{10}} = 0$) have been assumed for the order of magnitude calculations. The position x has been chosen, to correspond with the experimental setup. The expression for $\beta_e$ is the low frequency asymptotic expression of Levine-Schwinger[9]

$$\beta_e = 1/[\omega\, a(\, 0.6\, i + 0.25\, \omega\, a)\,]$$

This has also been used for the first transverse mode calculation. The elimination of the wall damping in the transverse mode calculation will raise its magnitude compared with the case of damping; consequently, this is a conservative comparison of the dominance of the plane wave mode over the transverse mode. The integrals in Eqs. (15) have been estimated by a) carrying out the $x_o$ integration as though $f_w$ were independent of $x_o$ and b) the transverse integrations have been estimated as

$$\int_S dS_o\, f_w\, \Psi^{\sigma}_{mn} \cong A_w \left[\frac{1}{S}\int_S \Psi^{\sigma}_{mn}\, dS\right]^{1/2}_S$$

where $A_w$ is an average (unknown) source strength. Shown in Fig. 1 are calculations for the plane wave mode and the first antisymmetric transverse mode (1,0), which is the first transverse mode to cut on as frequency rises. Starting from top to bottom, the plane wave mode at x = 0.655 with source contributions from 0 to x (00,1) is the dominant term. It shows the quarter wave resonance near $\omega = \pi/2$. Slightly lower in magnitude is the plane wave mode evaluated at x = 1, now using the source contribution from x = 0 to x = 1. The reason it is slightly lower in magnitude, even though the source contributes over the full can length, is that the impedance condition at the can exit plane requires nearly constant pressure, whereas there is no such restriction interior to the combustor. Much lower in magnitude is the plane wave contribution to the x = 0.655 position from the combustor position downstream of the transducer position. (00,2). Consequently, even if the combustor source strength were as large downstream as upstream of the transducer position it would not contribute to the transducer measurement. Finally, well down from the plane wave modes, is the first transverse mode contribution. It is almost completely cut off at the transducer location over the frequency range shown. Theoretically, it would cut on completely at a dimensionless frequency of 8.8 The frequencies of interest experimentally are well below this value so that the F function of Eq. (17) may indeed be neglected. The major conclusion, therefore, is that in Eq. (18) $\gamma^2 = 1$ should result over the frequency range of interest as long as the frequency is high enough that Eqs. (15) are a valid solution to the problem.

## Experiment

### Apparatus

The gas turbine combustor used in this study was described in Ref. (10). A schematic of the setup is shown in Fig. 2. A water-cooled pressure transducer capable of extracting signal above 135 dB re $2\times10^{-5}$ N/m$^2$ was located on the liner wall, 92 mm from the can exit plane. A near field 1/2 inch condensor microphone was located in the can exit plane, 113 mm to the side of the liner lip. This transducer measures the can exit plane dynamic pressure as long as the frequencies are restricted to wavelengths long compared with this separation distance. Far field microphones are employed to detect the onset of scattering from the burner hardware (non-monopole behavior of the can exit plane) as will be explained later.

All signals are recorded on FM tape for later digital Fourier analysis. The primary items of interest are spectral shapes and coherence analysis. Calibration procedures are therefore unimportant, except to be satisfied that the microphones are behaving linearly in voltage output vs dynamic pressure level.

### Results

Figure 3 displays the spectra obtained by fixed bandwidth frequency analysis of the interior microphone signal. Shown are the runs at extreme ends of the airflow and fuel/air ratio matrix. In all cases there are two regimes to the spectra. Below about 200 Hz the spectra are quite flat. Above this value the spectra undergo a hump. The upper frequency limit was chosen as 800 Hz, for reasons to be apparent later. Depending upon fuel/air ratio (speed of sound) a weak quarter wave resonance is seen in all curves in the vicinity of 400 Hz.

In contrast, look at Figure 4 which displays a typical near field microphone spectrum (although here a wider frequency range has been considered). At low frequency the spectrum falls off at roughly 13 dB/octave whereas the interior microphone measured a flat spectrum. By way of interest Figure 4 shows the 1/4, 3/4 and 5/4 wave resonance peaks. The major point is, however, that the near field spectrum has behavior similar to the interior microphone spectrum only above about 200 Hz. More documentation on this effect is shown by the several near field spectra in Fig. 5. Also shown is a typical far field microphone spectrum which is similar in shape to the near field spectra, except that ground reflection effects are seen in the spectrum.

Now consider Fig. 6 which shows the near to far field coherence which is high (nearly perfect coherence) over the range 100-600 Hz and is acceptably high even below 100 Hz. As long as the frequency is sufficiently low that the can is behaving as a monopole radiator the far field is quite coherent with the near field even in the presence of ground reflections; this occurs because ground reflections cause only a linear transform operation on the near field signal to recover the far field signal. Furthermore, in the frequency domain the distance traveled to the far field microphone only introduces a phase lag, again a linear transform operation which cancels out in coherence analysis. Above 600 Hz one concludes that scattering from the burner hardware is such that monopole behavior is destroyed; a single point measurement in the near field is insufficient to describe the total characteristics of the far field radiation. Consequently, below 600 Hz a near field measurement is adequate to describe the spectrum of the ultimately radiated sound power, and attention is focused only below 600 Hz.

Now view Fig. 7 which portrays the coherence between the interior and near field microphones for several run conditions. The coherence behavior is the same for all runs; it is above 0.5 between about 150 Hz and 600 Hz and is nearly unity over the range 200-500 Hz. As frequency drops below 150 Hz the coherence drops to nearly zero. The interpretation of these results is as follows. a) a source other than combustion noise is dominating the interior microphone measurement at frequencies below 150 Hz, b) because of the above analysis and the non-correspondence of the spectral shapes of the two microphones at low frequency the other noise source is hydrodynamic noise caused by the vortical turbulent motions and those motions do not provide propagational sound and c) above 600 Hz the low coherence is caused by the failure of a single point measurement in the near field to characterize the entire radiation pattern; the monopole radiation pattern has ceased. The drop in the near field spectrum at low frequency is faster than a dropoff proportional to frequency alone, indicating that $\dot{Q}_w$ is falling off at roughly 6-7 dB/octave below about 300 Hz. This appears to be the primary reason for the takeover of hydrodynamic pseudo-sound at low frequency.

## Discussion

The results presented here can clearly be expected to be apparatus-dependent, especially with regard to the frequency at which hydrodynamic noise and combustion noise are equivalent at an interior location. The only contention here is that generally such a transition at some frequency may be expected. In the experiment here there were only two basic noise sources - flow noise and combustion noise. In an installed configuration at least two other combustor-turbine interaction noises will come into the picture to confuse the results; there will be entropy noise[11] and vorticity-nozzle interaction noise,[12] both of which will cause propagational noise and which will be sensed by both interior and exterior microphones. These sources have been avoided here by directly discharging to the atmosphere.

A major point to be stressed is that combustion noise may be present in the far field signature even if there is little coherence between internal and external microphones. This was precisely the case at low frequency in these experiments. Consequently, some care in experiment design in installed configurations is required to determine the amount of pseudo-sound in the combustor as compared with propagational sound.

In the experiments here it was fortunate that the frequency content of combustion noise was low enough and the burner size was small enough that a) the plane wave mode dominated the interior acoustics and b) the can radiated basically as a monopole over the frequency range that contained most of the combustion noise. Severe complications in interpretation can be expected if this is not the case.

## References


1. Abdelhamid, A. N., Harrje, D. T., Plett, E. G. and Summerfield, M., "Noise Characteristics of Combustion Augmented Jets at Midsubsonic Speeds," AIAA J, 12, 336-392 (1974).
2. Gerend, R. P., Kumasaka, H. A. and Roundhill, J. P., "Core Engine Noise," Aeroacoustics: Jet and Combustion Noise; Duct Acoustics (Nagamatsu,ed.) AIAA, New York (1975) pp. 305-326.
3. Plett, E. G., Teshner, M. D. and Summerfield, M., "Combustion Geometry and Combustion Roughness Relation to Noise Generation," Second Interagency Symposium on University Research in Transportation Noise, Vol. II (1974) pp. 723-729.
4. Bendat, J. S., and Piersol A. G., Random Data: Analysis and Measurement Techniques, Wiley-Interscience, New York (1971) p. 32.
5. Strahle, W. C. and Shivashankara, B. N., "A Rational Correlation of Combustion Noise Results from Open Turbulent Flames," Fifteenth Symposium (International) on Combustion, The Combustion Institute, Pittsburgh (1975) pp. 1379-1388.
6. Chiu, H. H. and Summerfield, M., "Theory of Combustion Noise," Acta Astronautics, 1, 967-984 (1974).
7. Wahbah, M. M. and Strahle, W. C., "A New Method for Solving Problems of Sound Radiation for the Case of Low Mach Number," AIAA Paper No. 76-582 (1976).
8. Janardan, B. A., Daniel, B. R. and Zinn, B. T., "Characteristics of Response Factors of Coaxial Gaseous Rocket Injectors," NASA CR-134 788 (1975).
9. Levine, H. and Schwinger, J., "On the Radiation of Sound from an Unflanged Circular Pipe," Physical Review, 37, 383-406 (1948).
10. Strahle, W. C. and Shivashankara, B. N., "Combustion Generated Noise in Gas Turbine Combustors," Engineering for Power, 98, 242-246 (1976)
11. Cumpsty, N. A., "Excess Noise from Gas Turbine Exhausts," ASME Paper 75-6T-61 (1975).
12. Pickett, G. F., "Core Engine Noise due to Temperature Fluctuations Convecting through Turbine Blade Rows," Aeroacoustics: Jet Noise, Combustion and Core Engine Noise (Schwartz,ed.), AIAA, New York (1976) pp. 589-608.

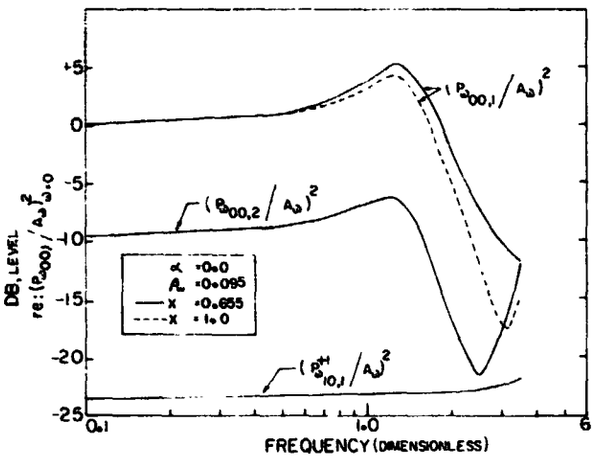


Figure 1. Relative magnitudes of various mode strengths at various combustor positions for a given combustion noise source strength.

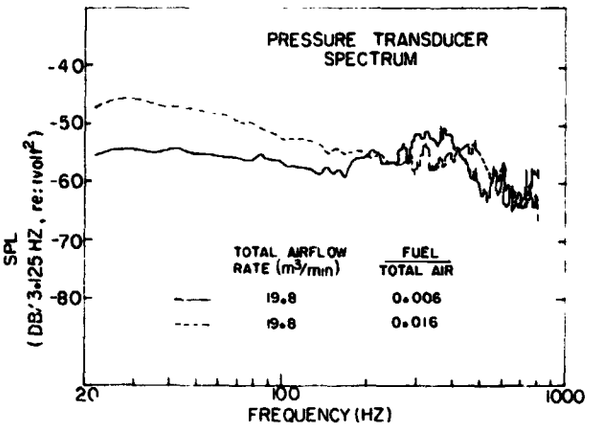


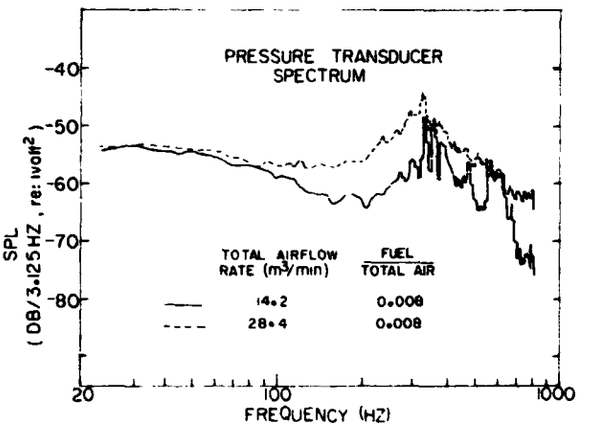


Figure 3. Interior microphone spectra as functions of airflow rate and fuel/total air. The fraction of air bypassed is approximately 26%.

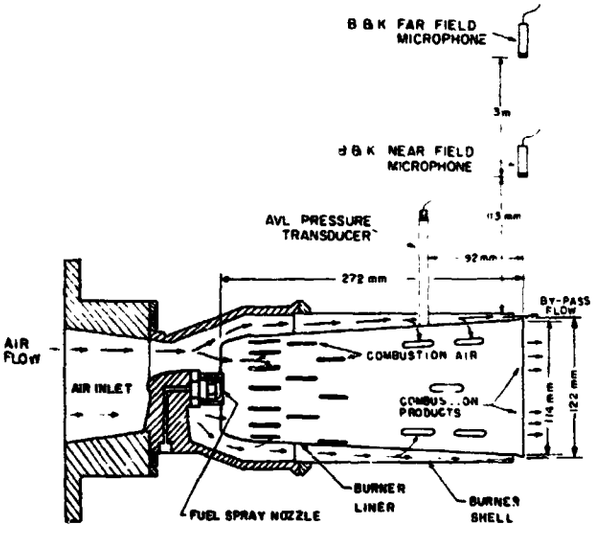


Figure 2. Schematic of experimental setup.

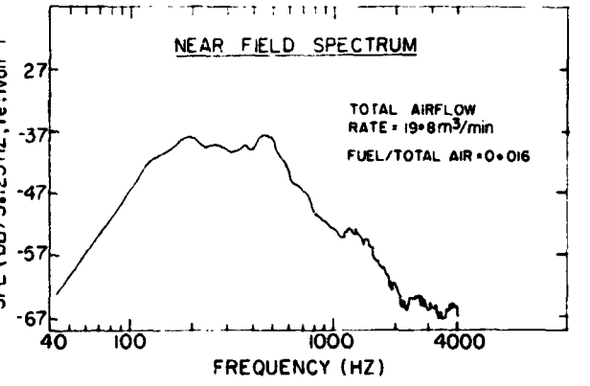


Figure 4. Typical near field microphone spectrum.

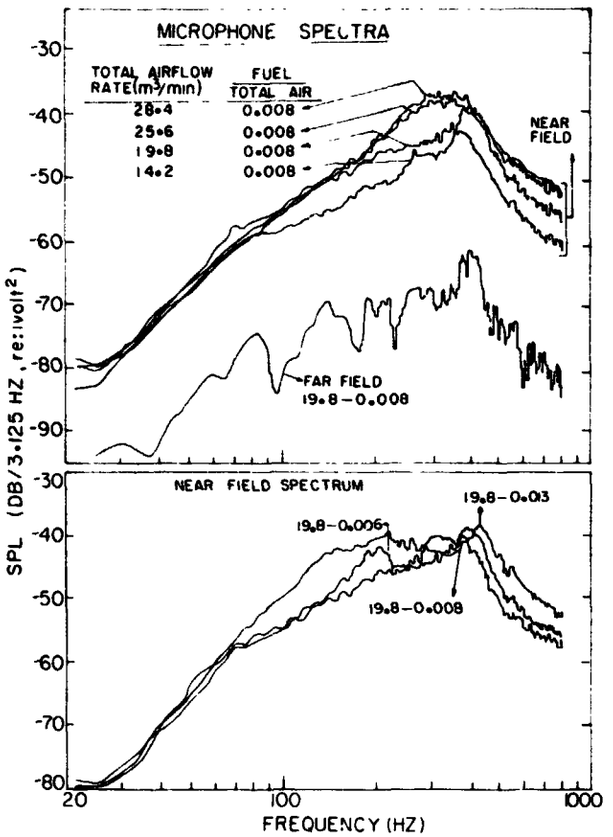


Figure 5. Near field spectra as a function of airflow and fuel/total air. Also shown is a typical far field spectrum.

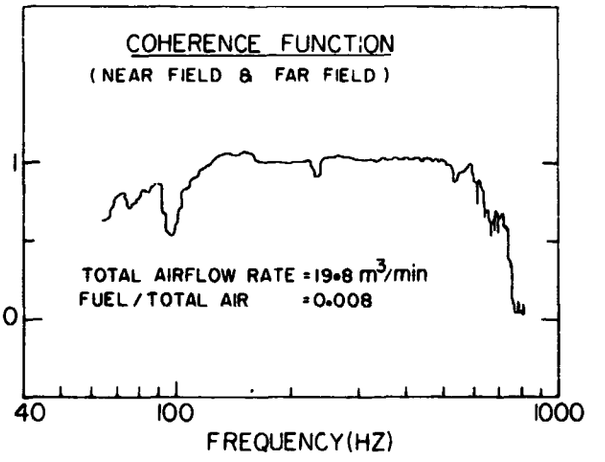


Figure 6. Coherence between the near and far field microphones.

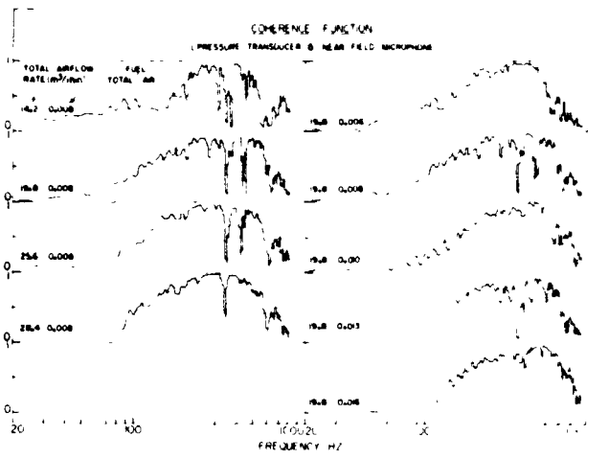


Figure 7. Coherence between the interior and exterior microphones for several run conditions.

## Appendix C

## Theory of Combustor Noise

### Formulation and Solution

The theory of Appendix B is used as the starting point here. The differential equations are based upon the linearized vorticity - acoustic field equations.[B1] Equation (11) of Appendix B is the acoustic equation to be solved, which is here reproduced as

$$\nabla^2 p_\omega + \omega^2 p_\omega = - f_\omega \qquad (C1)$$

where the nomenclature is defined in Appendix B. Equation (C1) is an acoustic field equation, independent of the turbulent, vortical part of the flow (by assumption), except as the two fields may interact at boundaries. Equation (C1) was derived on the basis of a low Mach number flow.

In Eq. (C1) the acoustic pressure is driven by fluctuations in the heat release throughout the combustor, represented by $f_\omega$. The boundary conditions applied to Eq. (C1) in Appendix B are given as Eqs. (14) in that appendix. The boundary condition at the combustor exit plane (x=1), however, was not the most general boundary condition, and here such a condition will be introduced. Since it was found in Appendix B that only the plane wave mode was important at the experimental frequencies of interest, only the plane wave mode will be treated here.

The most general boundary condition at the exit plane for the plane wave mode involves the axial velocity, pressure and entropy fluctuations in the form[C2]

$$u_{\omega_e} = \beta_e \frac{p_{\omega_e}}{\gamma} + \alpha \hat{\sigma}_{\omega_e} \qquad (C2)$$

where $\alpha$ is the entropy admittance coefficient, and the dimensionless entropy fluctuation is defined by $\sigma' \equiv \frac{\tilde{s}'}{\tilde{c}_p}$

and is equal to

$$\sigma' = \frac{1}{\gamma} \frac{p'}{\bar{p}} - \frac{\rho'}{\bar{\rho}}$$

for perfect gases. The oscillations of Eq. (C1) are isentropic ($\sigma' = 0$) and the primary source of $\sigma'$ is in temperature fluctuations produced by unequal heating of different fluid elements as they travel down the combustor. This is emphasized by Eq. (4) of Appendix B which may be written

$$\frac{D\sigma}{Dt} = \frac{(\gamma-1)}{\gamma} \dot{Q}$$

Both the acoustic pressure and the entropy fluctuation are consequently driven by heat release fluctuations. Moreover, they interact at the boundary through Eq. (C2). It must be emphasized, therefore, that entropy noise (noise due to $\sigma$) and direct combustion noise (noise due to f) are related, but not identical.

The superscript $\hat{}$ on $\sigma_{\omega_e}$ in Eq. (C2) is to emphasize that the plane wave mode requires a cross section average of $\sigma_\omega$; that is,

$$\hat{\sigma}_{\omega_e} \equiv \frac{1}{S} \int_S \sigma_{\omega_e} \, dS \qquad \text{(C3)}$$

Using the nondimensionalization scheme of Appendix B and the fact that $\sigma'$ is dominated by temperature fluctuations

$$\sigma_{\omega_e} = \frac{T_{\omega_e}}{\bar{T}}$$

where T is temperature. These temperature fluctuations are presumed known from some independent measurement.

The boundary conditions at the side wall and head end are the same as in Eqs. (14) of Appendix B. The solution to Eq. (C1) then follows from standard methods for an interior wall pressure measurement point <u>downstream</u> of the

combustion zone.

$$p_{\omega}(x,a,\theta) = p_{\omega_{00,1}} - \frac{i\omega\gamma\alpha}{ik_{oo}S} \frac{1+\eta_{oo}}{D_{oo}} \cos k_{oo}x \quad \hat{\sigma}_{\omega_e} \tag{C4}$$

where the nomenclature is the same as in Appendix B. The effect of the exit plane entropy fluctuation is to add a term to the solution proportional to $\alpha\hat{\sigma}_{\omega_e}$. In the case of experiments with no nozzle $\alpha = 0$; hence there is no effect of the entropy fluctuation in noise generation.

Now consider three microphone positions at $x = x_0$, $x = 1$ and at the nozzle exit plane. Denote the plane wave pressures there as $p_{\omega_0}$, $p_{\omega_1}$, and $p_{\omega_2}$. In general the true measured pressure at an interior microphone position will be contaminated with hydrodynamic noise which does not propagate to the near field, considered as the $p_{\omega_2}$ microphone if it is placed near, but outside of, the jet stream. At $x = x_0$, Eq. (C4) may be rewritten as

$$p_{\omega_o} = A_{\omega} f_1(\omega) + \hat{\sigma}_{\omega_e} f_2(\omega) + H_0(\omega) \tag{C5}$$

where H is the hydrodynamic noise, $f_1$ and $f_2$ are frequency dependent transfer functions and $A_{\omega}$ is the transform of the weighted heat release fluctuation

$$A_{\omega} = \int_V f_{\omega} \cos k_{00} x \, dV$$

At the nozzle entrance plane, the acoustic pressure will also be computed from Eq. (C4) with an additional hydrodynamic noise contribution

$$p_{\omega_1} = A_{\omega} f_3(\omega) + \hat{\sigma}_{\omega_e} f_4(\omega) + H_1(\omega) \tag{C6}$$

Finally, there are the acoustic transmission generation and reflection processes due to the presence of a nozzle at the exit plane. It will be assumed that the nozzle is sufficiently short (compared with a wavelength or length of an entropy pulse) that quasi-steady short nozzle theory may be

used.[C2] In such a case the two conditions are a) conservation of mass and b) conservation of stagnation energy. For the acoustic part of $p_{\omega_{1_a}}$, which excludes $H_1$, these conditions yield

$$\frac{p_{\omega_{1_a}}}{\gamma \bar{p}_1}\left(1 + \frac{\beta_1}{M_1}\right) - \frac{p_{\omega_2}}{\gamma \bar{p}_2}\left(1 + \frac{\beta_2}{M_2}\right) = -\frac{\alpha \hat{\sigma}_{\omega_e}}{M_1}$$

$$\frac{p_{\omega_{1_a}}}{\gamma \bar{p}_1}(1 + M_1 \beta_1) - \frac{z_1}{z_2}\frac{p_{\omega_2}}{\gamma \bar{p}_2}(1 + \beta_2 M_2) = \left[\frac{M_1^2 - M_2^2}{2z_2} - \alpha M_1\right]\hat{\sigma}_{\omega_e} \tag{C7}$$

with $z = 1 + \frac{\gamma - 1}{2} M^2$, and isentropic oscillations have been assumed. Since in the absence of entropy fluctuations Eqs. (C7) may be expected to have a solution, the determinant of the solution matrix must be zero, yielding

$$\beta_1 = \frac{(1 - z_1/z_2) + \beta_2 (1/M_2 - z_1 M_2/z_2)}{\frac{z_1}{z_2}\frac{(1 + M_2\beta_2)}{M_1} - M_1(1 + \beta_2/M_2)} \tag{C8}$$

Moreover, Eqs. (C7) must yield a solution with $\hat{\sigma}_{\omega_e}$ finite. Consequently,

$$\alpha = \frac{(M_2^2 - M_1^2)(1 + \beta_2/M_2)}{2 z_2\left[\frac{z_1}{z_2}\frac{(1 + M_2 \beta_2)}{M_1} - (1 + \beta_2/M_2) M_1\right]} \tag{C9}$$

Equation (C9) emphasizes the previously mentioned fact that as $M_2 \to M_1$, $\alpha \to 0$.

The only item left to close the solution is $\beta_2$. Reference (C3) shows that at low values of $M_2$ the fact that there is a temperature mismatch between the combustor jet flow and the surroundings does not greatly alter $\beta_2$ over its Levine-Schwinger value.[C4] Using the low frequency limiting form,

$$\beta_{2_{LS}} = \frac{1}{\omega a_2 [0.6i + 0.25 \omega a_2]} \tag{C10}$$

where $a_2$ is the radius of the nozzle outlet. On the other hand, near $M_2 = 1$, the choking condition yields $\beta_2 = (\gamma-1)/2$. For the approximate calculations here a linear relation is used for Mach numbers between 0 and 1; that is,

$$\beta_2 = \beta_{2_{LS}} (1 - M_2) + M_2 (\gamma - 1)/2 \tag{C11}$$

The first of Eqs. (C7) and Eq. (C6) may then be written as

$$p_{\omega_2} = \left[ p_{\omega_{1_a}} + \frac{\alpha\gamma\hat{\sigma}_{\omega_e}}{M_1 (1+\beta_2/M_2)} \right] (z_1/z_2)^{\frac{\gamma-1}{\gamma}}$$

$$= \left\{ A_\omega f_3 + \hat{\sigma}_{\omega_e} \left[ \frac{\alpha\gamma}{M_1(1+\beta_2/M_2)} + f_4 \right] \right\} (z_1/z_2)^{\frac{\gamma-1}{\gamma}}$$

$$= p_{\omega_{1_a}} f_5(\omega) + \hat{\sigma}_{\omega_e} f_6 \tag{C12}$$

The experiments of Appendix B verify that the hydrodynamic noise, $H_1$ and $H_0$, is not propagational to position 2 and no hydrodynamic noise is present in the $p_2$ signal if the microphone is slightly outside of the jet flow. Combustion noise dominates the situation, at least when no nozzle is present.

Now the major fact revealed by Eqs. (C6) and (C12) is that entropy noise and combustion noise have different transmission characteristics to the $p_2$ microphone (which is also coherent with the far field microphone at the frequencies under consideration). From Eq. (C12), $p_{\omega_2}$ depends upon both $p_{\omega_1}$ and $\hat{\sigma}_{\omega_e}$, but from Eq. (C6) $p_{\omega_1}$ depends on $A_\omega$ (combustion noise) and $\hat{\sigma}_{\omega_e}$ (entropy noise). Depending upon the behavior of $f_3$, $f_4$, $f_5$, and $f_6$, which are all different, it is possible to have the following possibilities:
Position 1, $\sigma$ dominant, Position 2, $\sigma$ dominant; Position 1, $\sigma$ dominant, Position 2, $p_{\omega_1}$ dominant which means $\sigma$ is still dominant; Position 1, A dominant, Position

2,σ dominant, which means that combustion noise dominates the combustor interior while entropy noise is the strongest exterior noise; Position 1, A dominant, Position 2, $p_{\omega_1}$ dominant which means that combustion noise dominates the exterior noise.

The distinction between an entropy noise and a combustion noise dominated case becomes a bit unclear when one recalls that they are both fundamentally linked to the heat release fluctuations. For the moment, however, consider that $A_\omega$ and $\hat{\sigma}_{\omega_e}$ are statistically uncorrelated, and this point will be returned to in a later appendix.

Calculations

Assuming statistical independence of $A_\omega$, $\hat{\sigma}_{\omega_e}$ and H, the ensemble average, one sided spectral densities of the measured pressures may be constructed from the Fourier transforms in Eqs. (C5, C6 and C12). Denoting a one sided spectral density by G with a subscript for the quantity under consideration, there results

$$G_{p_0} = G_A f_1^2 + G_S f_2^2 + G_{H_0}$$

$$G_{p_1} = G_A f_3^2 + G_S f_4^2 + G_{H_1}$$

$$G_{p_2} = G_{(p_1 - H_1)} f_5^2 + G_S f_6^2 \qquad \text{(C13)}$$

The spectral densities are dimensionless by construction when $\tilde{\bar{p}}_1$ is the pressure used for nondimensionalizing and the time unit is $\tilde{\ell} / \tilde{\bar{c}}_1$. In the calculations all numbers have been plotted as a spectrum dimensionless in pressure units but on a per Hertz basis.

Consider first the case with no nozzle. Sample calculations have been made for the 19.8 $m^3$/min air flow case at an overall fuel/air ratio of 0.016; Figure

7 of Appendix B shows the coherence between the interior and exterior microphones for this run. In the experiments the position of the interior microphone is at $x = x_0 = 0.655$. For this case $M_1 = M_2 = 0.1$ and $\sigma = 0$, so only $G_A$ and $G_H$ enter the picture. A spectral peak corresponding to the first quarter wave resonance occurs at 450 Hz for this case and experimentally there is nearly perfect coherence between $p_0$ and $p_2$. Moreover, independent experiments have shown that $p_2$ senses no hydrodynamic noise at its location out of the jet flow. Consequently, at 450 Hz both $p_0$ and $p_2$ are sensing combustion noise almost completely. The experimental spectrum for $p_0$ is shown in Fig. C1a. A value of $\beta_\omega$ is chosen so that the theoretical spectrum ($f_1^2$) best osculates the spectral peak of $G_{p_0}$; this value is 0.06 which indicates a hard, but not too hard, behavior of the liner walls. This determines $G_A$ at the 450 Hz point. Since the physical location of the $p_2$ microphone is not precisely at the exit plane, a calibration factor to multiply the experimental $G_{p_2}$ is obtained knowing $G_A$ at 450 Hz and

$$G_{p_2} = G_A f_3^2 = G_A f_5^2$$

The calibration factor is then applied to the measured $p_2$ spectrum and the corrected spectrum represents the $p_2$ spectrum which would have been measured at the exit plane. This is shown in Fig. C1a. Since $G_{p_2}$ senses only combustion noise, $G_A$ may be calculated by $G_A = G_{p_2}/f_3^2$ as a function of frequency; this is shown on Fig. C1a. Knowing $G_A$, one can calculate $G_{H_0}$ from $G_{H_0} = G_{p_0} - G_A f_1^2$. This is shown in Fig. C1a and is the derived hydrodynamic noise. This subtraction process becomes highly sensitive to small experimental errors when $G_H$ falls more than 5-6 dB below $G_{p_0}$; if this happens $G_{H_0}$ is arbitrarily set to zero. One sees that the interior microphone is dominated by hydrodynamic noise at frequencies less than, say 150 Hz.

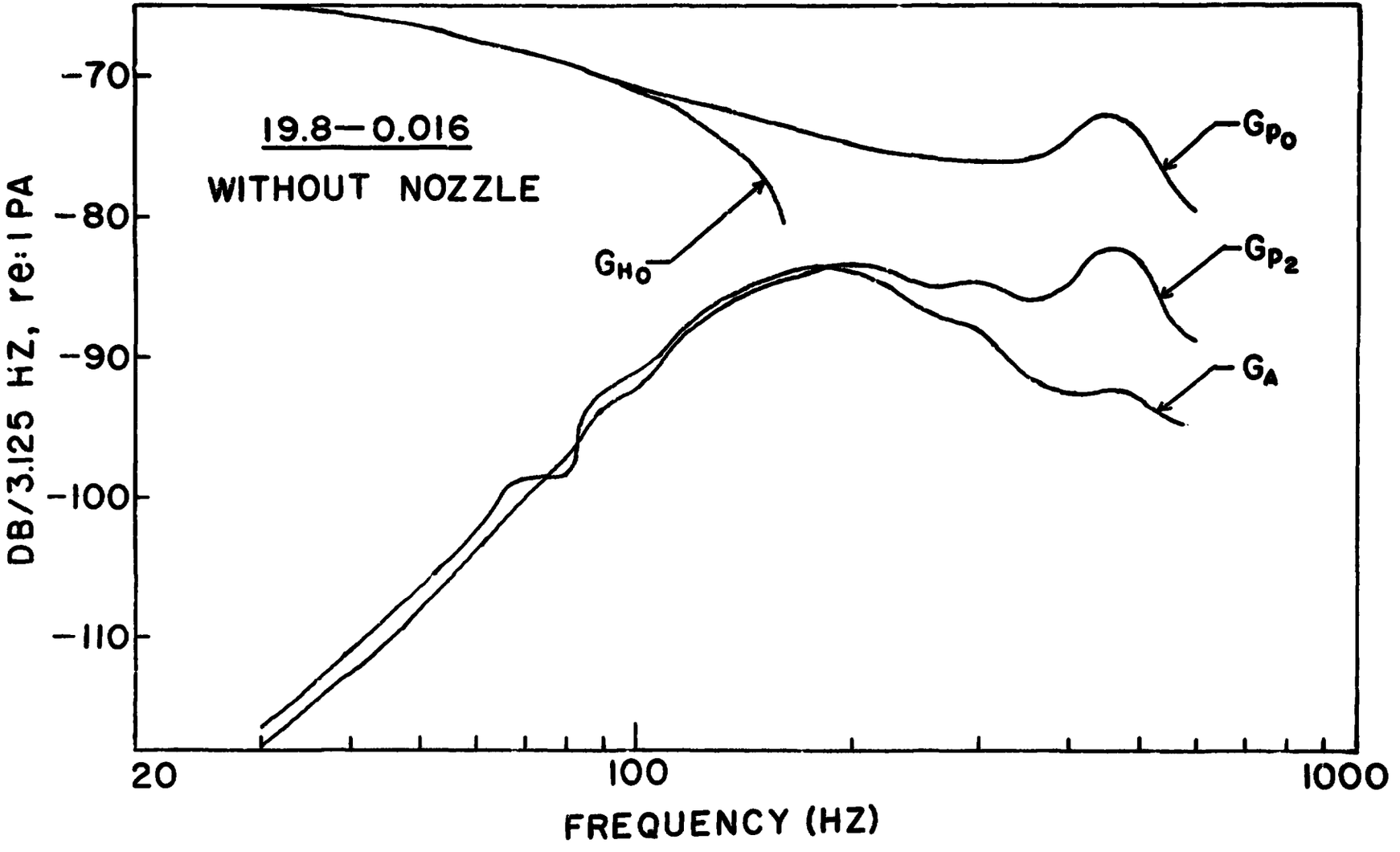


Figure C1a. No-nozzle case spectra for the interior microphone, derived heat release fluctuation, near field microphone and derived hydrodynamic noise.

As a check on this procedure, which assumes only two noise sources present at the interior microphone and one source at the exterior microphone, the coherence function between the $p_0$ and $p_2$ microphones may be computed.(C5) This is

$$\gamma^2 = \frac{1}{1 + \frac{G_{H_0}}{G_A f_1^2}}$$

It is computed and compared with experiment in Fig. C1b and the agreement is very good. The computed function is higher than the experimental function everywhere, which it should be because in reality there is some electronic noise and a low level jet noise which contaminates the two signals.

Guided by this successful separation of combustion and hydrodynamic noise, it now remains to calculate the effects of entropy noise. For this, independent measurements are required for $\hat{\sigma}_{\omega_e}$. These are described in Appendix D. For these calculations $G_S$ is known from those experiments. It is assumed in the calculation that $G_{H_0}$ remains the same with the nozzle on or off. Calculations are made for two cases, one with a contraction ratio of 3:1, which at the same mass flow and fuel/air ratio yields $M_1 = 0.1$, $M_2 = 0.33$, and one for a contraction ratio yielding $M_2 = 1.0$. It is moreover assumed that $G_A$ is unchanged with a nozzle on (since the pressure is only varied over a factor of two in the combustor, this is not expected to yield a large error).

Shown in Fig. C2a are the components of the calculated $G_{p_0}$, where $G_{H_0}$ has been omitted for clarity (see Fig. C1a), for the "short nozzle" case (low contraction ratio). It is seen that the entropy noise contribution to the signal is small, so that for practical purposes the interior microphone would be dominated by combustion noise. Notice that there is a strong change in the computed spectral shape, as compared with $G_{p_0}$ in Fig. C1a. Since the calculations were only carried to 600 Hz the resonance peak, which has shifted to a higher

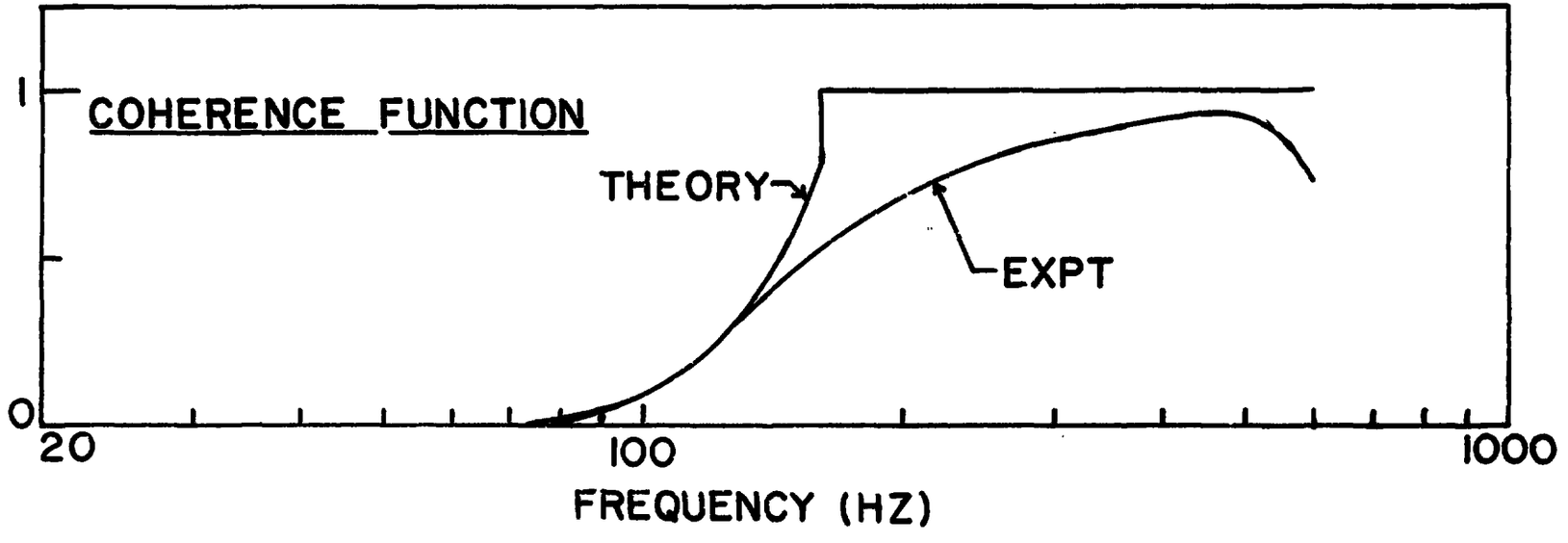


Figure C1b. Coherence between the interior and near field microphones for the no-nozzle case - theory.

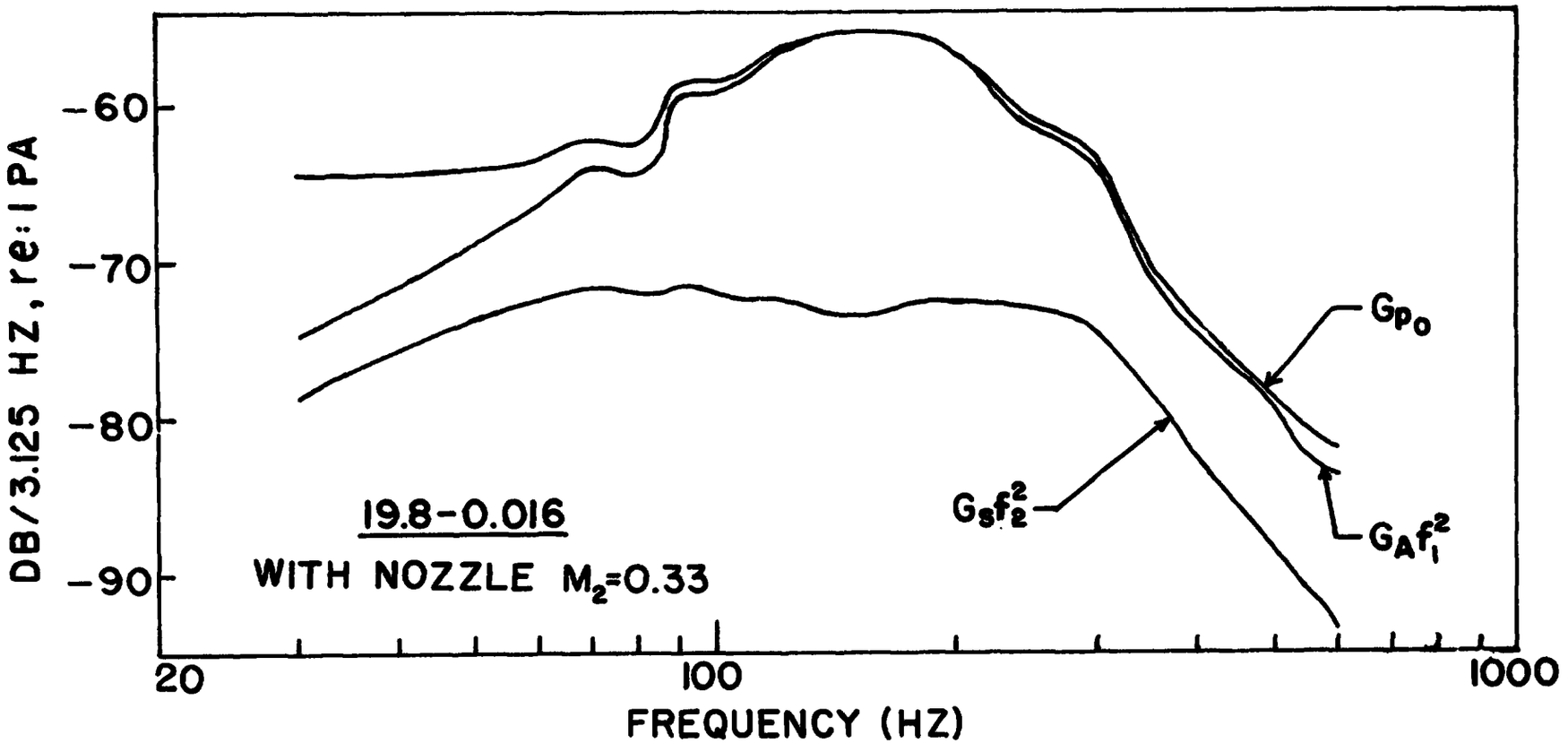


Figure C2a. Total noise at the interior microphone location and its components from combustion and entropy noise. Low contraction ratio case.

frequency in the presence of a nozzle, does not appear. Continuing, $G_{(p_1-H_1)}$ is computed and then $G_{p_2}$. The results are shown in Fig. C2b. It is evident that the entropy contribution is still negligible, but approaching the combustion noise curve at the higher frequencies.

The calculations are reported for the choked nozzle case and are shown in Figs. C3a and C3b. The results are that the interior microphone is dominated by combustion noise but the transmitted noise becomes entropy dominated above 210 Hz. Moreover, there is an elevation of the high frequency content of the noise.

Conclusion

The conclusion is therefore clear, but may be due to the particular hardware used in the experiments. At sufficiently high frequency and under choked or nearly choked conditions, entropy noise may be the dominant noise source in combustors. Under sufficiently low nozzle pressure drop combustion noise will dominate. These theoretical results are borne out by the experimental results in Appendix D. It must be cautioned that because of the many approximations used in the analysis that the results should be viewed in a qualitative sense only. Moreover, the assumption in the calculations that $G_A$ and $G_S$ are independent is not strictly true, as will be seen in Appendix E.

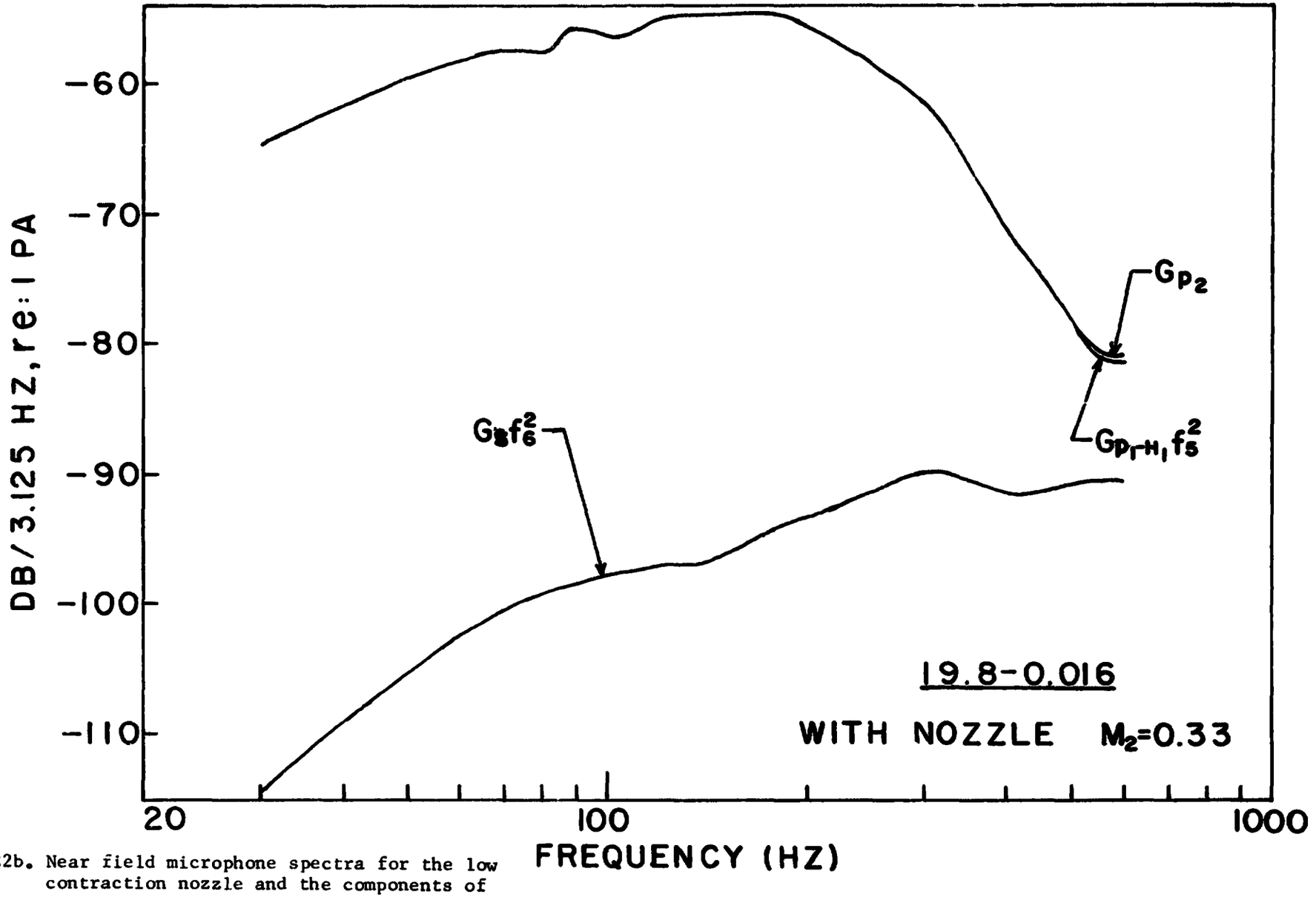


Figure C2b. Near field microphone spectra for the low contraction nozzle and the components of this noise from the interior microphone and entropy noise.

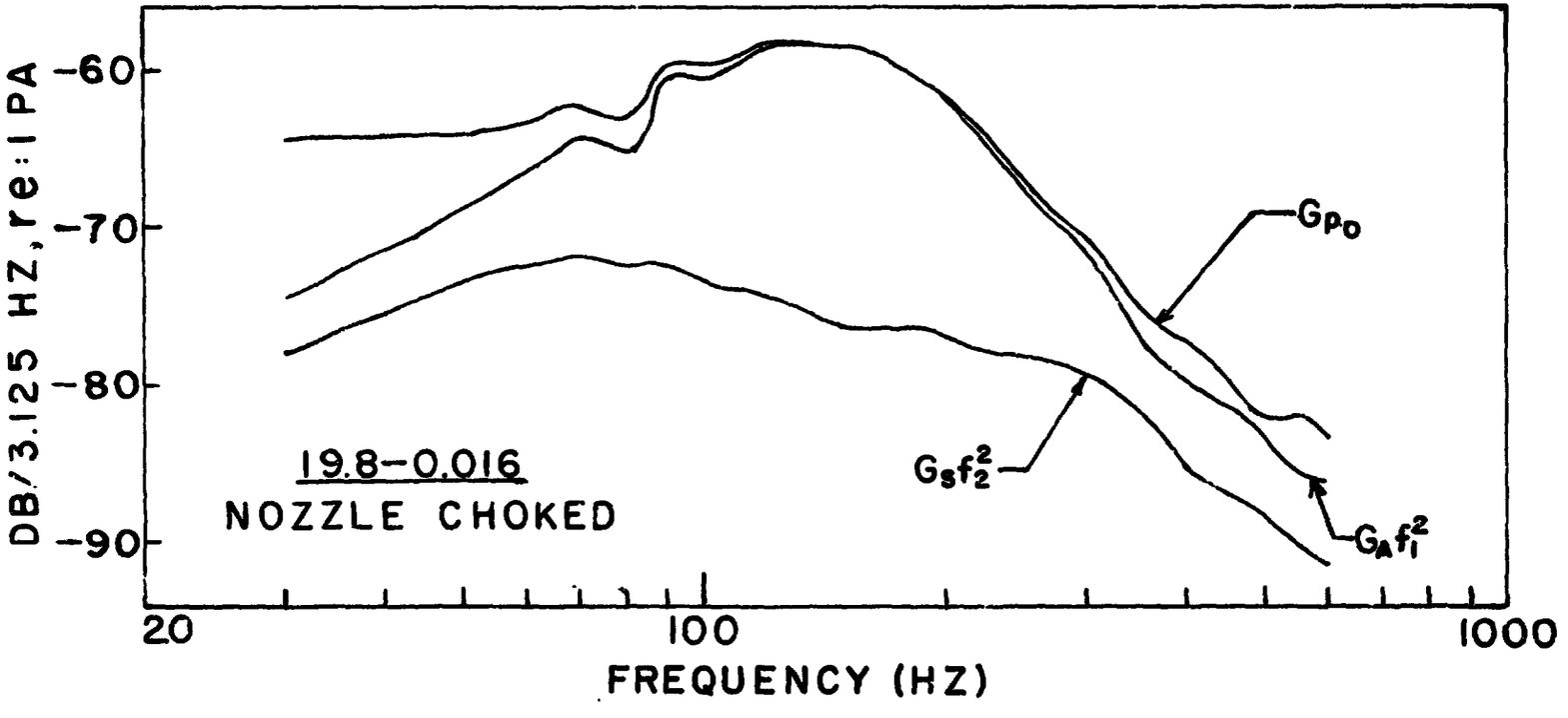


Figure C3a. Choked nozzle interior microphone spectra and the combustion and entropy noise components.

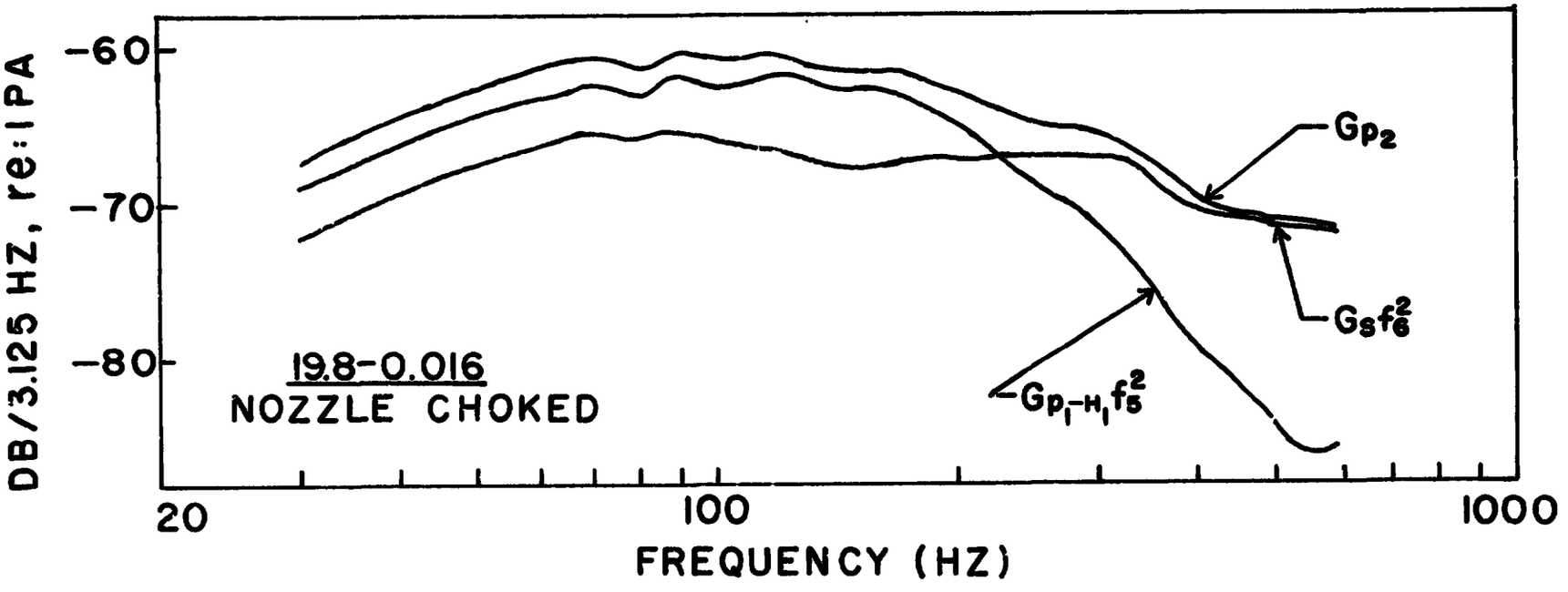


Figure C3b. Choked nozzle near field microphone spectra and the interior microphone and entropy noise components.

## References


C1. Goldstein, M. E., Aeroacoustics, Chapt. 5, McGraw-Hill, New York (1976).

C2. Crocco, L. and Sirignano, W. A., "Behavior of Supercritical Nozzles under Three Dimensional Oscillatory Conditions," AGARDograph No. 117, NATO, 1967.

C3. Wahbah, M. M. and Strahle, W. C., "Sound Radiation from Ducts for the Case of Low Mach Number," AIAA Journal, 15, 553-560 (1977)

C4. Levine, H. and Schwinger, J., "On the Radiation of Sound from an Unflanged Circular Pipe," Physical Review, 37, 383-406, 1948.

C5. Bendat, J. S. and Piersol, A. G., Random Data: Analysis and Measurement Procedures, Wiley, New York (1971).

## Appendix D

## Entropy Noise

### General

This section deals with combustion and entropy noise radiation characteristics and the experimental procedures for separating them. Combustion noise radiation characteristics and the ways of separating them from the hydrodynamic noise have been explained in detail in Appendix B. Entropy noise is generated in turbopropulsion systems when combustion generated hot spots are accelerated through a region of mean pressure gradient. In the present program, such a pressure gradient is imposed on the hot gases by attaching to the burner exit a convergent nozzle of area reduction 3:1 or an orfice plate with 9 holes of 14 mm diameter each and having an effective area reduction of 10.5:1. An exit Mach number, $M_2 = 0.20$, is obtained with the above nozzle whereas at high Mach numbers, $M_2 = 0.6$, 0.8 and 1.0, the jet is exhausted through a multi-hole orfice plate, rather than a single opening nozzle, to keep the jet noise interference low.

### Experimental Apparatus

The facility used for the present investigation is the same as that described in Appendix B. The experimental set-up with the relative locations of the transducers is shown in Fig. D1. The pressure fluctuations inside the combustor and the near field and the far field radiated sound pressures have been measured through a photocon pressure transducer and Brüel and Kjaer type 4134, 12 mm condenser microphones. The reason for including a near field microphone in the measurement scheme is twofold. At higher exit Mach numbers, the jet noise is expected to contaminate the exterior radiated core noise signals. In that case, the near field microphone by virtue of its location, will receive more contribution from core noise radiation with a lesser degree of contamination from a small local area of the jet. However, the far field microphone signal may be

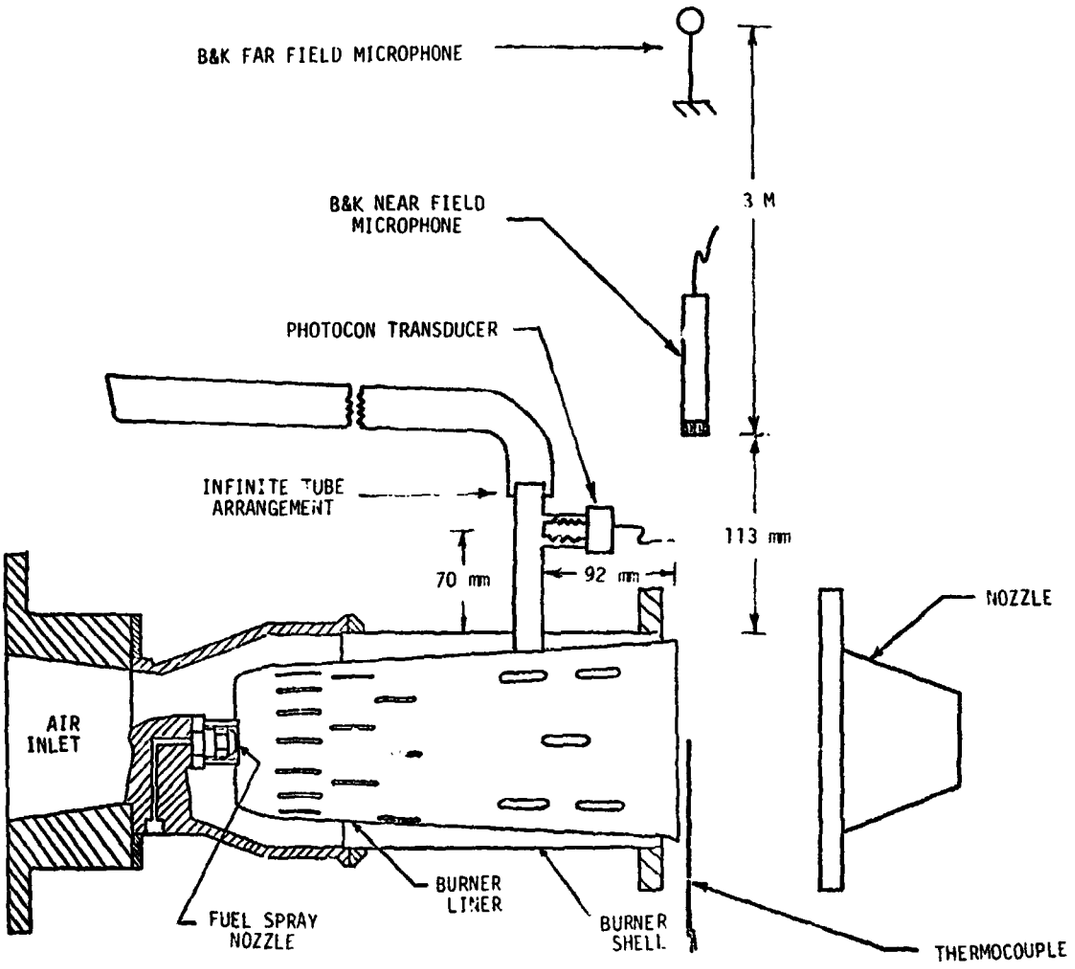


Figure D1. Schematic of experimental set-up.

dominated by jet noise as it sees the whole jet. This means that the near field signal, rather than the far field one, can be used with more confidence to represent the exterior radiated core engine noise. The second reason is that the far field microphone spectrum is masked by severe ground reflection effects, as shown earlier in Fig. 5 of Appendix B, whereas the near field microphone, by virtue of its close location to the burner exit, is free from these effects. Since the entropy noise study requires the details of the combustion generated hot spots, a measurement program has been carried out to obtain the temperature fluctuation characteristics. Fast response chromel-alumel thermocouples of wire diameter 0.025 mm are used to record the temperature fluctuations at the burner exit plane as shown in Fig. D1. The time constants of the thermocouples are determined as explained in Appendix F, and the thermocouple signals are compensated for these time constants later during data analysis by suitable modification of the Fourier Analyser programming. All the signals, after amplification, are recorded on an Ampex FR 1300, 14 channel magnetic tape recorder at a tape speed of 30 ips. The recorded signals are then subjected to spectral analysis and coherence function estimates through a HP 5451A Fourier Analyser system.

Results

Spectral Characteristics: An exit Mach number, $M_2$=0.05, represents the burner can operating without a nozzle while $M_2$=0.20 belongs to the convergent nozzle case and $M_2$=0.6, 0.8 and 1.0 come through the use of the orifice plate. The airflow rates vary between 7.0 and 19.8 $m^3$/min.,with the overall fuel/air ratio maintained constant at 0.016 for all cases. Out of a wide range of test runs, only the above conditions are selected for the purpose of comparison of the results. Fig. D2 shows the spectra of the interior pressure fluctuations. The upper frequency limit is chosen as 2000Hz because the information of interest falls below this limit. Figure D2a illustrates the spectral changes with the increasing pressure drop across the combustor as the exit termination is changed for a fixed airflow rate and fuel/air ratio, whereas

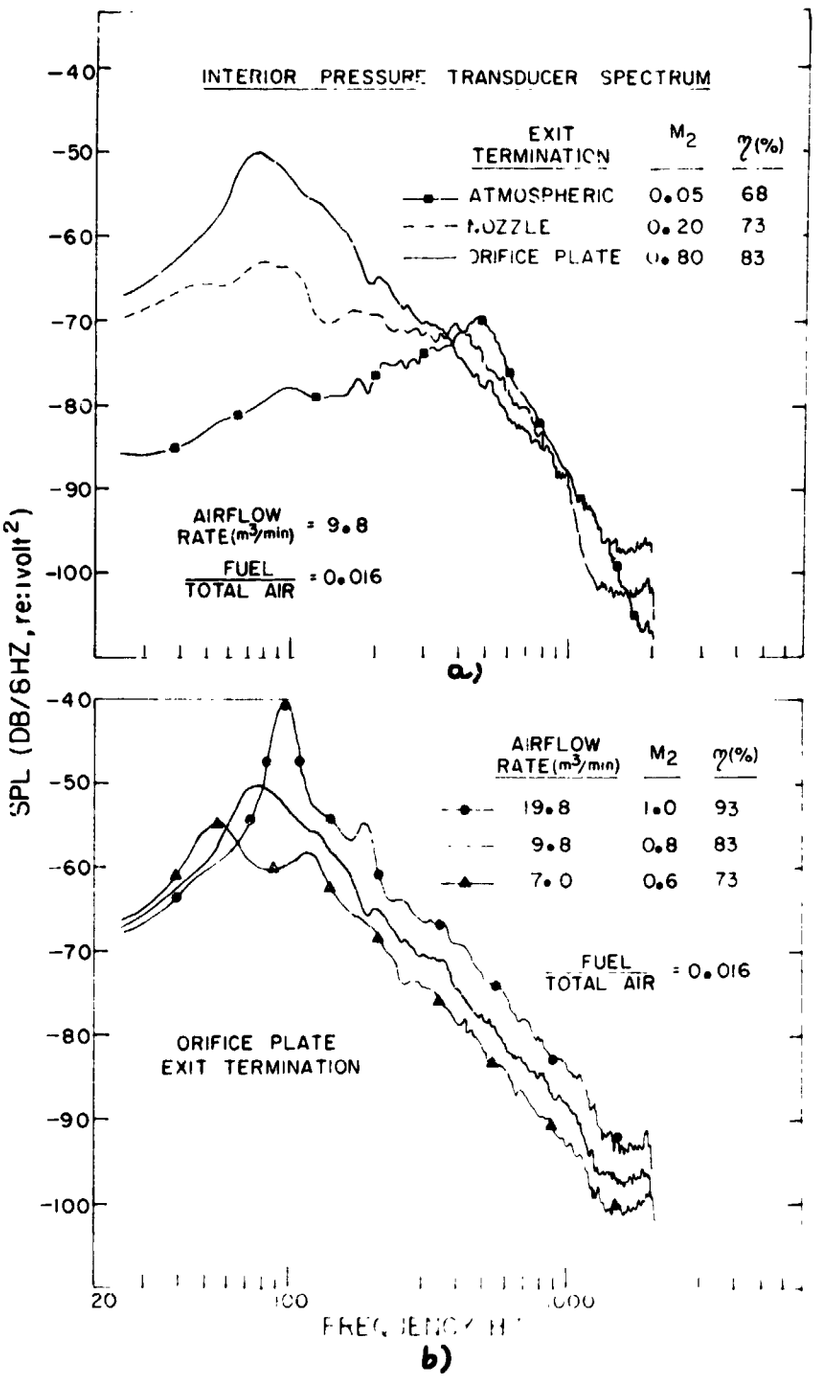


Figure D2. Interior photocon spectra as a function of airflow rate and fuel/total air.

Figure D2b shows the spectral behavior with the increasing pressure drop across the orifice plate for varying airflow rates and a fixed fuel/air ratio. It can be seen from Fig. D2a that as the exit contraction ratio is increased, the spectral level rises significantly with an increase in the exit Mach number, in the lower frequency range of 0-300 Hz. Around 300 Hz, all attain almost the same level, and then they fall off rapidly at the same rate (10 dB/octave) with increasing frequency. Another observation made here is that the interior spectrum corresponding to the exit Mach number, $M_2 = 0.05$, exhibits a quarter wave resonance peak around 500 Hz. With an increase in the exit contraction ratio corresponding to high Mach number cases, this resonance peak should shift to a higher frequency range (800-1000 Hz), tending towards a half wave resonance. On the contrary, these peaks have disappeared in the high Mach number cases. Such peaks have been seen in experiments not reported here, when using an AVL interior transducer. The occurance of a peak around 100 Hz in the case of high Mach numbers is explained at the end of this section.

Fig. D3 shows the near field spectra for the same run conditions. While at low exit Mach numbers, there is a familiar combustion noise hump, high Mach number cases exhibit no such characteristics. The near field spectra, pertaining to high Mach number cases, do not resemble the usual combustion noise spectra. The change in the spectral shapes at high Mach numbers could mean either entropy noise domination or jet noise contamination of the near field signal. To investigate the above speculation, two checks were made. First, the scaling of the near field sound power level with exit velocity was obtained. The exponent on velocity in high Mach number cases was higher than value obtained at low Mach number cases. However, the value of this exponent was far below the one corresponding to the jet noise velocity scaling law. This means that the near field microphone receives a greater contribution from core engine noise radiation although there is jet

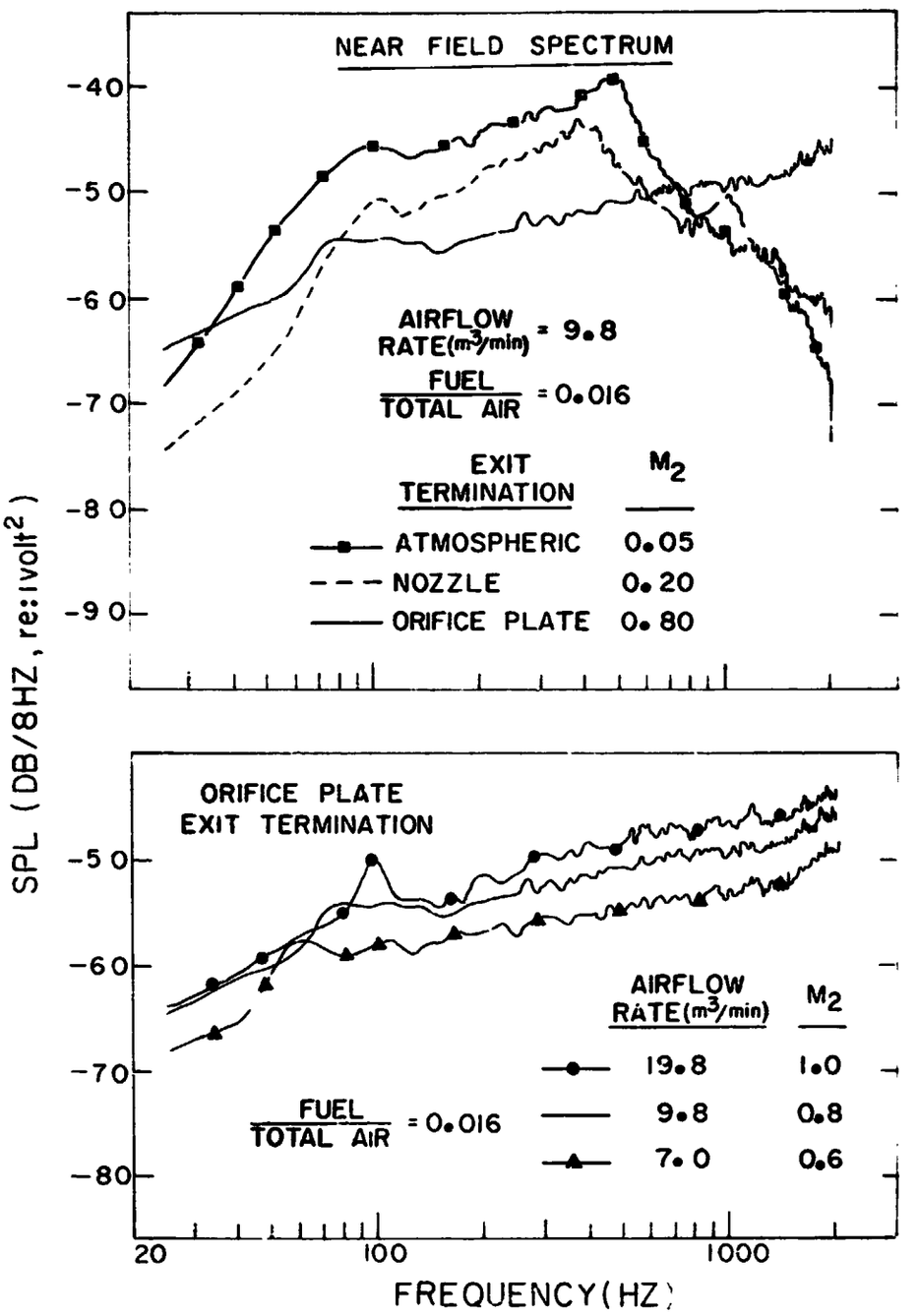


Figure D3. Near field spectra as a function of airflow rate and fuel/total air.

noise contamination to a lesser degree. Secondly, a spectral analysis of the near field signals was carried out. Fig. D4 shows a comparison of the near field spectra of the hot exhaust at $M_2 = 0.6$ with the cold flow of identical exit velocity. It can be seen that the spectrum level with the combustion on is higher than that of the exit-velocity-matched cold flow by at least 3 to 4 db in the frequency range of 150-1000 Hz. This gives some confidence that the core engine noise dominates the jet noise, at least in the frequency range of interest to the present investigation. Later in this section, it is shown through coherence function analysis that it is indeed the entropy noise that contributes significantly to the near field signal at high exit Mach numbers.

Typical spectra of the temperature fluctuations at the burner exit plane are shown in Fig. D5 The spectral shapes of the temperature fluctuations, corresponding to different exit terminations, as seen from Fig. D-5, are found to be very similar. The temperature fluctuation spectrum is a broad band one and low frequency in nature. The spectrum gradually falls off with an increase in frequency. The r.m.s. temperature fluctuations are found to vary within a range of 9 to 14% of the mean temperature for various cases.

The theoretical evaluation of entropy noise requires a knowledge of the spatial correlation length scales of the temperature fluctuations. Two thermocouples of the same size (0.025 mm wire diameter) have been used for this correlation study. One of the thermocouples monitors the temperature fluctuations at a fixed place at the burner exit plane while the other one registers the signals at various locations, moving radially away from the former. The fixed and the moving thermocouple signals have been cross-correlated and normalized to obtain the cross-correlation coefficients. The cross-correlation coefficient, as a function of the separation distance between the two thermocouples, is shown in Fig. D6 for two cases corresponding to the thermocouple traverse along two

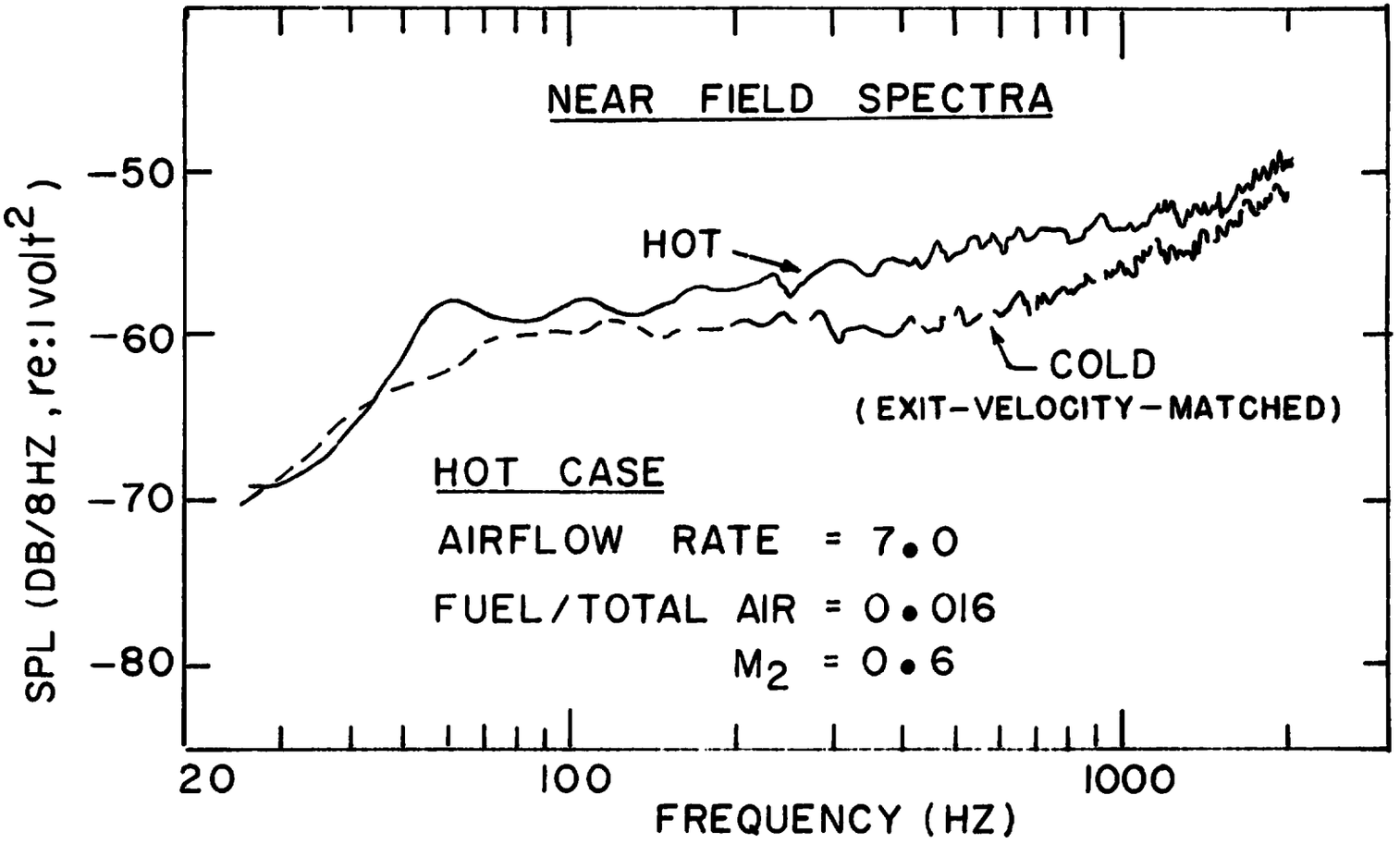


Figure D4. Comparison of hot and exit-velocity-matched cold near field spectra.

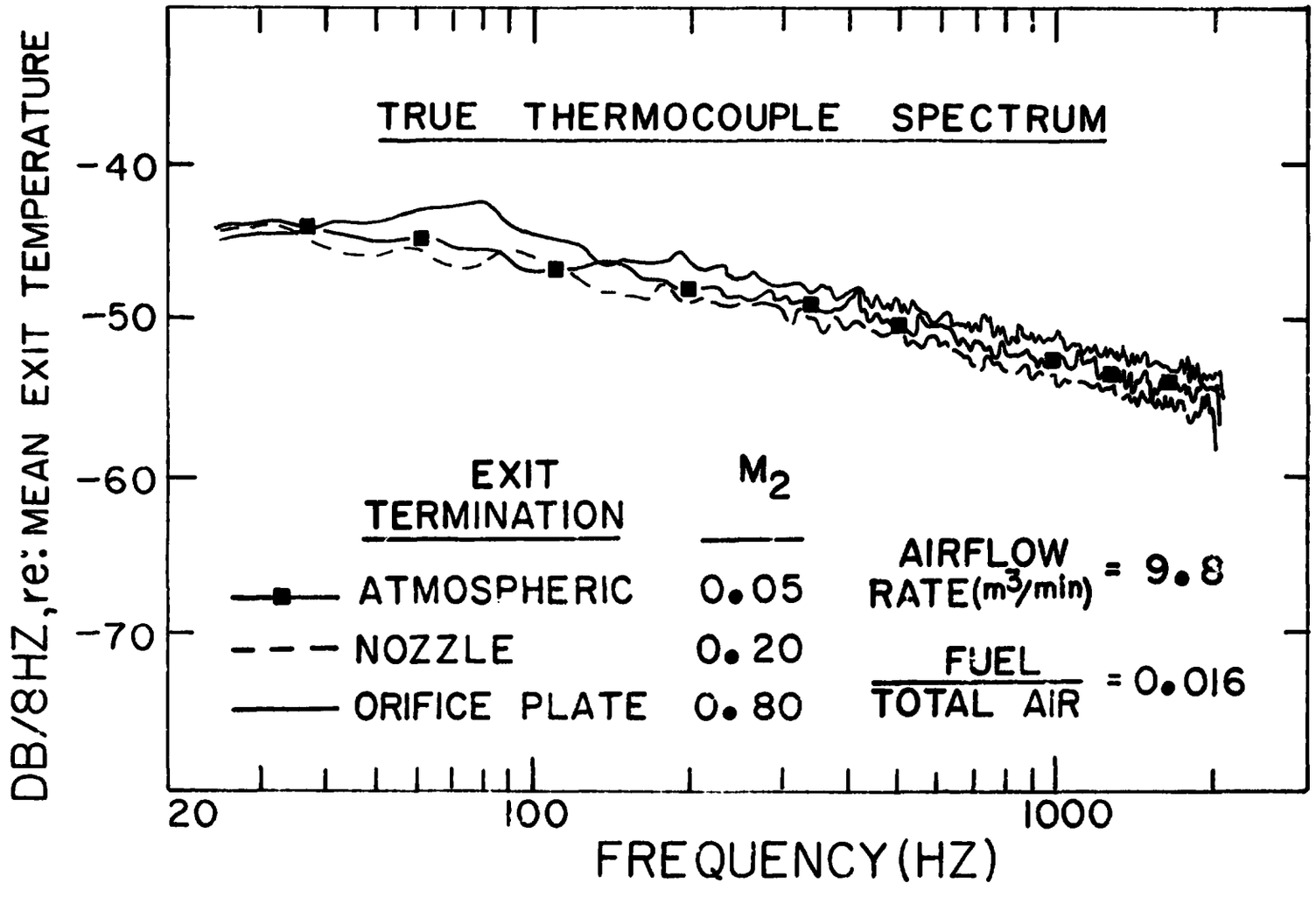


Figure D5. Temperature fluctuation spectra for a few typical operating conditions.

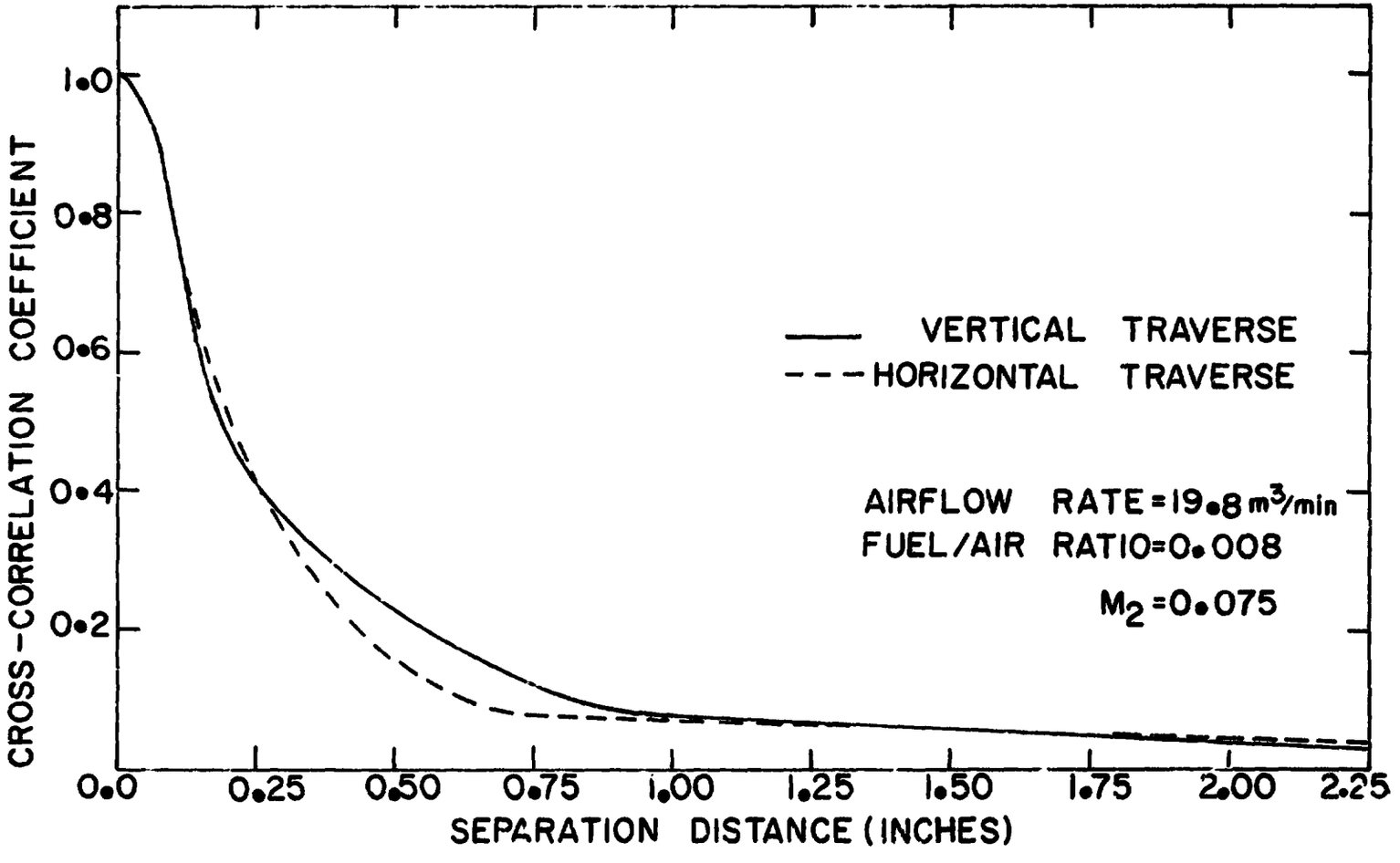


Figure D6. Cross-correlation coefficients as a function of separation distance between two thermocouples for different traverse directions.

different radial directions. In both cases, the temperature fluctuations seem to be correlated over a distance of about 12 mm at the burner exit plane, thereby suggesting a temperature eddy of about 12 mm in size. The constancy of the correlation length scales in various radial directions demonstrates the axi-symmetric nature of the thermal eddies. The similarity in the correlation analysis results for two different test conditions is brought out in Fig. D7 In all the above cases, the cross-correlation is found to be positive everywhere, with a long tail.

It is important to note that the spectral characteristics of the temperature fluctuations mentioned in the above paragraphs were obtained through single point thermocouple measurements at the burner exit plane. However, the entropy noise calculations require the quantities averaged over the burner exit area. The relationship between the single point thermocouple measurements and the area averaged quantities are established below.

Let $T'$ and $\bar{T}$ represent the fluctuating and mean temperature measured at a point at the burner exit plane by a thermocouple and a ratio $\sigma'$ be defined as

$$\sigma' = \frac{T'}{\bar{T}} = \frac{s'}{C_p} \tag{D-1}$$

where $s'$ is the fluctuating entropy component and $C_p$ is specific heat at constant pressure. However, the entropy noise evaluation requires $\hat{s}_\omega$ given by

$$\hat{s}_\omega = \frac{1}{A_e} \int_{A_e} \sigma_\omega \, dA \tag{D-2}$$

where $A_e$ is the burner exit area, and the subscript $\omega$ represents Fourier transform of the corresponding primed quantities. If the cross-correlation properties of the temperature fluctuations are invarient across $A_e$, it may be shown that

$$S_{\hat{s}\hat{s}} = \frac{A_{cor}}{A_e} S_{\sigma\sigma} \; ; \; S_{\hat{s}i} = S_{\sigma i} \; ; \gamma^2_{\hat{s}i} = \frac{A_e}{A_{cor}} \gamma^2_{\sigma i} \tag{D-3}$$

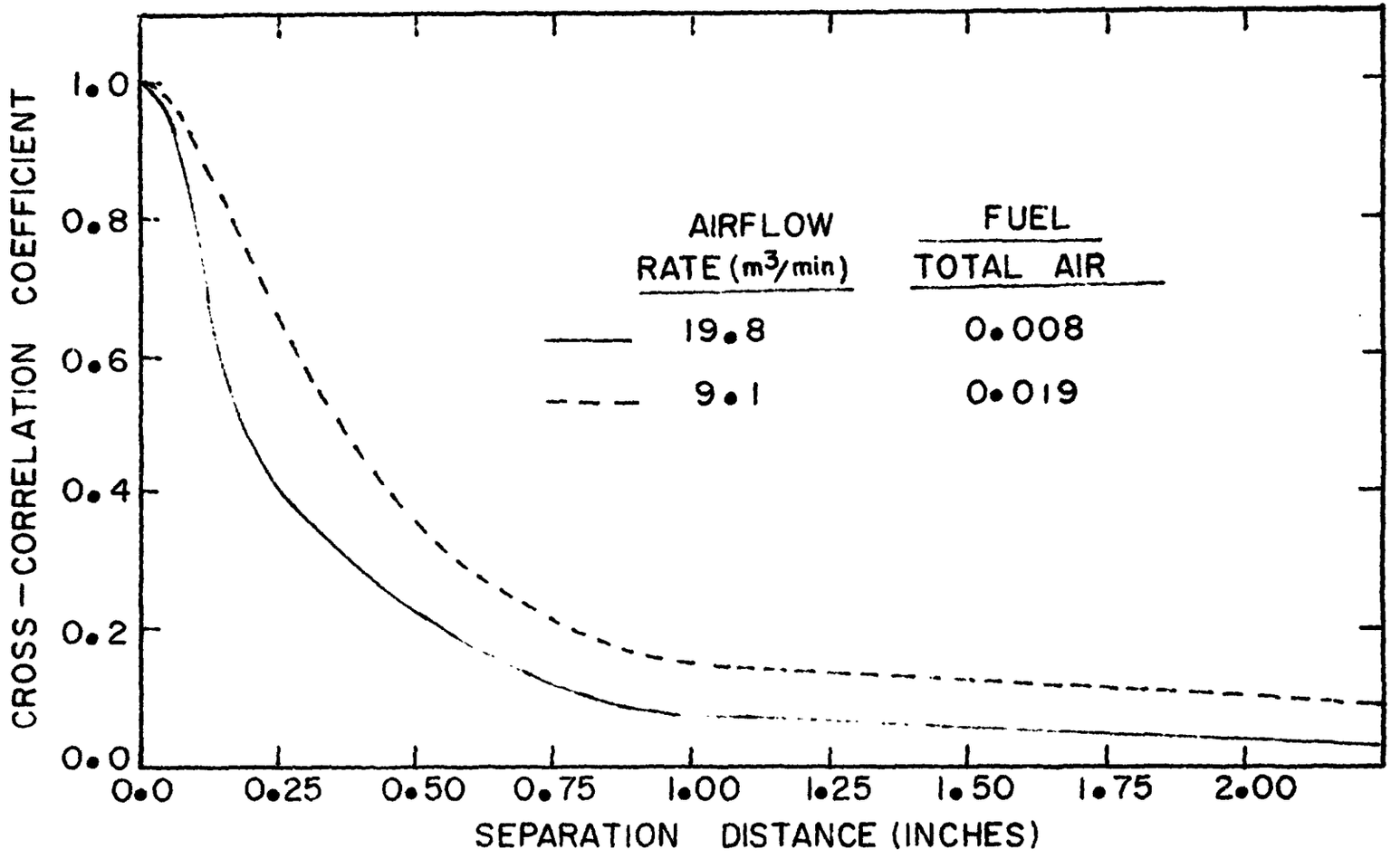


Figure D7. Cross-correlation coefficients as a function of separation distance for different operating conditions.

where S and $\gamma^2$ represent the spectral and coherence estimate, respectively, of the subscripted quantities and i stands for any dummy point on the burner exit plane. $A_{cor}$ refers to the area over which the temperature fluctuations are correlated at the burner exit plane and is given by

$$A_{cor}(\omega) = \frac{\int dA(\vec{d}) \int dA(\vec{r}) \; \sigma_\omega(\vec{r}) \, \sigma^*_\omega(\vec{r}+\vec{d})}{S_{\sigma\sigma} A_e} \qquad \text{(D-4)}$$

where $\vec{r}$ is a vector representing any point on the burner exit plane and $\vec{d}$ is a vector representing the separation distance between any two $\vec{r}$'s. It is obvious from the above expressions that the area averaged quantities can be derived from the single point thermocouple measurements, once the correlation area as a function of frequency is evaluated through Eq.(D-4). The variation of the normalized correlation area with the frequency, as obtained by a single radial thermocouple traverse, is shown in Fig. D8. For reasons to be explained later, an average correlation area is also computed. This average one is computed from three correlation areas obtained through radial as well as circumferential thermocouple cross-correlations without any end attachment and radial cross-correlations with the orifice plate attached. The airflow rate and fuel/air ratio were kept constant at 9.1 $m^3$/min. and 0.019 respectively in the above three test runs. This average temperature correlation area is also shown in Fig. D8. It can be seen from Fig. D8 that the low frequency temperature fluctuations are correlated over a larger area compared to the high frequency fluctuations as is reasonable. Since the correlation area is a measure of the eddy size, it can be said that an eddy representing the low frequency fluctuations is larger in size compared to that of a high frequency one.

Coherence Estimates. So far, the spectral characteristics of the individual signals have been discussed in detail. It will be expedient at this stage to look at the coherence between the various signals. As already mentioned in Appendix B, coherence estimates between two signals will bring out the true linear relationship between them. Coherence analysis among the interior, near and

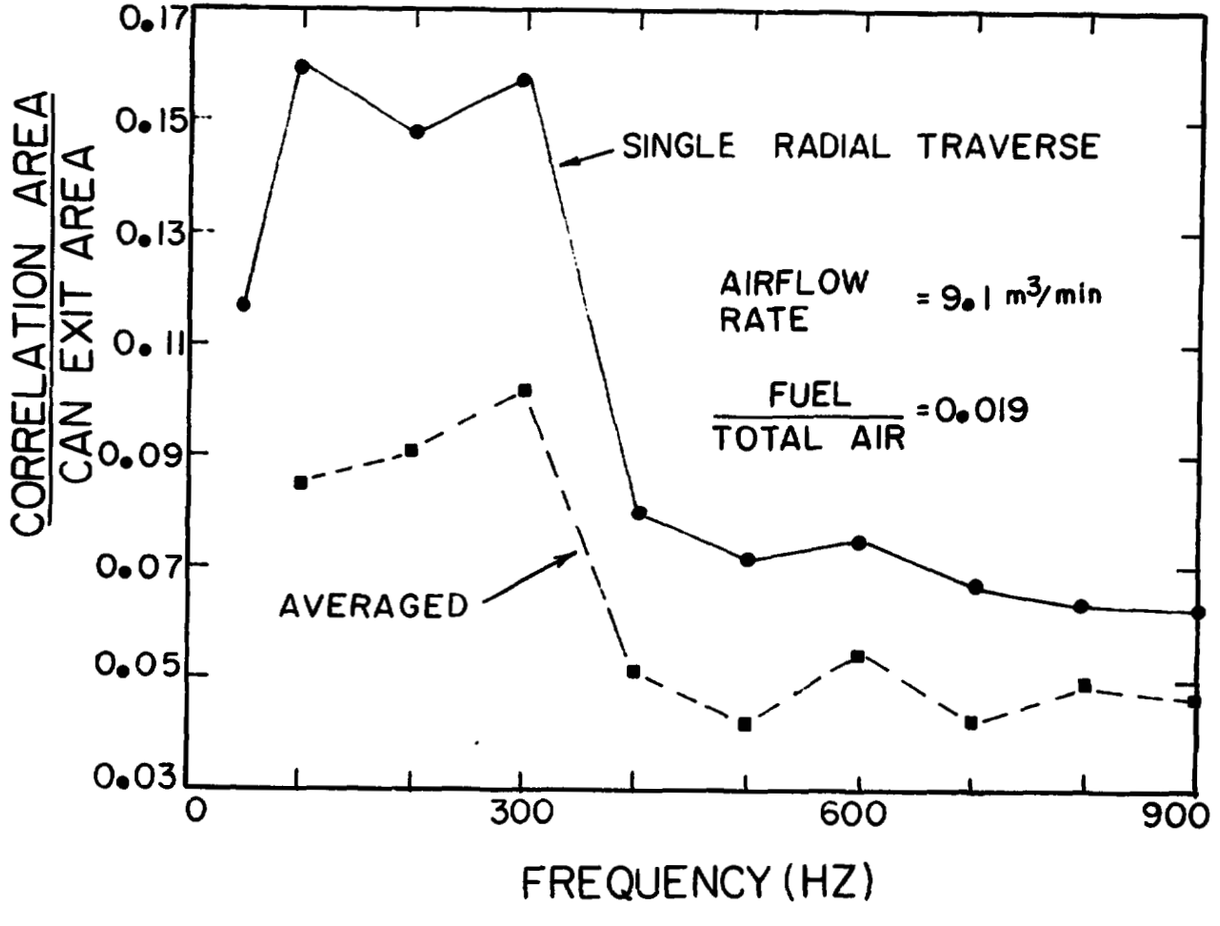


Figure D8. Frequency distribution of normalized temperature fluctuations correlation area.

far field signals is explained below. Various noise sources and their associated transmission paths are illustrated in Fig. D9. The near field signal is expected to contain contributions from the two interior sources, namely combustion and entropy noise sources as well as from the exterior jet noise. Hence, the coherence between the interior and near field signals has to be evaluated on the basis of a multiple input problem. In such cases, the degree of linear relationship between any single cause and the effect is best revealed through the partial coherence function analysis which cancels out the effects of the other extraneous inputs. The theory of partial coherence functions and the procedures for evaluating them are described in detail in Ref. D1.

The results of the coherence estimates between the interior and the near field signals are shown in Figs. D10 - D13. It is important to note that the interior sources, namely, the interior pressure transducer and the thermocouple signals, may or may not be correlated. In either case, the coherence analysis takes care of the situation except that in the uncorrelated case, the expressions become simpler. The significance of the experimental coherence results can be best explained with the help of some analytical expressions for coherence estimates based on the model shown in Fig. D9. For the purpose of explanation, a model of an uncorrelated case will be assumed because of its simpler analytical expressions, although the same conclusions can be arrived at, even in the case of correlated inputs. For the uncorrelated interior sources, the model shown in Fig. D9, yields the following expressions[D1]:

Ordinary Coherence Estimate.

Interior and near field microphones = $\gamma^2_{1y} = \dfrac{1}{1+\left(\dfrac{|H_2|^2 \bar{S}_{22} + \bar{S}_{zz}}{|H_1|^2 \bar{S}_{11}}\right)}$

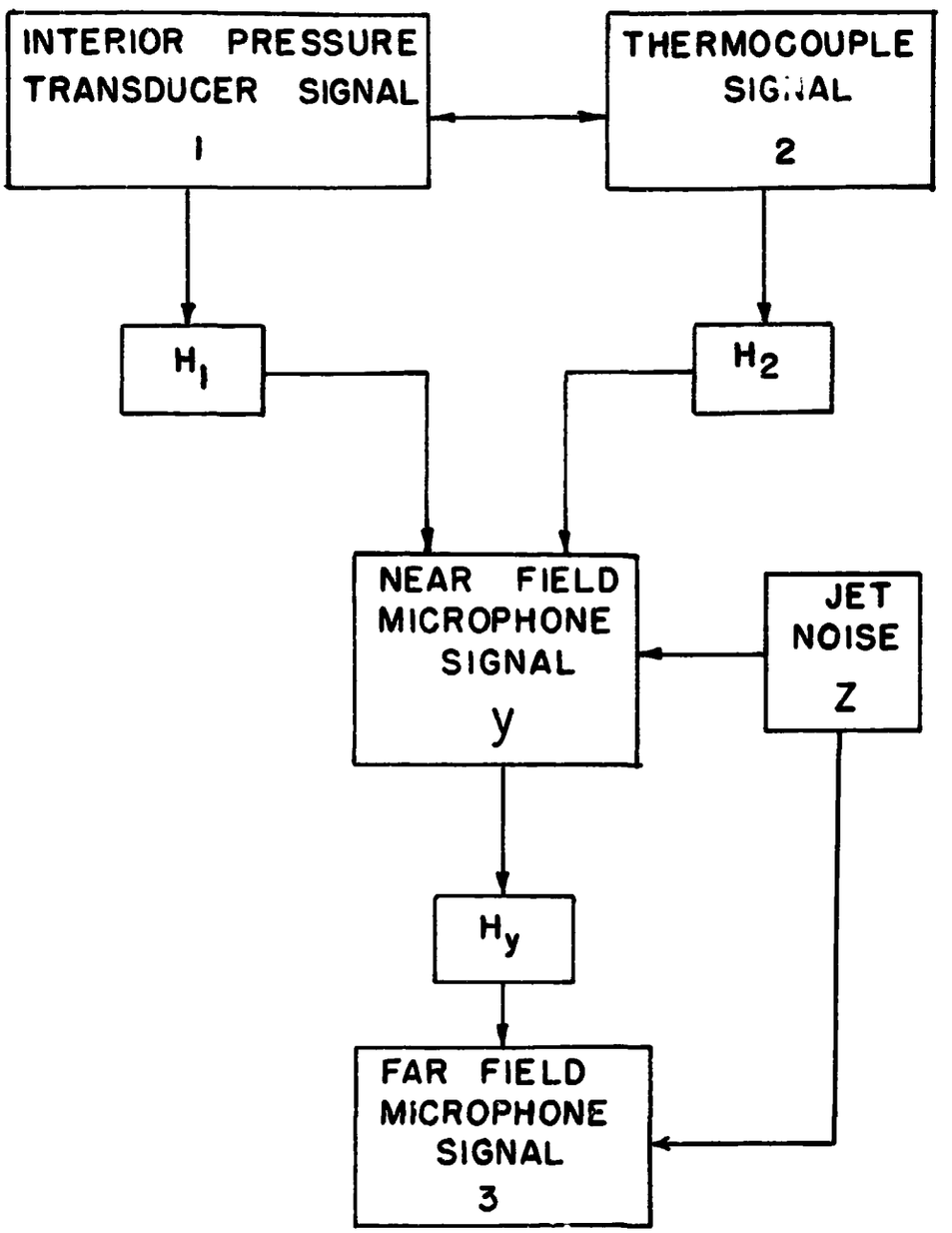


Figure D9. Noise sources model for coherence estimates.

Thermocouple and near field microphone = $\gamma^2_{2y} = \dfrac{1}{1+\left(\dfrac{|H_1|^2\bar{S}_{11} + \bar{S}_{zz}}{|H_2|^2\bar{S}_{22}}\right)}$

(D-5)

Partial Coherence Estimate.

Interior and near field microphones with entropy noise effect removed : $\gamma^2_{1y,2} = \dfrac{1}{1+\left(\dfrac{\bar{S}_{zz}}{|H_1|^2\bar{S}_{11}}\right)}$

(D-6)

Thermocouple and near field microphone with interior microphone effect removed : $\gamma^2_{2y,1} = \dfrac{1}{1+\left(\dfrac{\bar{S}_{zz}}{|H_2|^2\bar{S}_{22}}\right)}$

where $\bar{S}$ denotes the many sample averaged power spectral densities of the subscripted source. Returning to the coherence results, it can be seen from Figs. D10 and D11 that the ordinary coherence function level between the interior and near field microphones generally decreases with an increase in the exit Mach number, while that between the thermocouple and the near field increases. This result, interpreted through the Eqs. (D-5) suggests that the entropy noise contribution available to the near field microphone starts dominating the combustion noise contribution to the near field microphone signal, with the increase in the exit Mach number. Stated otherwise, there is a gradual transition from a combustion noise dominated situation at low Mach numbers to an entropy noise dominated one at high Mach numbers.

The partial coherence estimates, a more reliable procedure for the multiple-input problem, also confirm the above results in Figs. D12 and D13. It can be seen from these figures that with the increase in the exit Mach number, the partial coherence estimate obtained between the thermocouple and the near field signals, with the interior microphone effects removed, rises above the partial co-

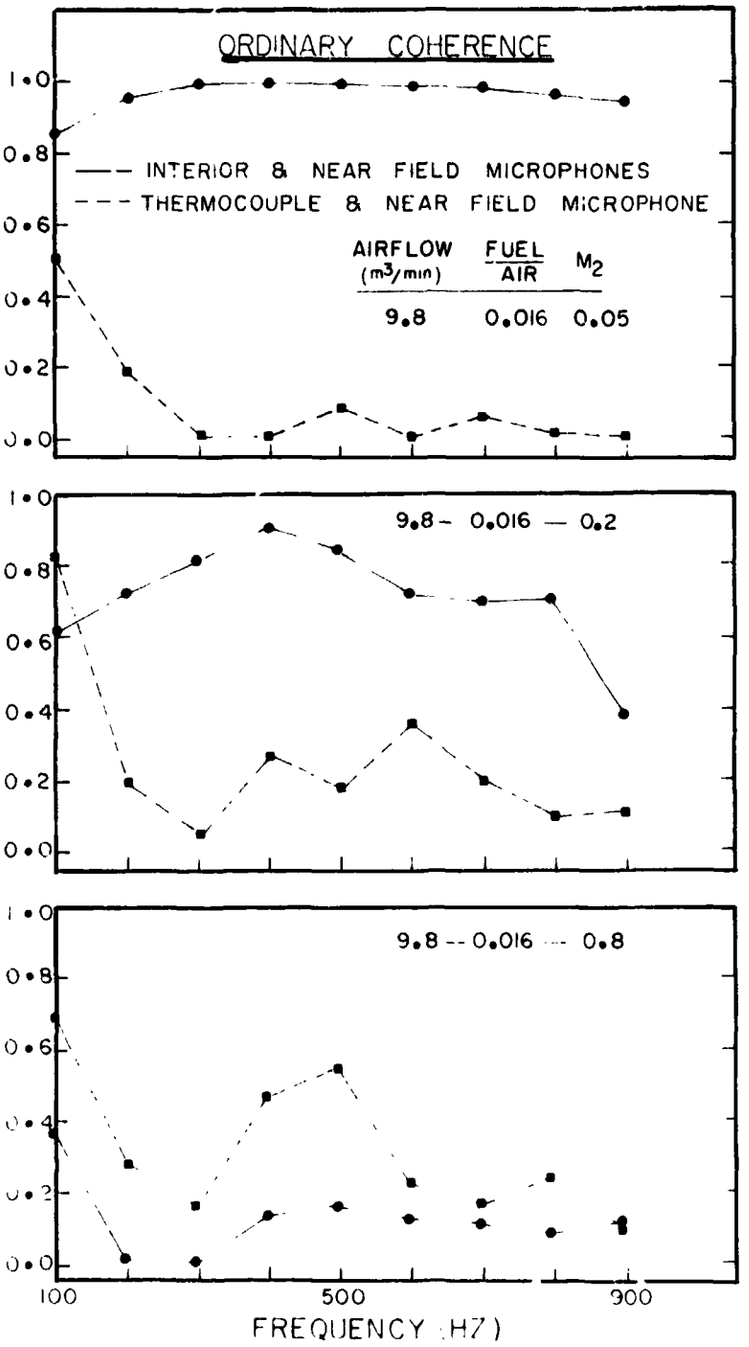


Figure D10. Ordinary coherence estimates between interior and near field signals for a fixed airflow rate and fuel/air ratio varying exit terminations.

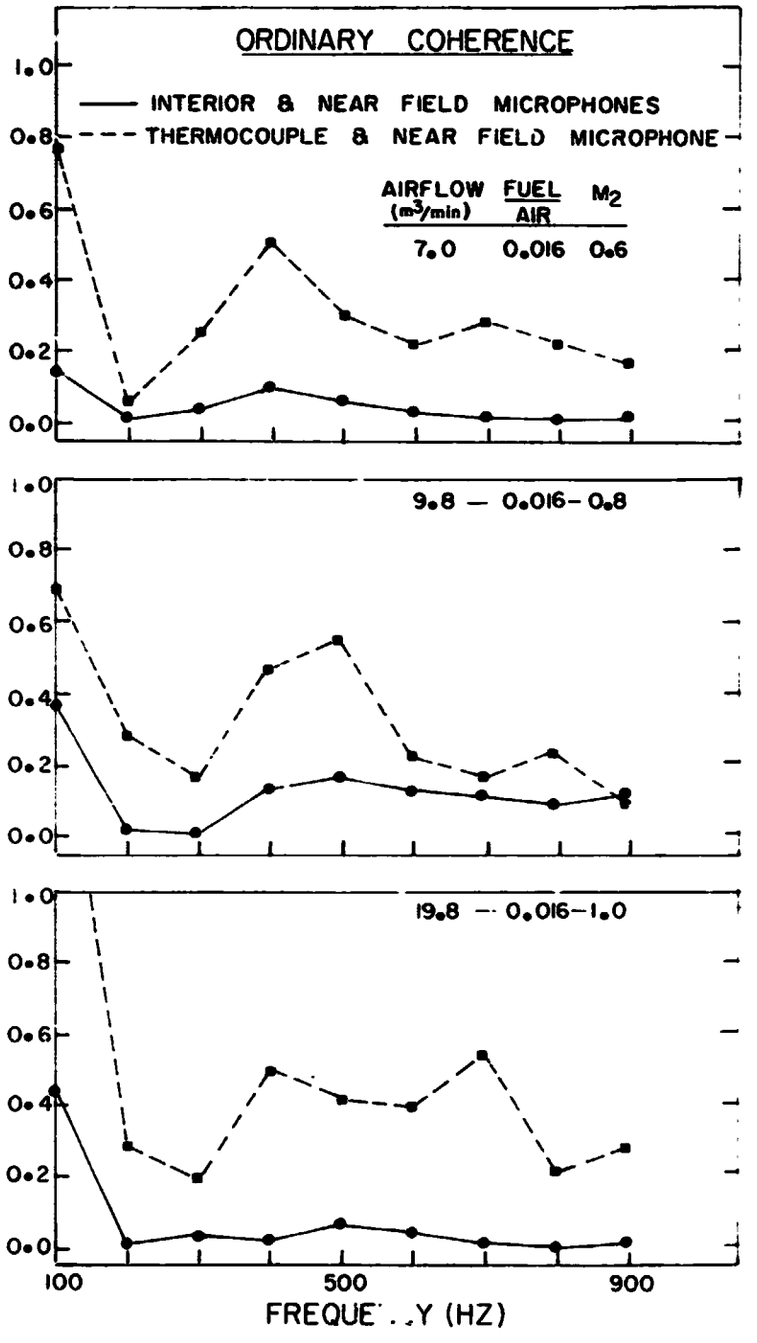


Figure D11. Ordinary coherence estimates between interior and near field signals for a fixed exit termination and fuel/air ratio with increasing airflow rates.

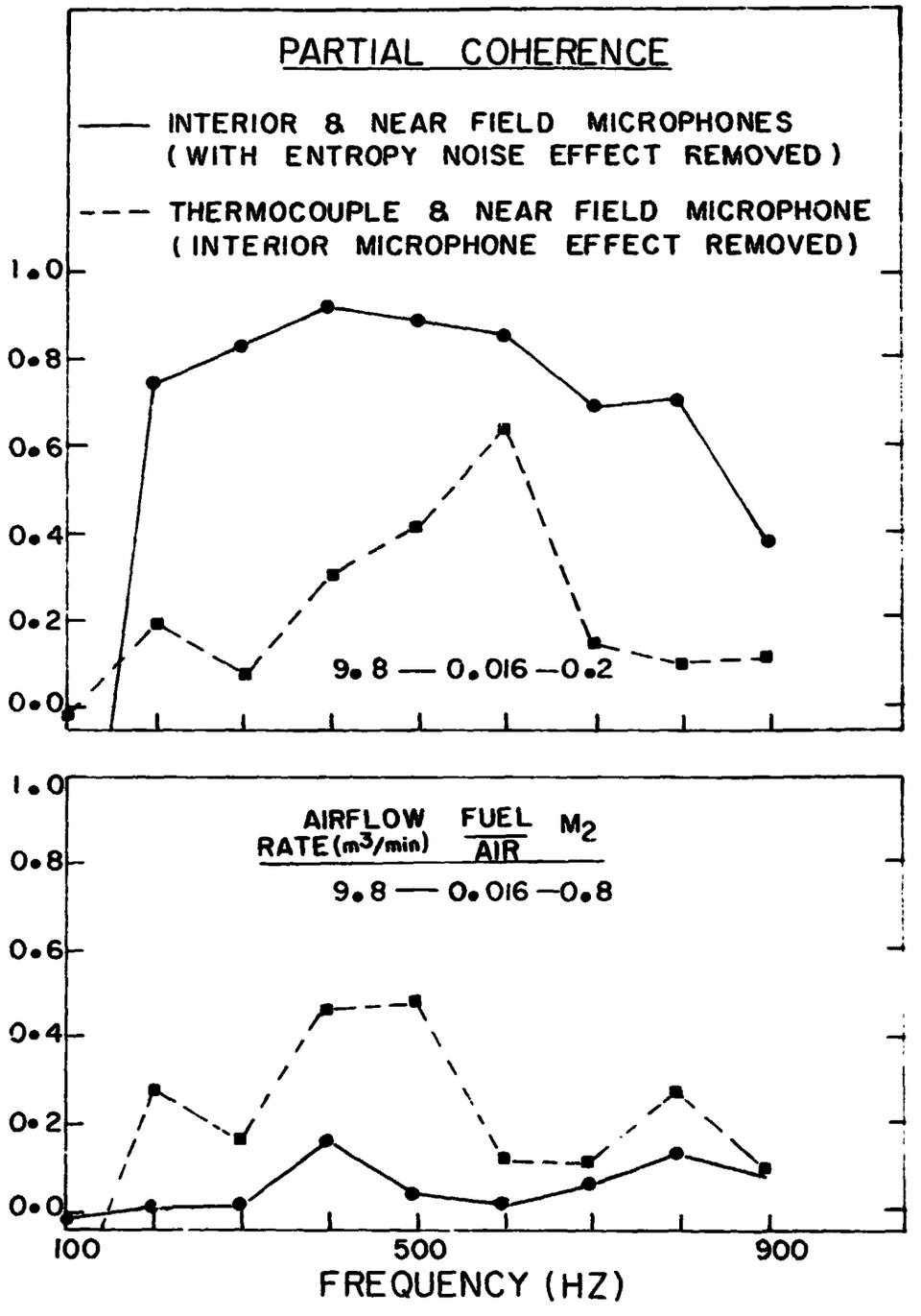


Figure D12. Partial coherence estimates between interior and near field signals for a fixed airflow rate and fuel/air ratio with varying exit terminations.

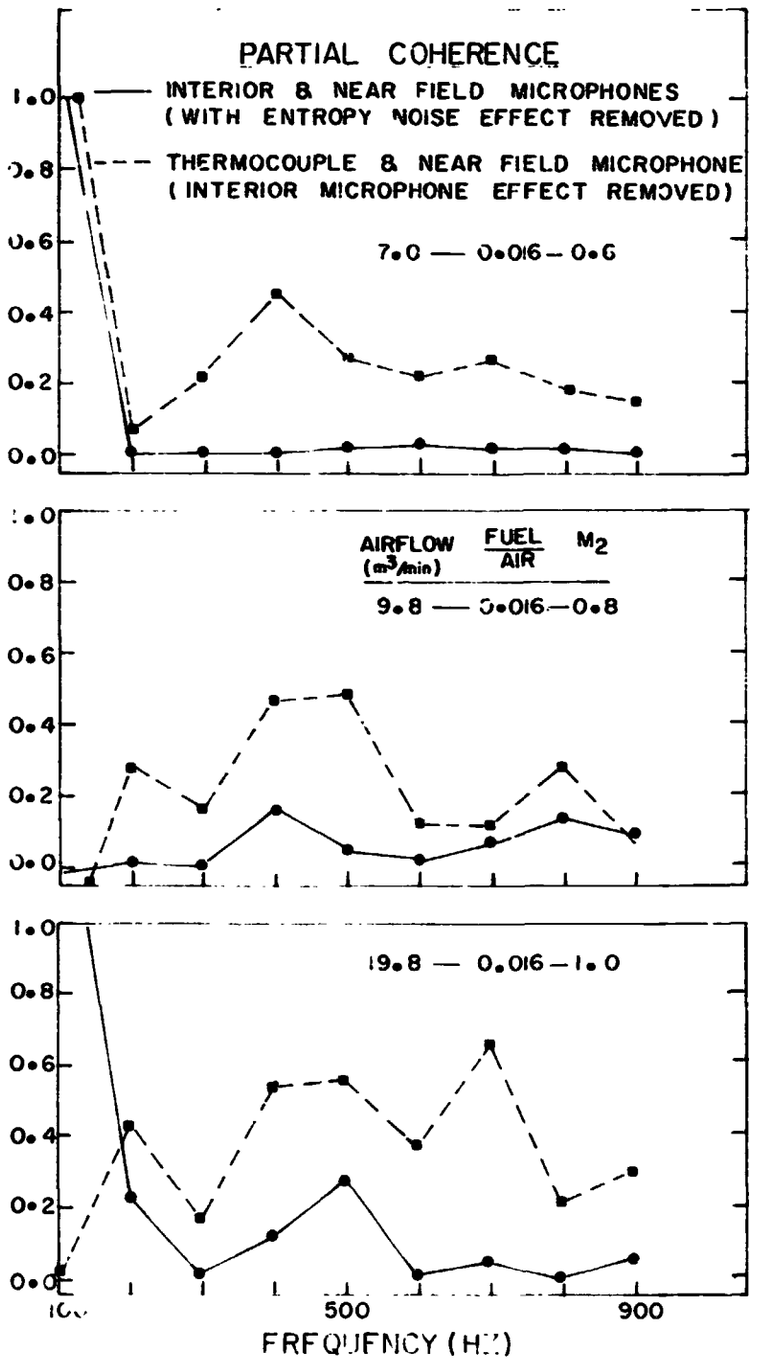


Figure D13. Partial coherence estimates between interior and near field signals for a fixed exit termination and fuel/air ratio with increasing airflow rates.

hereuce levels evaluated between the interior and the near field microphone signals, with the effect of the entropy noise removed. This partial coherence result, with the help of the Eqs. (D-6) reestablishes the previous result that the entropy noise starts dominating the near field signal with the increase in the exit Mach number. In other words, the partial coherence analysis also reaffirms the results of the ordinary coherence function analysis that a combustion noise domination of the near field signal at low Mach numbers yields to an entropy noise domination at high Mach numbers. It is important to note that in all the above partial coherence calculations the single point thermocouple measurements were converted into area averaged quantities using Eqs. D-3 and D-4 which involve the ratio $(A_e/A_{cor})$. A look at Fig. D8 reveals a significant difference in the correlation area values computed in two different ways. The coherence results, discussed above, are based on the correlation area obtained from a single radial traverse of the thermocouple at the burner exit plane without any nozzle or orifice plate attachment. It is informative to see how sensitive the coherence estimates are to the correlation area values. Referring to Fig. D9, the partial coherence estimate between 1 and y, with the effects of 2 subtracted out by a linear least-square prediction, is given as follows.(D1)

$$\gamma^2_{1y,2}(f) = \gamma^2_{1y} \frac{\left(1 - \frac{A_e}{A_{cor}} \frac{\bar{S}_{1y}}{\bar{S}_{22}} \frac{\bar{S}_{2y}}{\bar{S}_{1y}}\right)}{\left(1 - \frac{A_e}{A_{cor}} \gamma^2_{12}\right)\left(1 - \frac{A_e}{A_{cor}} \gamma^2_{2y}\right)} \qquad \text{(D-7)}$$

The symbols used above have been explained in the previous equations and the ratio $(A_e/A_{cor})$ appears in the above equation to obtain the area averaged quantities from single point thermocouple measurements, as explained in the Eqs. (D-3 and 4). For a given test run, the spectral and ordinary coherence estimates, after ensemble averaging and spectial smoothing, have very stable values. Hence,

the accurate estimation of the partial coherence estimate in Eq. (D-7) depends heavily on the confidence with which $A_{cor}$ can be computed for a given $A_e$. Fig. D8 compares the correlation area obtained in two different ways. As explained in the previous section, the average correlation area is computed from the three correlation areas obtained through the radial as well as the circumferential thermocouple cross-correlations at the burner exit plane without any end attachment and the radial cross-correlations at the burner exit plane with the orifice plate attached. The other one is obtained by a single radial traverse of the thermocouple across the burner exit plane without any end attachment. It can be seen from Fig. D8 that there is about 2:1 change in the values when computed in two different ways. For a given set of spectral values, this change may drive the bracketed quantities in Eq. (D-7) to fluctuate between very low positive values and negative ones, thereby altering the partial coherence estimates significantly. Fig. D14 shows the partial coherence estimate based on this average correlation area for a few typical cases. A comparison of Figs. D12 and D14 with the help of Fig. D8 indicates that a decrease in the correlation area values generally increases the partial coherence estimates, with its effect being felt more on the coherence between the thermocouple and the near field signals than on the one between the interior and the near field microphones. The above arguments lead to the fact that a sufficiently accurate determination of the temperature correlation area distribution is vital for a reliable estimation of the partial coherence. This may be achieved by using a large number of thermocouples at the burner exit plane so as to obtain more details about the spatial distribution of the temperature fluctuations. The extraordinarily high coherence at about 100 Hz in the case of high Mach numbers is explained at the end of this section. It is important to note that the coherence values in some cases, even after ensemble averaging, are found to be in the range of the statistical errors associated with the coherence estimates. With a view to increasing the reliability of the results, a spectral

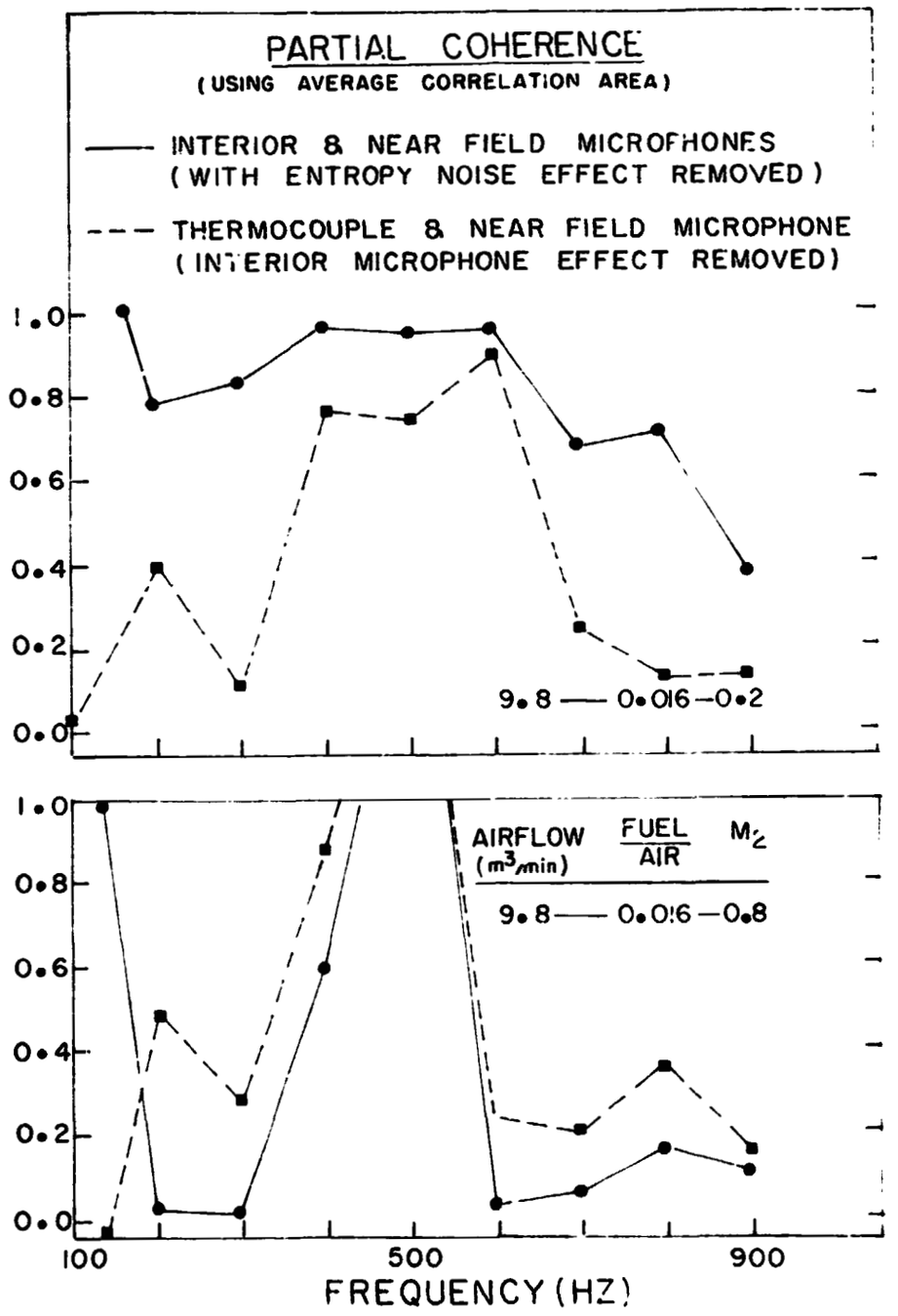


Figure D14. Partial coherence estimates between interior and near field signals for different exit terminations, using average temperature correlation area.

smoothing technique has been employed in which the spectral estimates corresponding to 9 adjacent frequency bands have been averaged. This process reduces the frequency resolution but improves the statistical stability.

The results of the ordinary coherence estimates between the near and far field microphones are presented in Fig. D15. A good coherence level exists at low exit Mach numbers. This is attributable to the fact that at these low Mach numbers, the combustion noise contribution to the exterior radiated sound is very high, and, further, its low frequency nature yields to a monopole radiation pattern. However, at high exit Mach numbers, the coherence level starts decreasing as shown in Fig. D15. This may be due to the fact that with the increasing exit Mach number, the jet noise starts contaminating the core noise radiation. The far field microphone signal is contaminated to a greater degree than that of near field as the former receives the effect of whole jet. However, the near field microphone receives greater contribution from core noise radiation with a lesser degree of contamination by jet noise. This leads to low coherence levels between near and far field signals at high exit Mach numbers.

It can be seen from the coherence results of Fig. D10 to D15 that in the high Mach number cases, the coherence suddenly jumps to a high value in the vicinity of 100 Hz. The interior and the near field microphone spectra as well as the thermocouple spectra exhibit a similar behavior at the corresponding frequencies, as shown in Figs. D2, D3 and D5. Many possibilities for the occurance of this low frequency peak have been investigated. A speculation about the contribution by the burner stand or the probe to this peak has to be discounted, because this occurs only in the high Mach number cases and, moreover, the corresponding cold flow tests do not exhibit this trend. A suspicion on a longitudinal resonance phenomenon is ruled out because the resonant frequency of the combustor, calculated from the speed of sound within the burner rig and the length of the

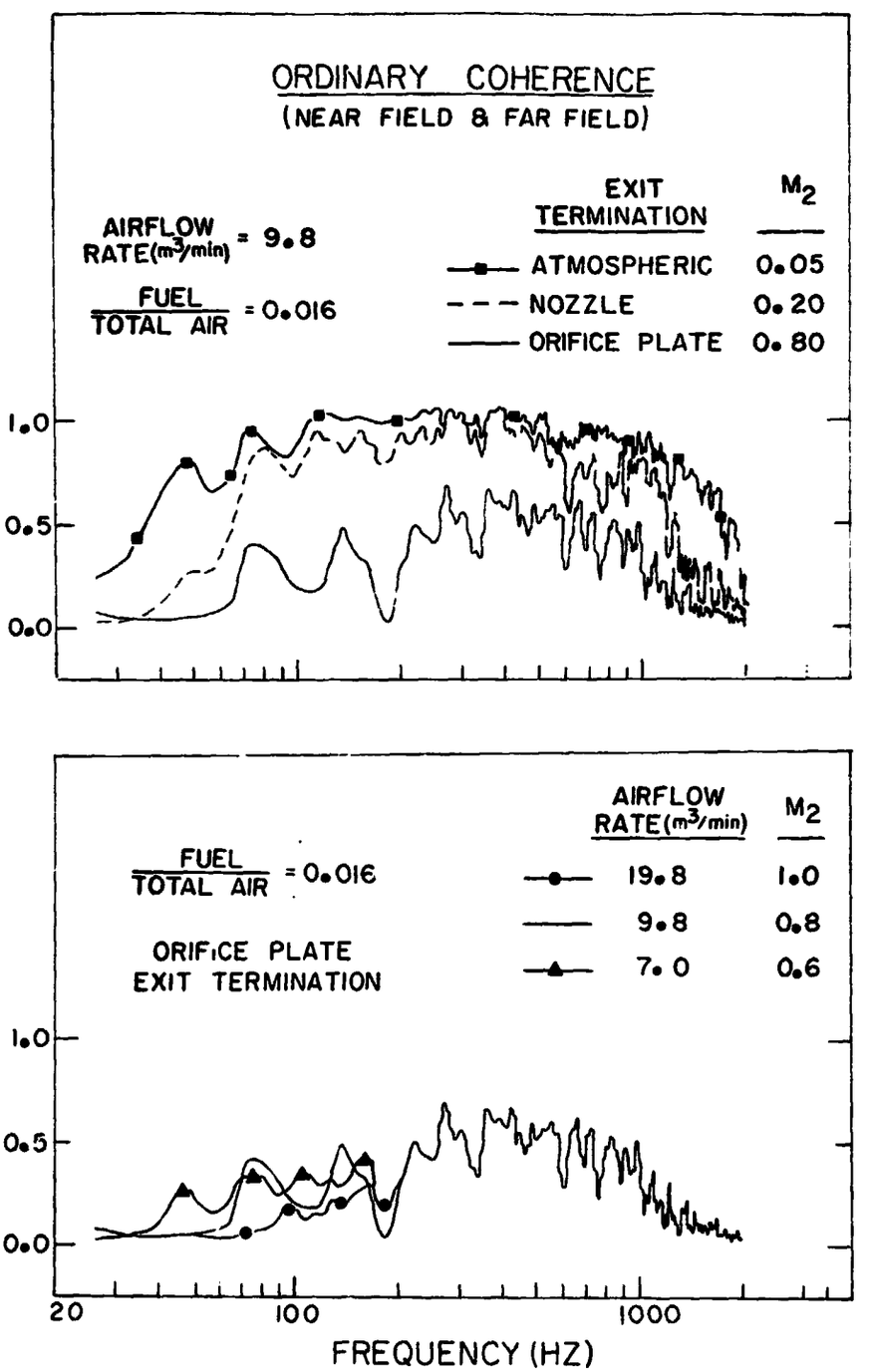


Figure D15. Ordinary coherence estimates between near and far field microphones.

combustor, falls in the range of 400-800 Hz, depending on the nature of the exit termination, as supported experimentally by Fig. D2. A strong possibility is that there may be an acoustic coupling between the interior pressure waves and the fuel/air ratio. Pressure waves traveling towards the head end of the burner will bring out a change in the density of the air which brings a change in the fuel/air ratio. This changes the temperature of the fluid traveling towards the nozzle. The temperature change encountering the nozzle in turn produces a new set of pressure waves, augumenting the old set. It is believed that this acoustic feed-back is mainly responsible for the observed low frequency (about 100 Hz) peak, since the frequency of the phenomenon should be governed by the flow speed and the burner length. Calculations show that this frequency falls in the range of 100-200 Hz. This peak, while interesting, is not too significant as far as the overall sound output is concerned in these experiments.

Finally, note from Eqs. (D-6) that the partial coherence function should be unity if there are no intervening noise sources other than the two under consideration ($S_{zz} = 0$). A partial coherence of unity was not achieved with either partial coherence function for either area correlation curve. Moreover, this was not even achieved for runs where the jet noise contamination was low. One could possibly conclude, therefore, that there are some unconsidered noise sources which are important to the core noise problem. Unfortunately, the partial coherence function is relatively sensitive to the correlation area measurements so that this conclusion appears weak. On the other hand, the partial coherence function between the interior and near field microphones should not suffer from errors in the correlation area, and at high exit Mach number there is indeed low partial coherence between these two microphones. There is the suspicion, therefore, that at least one other noise source is present which was not investigated in this program. The most likely candidate appears to be vorticity-nozzle interaction noise, which deserves investigation in a future program.

## References

D1. Bendat, J. S., and Piersol, A. G., Random Data: Analysis and Measurement Technique, Wiley-Interscience, New York (1971).

Appendix E

## The Relation Between Direct Combustion and Entropy Noise

In Appendix C it was shown that in the absence of any containment to an interior microphone that the pressure transform is of the form

$$p_\omega = f(\omega) \int_V dV\, \dot{Q}_\omega \cos k_{oo} x \tag{E1}$$

where $f(\omega)$ is a frequency dependent transfer function, V is the combustor volume, $k_{oo}$ is the plane wave mode wave number and $\dot{Q}_\omega$ is the transform of the dimensionless heat release fluctuation. Also, it was shown that the entropy follows the equation

$$\frac{D\sigma}{Dt} = \frac{\gamma-1}{\gamma}\,\dot{Q}$$

which upon linearization and application of the Fourier transform becomes

$$i\omega\sigma_\omega + \bar{\vec{v}} \cdot \nabla\sigma_\omega + \vec{v}_\omega \cdot \nabla\bar{\sigma} = \frac{\gamma-1}{\gamma}\,\dot{Q}_\omega \tag{E2}$$

Assuming the mean flow is nearly one dimensional, Eq. (E2) becomes

$$i\omega\sigma_\omega + \bar{u}\,\frac{\partial\sigma_\omega}{\partial x} + u_\omega\,\frac{d\bar{\sigma}}{dx} = \frac{\gamma-1}{\gamma}\,\dot{Q}_\omega$$

Taking a cross section average by the operation $\frac{1}{S}\int dS$,

$$\bar{u}\,\frac{d\hat{\sigma}_\omega}{dx} + i\omega\hat{\sigma}_\omega + u_{\omega_{oo}}\,\frac{d\bar{\sigma}}{dx} = \frac{\gamma-1}{\gamma}\,\frac{1}{S}\int_S \dot{Q}_\omega\, dS \tag{E3}$$

For purpose of analysis it will be assumed that the convective term $u_{oo}\,d\bar{\sigma}/dx$ is negligible compared with the fluctuations in $\hat{\sigma}_\omega$ due to $\dot{Q}_\omega$. This appears justified if $u_{\omega_{oo}}$ is only the acoustic velocity, but theoretically the turbulent fluctuation (vortical part) should also be considered. More sophisticated analysis can reexamine this issue in future work. Equation (E3) may then be written

$$\frac{d\hat{\sigma}_\omega}{dx} + \frac{i\omega}{\bar{u}}\,\hat{\sigma}_\omega = \frac{\gamma-1}{\gamma\bar{u}}\,\frac{1}{S}\int_S \dot{Q}_\omega\, dS \tag{E4}$$

If the boundary condition is applied that there is no combustion, and, hence, no fluctuation in $\sigma$ at $x = 0$, the solution to Eq. (E4) may immediately be written as (evaluated at the exit plane)

$$\hat{\sigma}_{\omega_e} = \frac{\gamma-1}{\gamma S} \; e^{-i\omega_o \int_o^1 \frac{dx}{\bar{u}}} \int_o^1 \frac{e^{i\omega_o \int_o^x \frac{dx'}{\bar{u}}}}{\bar{u}} \, dx' \int_S \dot{Q}_\omega \, dS$$

which may be computed (since S = V in the non-dimenionalization scheme used)

$$\hat{\sigma}_{\omega_e} = \frac{\gamma-1}{\gamma} \; e^{-i\omega_o \int_o^1 \frac{dx}{\bar{u}}} \; \frac{1}{V} \int_V dV e^{i\omega_o \int_o^x \frac{dx'}{\bar{u}}} \; \frac{\dot{Q}_\omega}{\bar{u}} \tag{E5}$$

Equation (E5) may be written as

$$\hat{\sigma}_{\omega_e} = g(\omega) \int_V e^{i\omega_o \int^{x'} \frac{dx'}{\bar{u}}} \frac{\dot{Q}_\omega}{\bar{u}} \, dV \tag{E6}$$

where $g(\omega)$ is a deterministic transfer function. It can already be seen that there is a remarkable similarity between Eq. (E6) and Eq. (E1). This is especially true if $\omega/\bar{u}_{max} << 1$ in which case $\cos k_{oo} x$ and the exponential terms in Eqs. (E1) and (E6) are unity. With the nondimensionalization scheme used here $\omega \bar{u}_{max} \approx 1$ corresponds to the physical frequency being of the same order of magnitude as the inverse of a fluid particle stay time in the combustor. In the opposite limit $\omega/\bar{u}_{max} << 1$ there is extremely rapid phase rotation of the exponential factor in Eq. (E6) as the x-integration is carried out which would destroy any phase coherence between Eq. (E1) and (E6).

The expected situation is, consequently, near perfect coherence between $p_\omega$ and $\hat{\sigma}_{\omega_e}$ [except for the factor $\bar{u}$ in the denominator of Eq. (E6)] at low frequency, changing to zero coherence at high frequency. The transition whould take place where $\omega \approx \bar{u}_{max}$. In the current experimental hardware the physical frequency is roughly 200 Hz.

$\hat{\sigma}_{\omega_e}$ is the cross section average transform of the entropy fluctuation. A point measurement will be expected to yield lower coherence, as discussed in Appendix D. The coherence function, for a nozzle-off case, between a point temperature measurement and the wall pressure fluctuation is shown in Fig. E1. The drop in coherence at very low frequency is believed due to the hydrodynamic noise contamination of the interior microphone, as discussed earlier. The drop-off above 150-200 Hz is the transition from coherence to incoherence between $p_\omega$ and $\sigma_{\omega_e}$.

This phenomenon is shown also in Fig. E2 where the cross correlation coefficient between $p'$ and $\sigma'$ is shown. Although detailed interpretation of this curve is impossible because Eqs. (E6) and (E1) contain complicated phase information, it is readily observed that a) a strong cross correlation exists and b) the "frequency" of the cross-correlation oscillation is roughly 130 Hz, which is of the expected magnitude.

The major conclusion is that above about 200 Hz it is permissible to assume statistical independence of combustion noise and entropy noise, whereas at lower frequencies they are intimately connected. This transition frequency, of course, depends upon the flow speed and burner size.

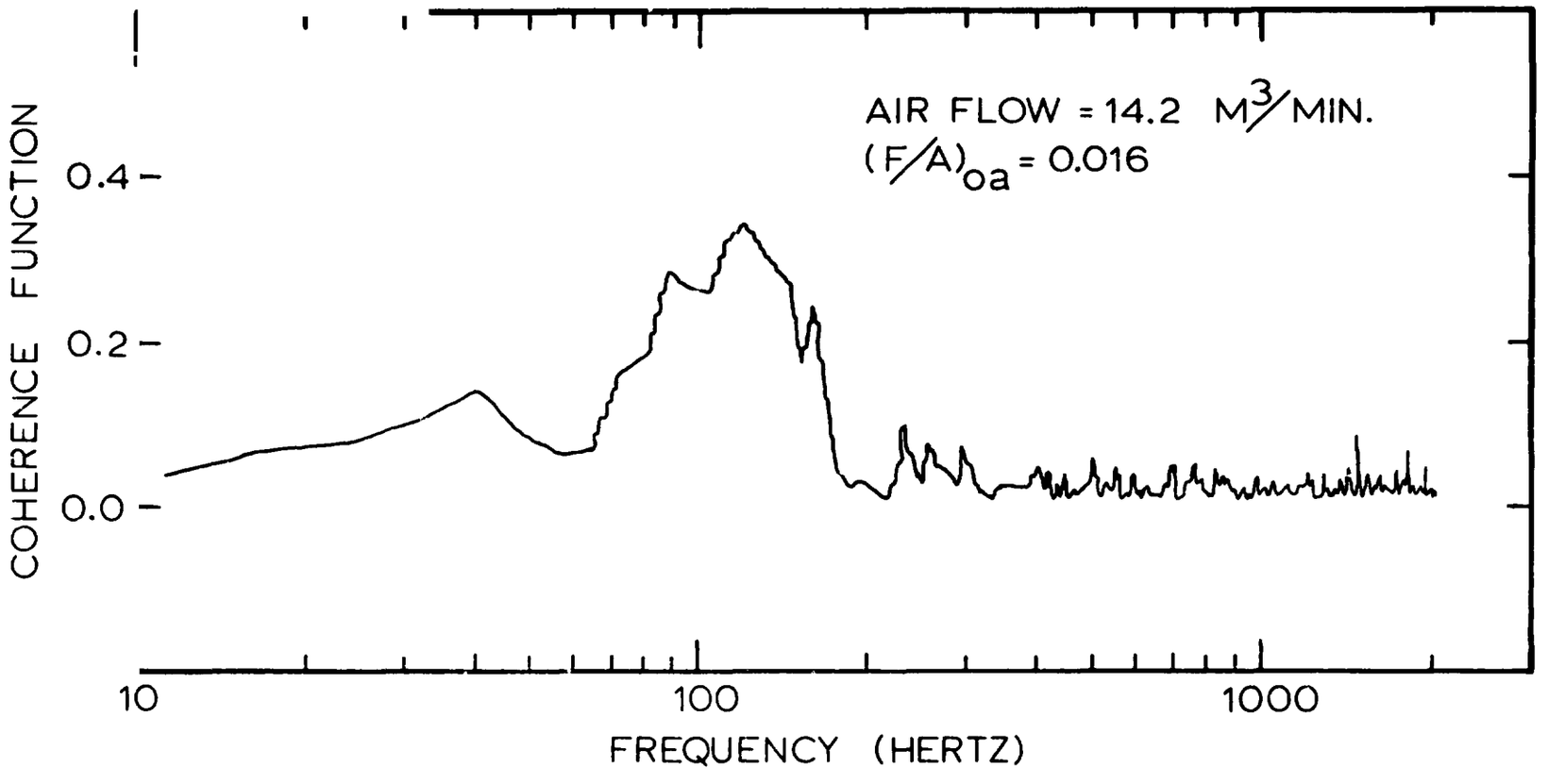


Figure E1. Nozzle off coherence between an exit plane thermocouple and an interior microphone.

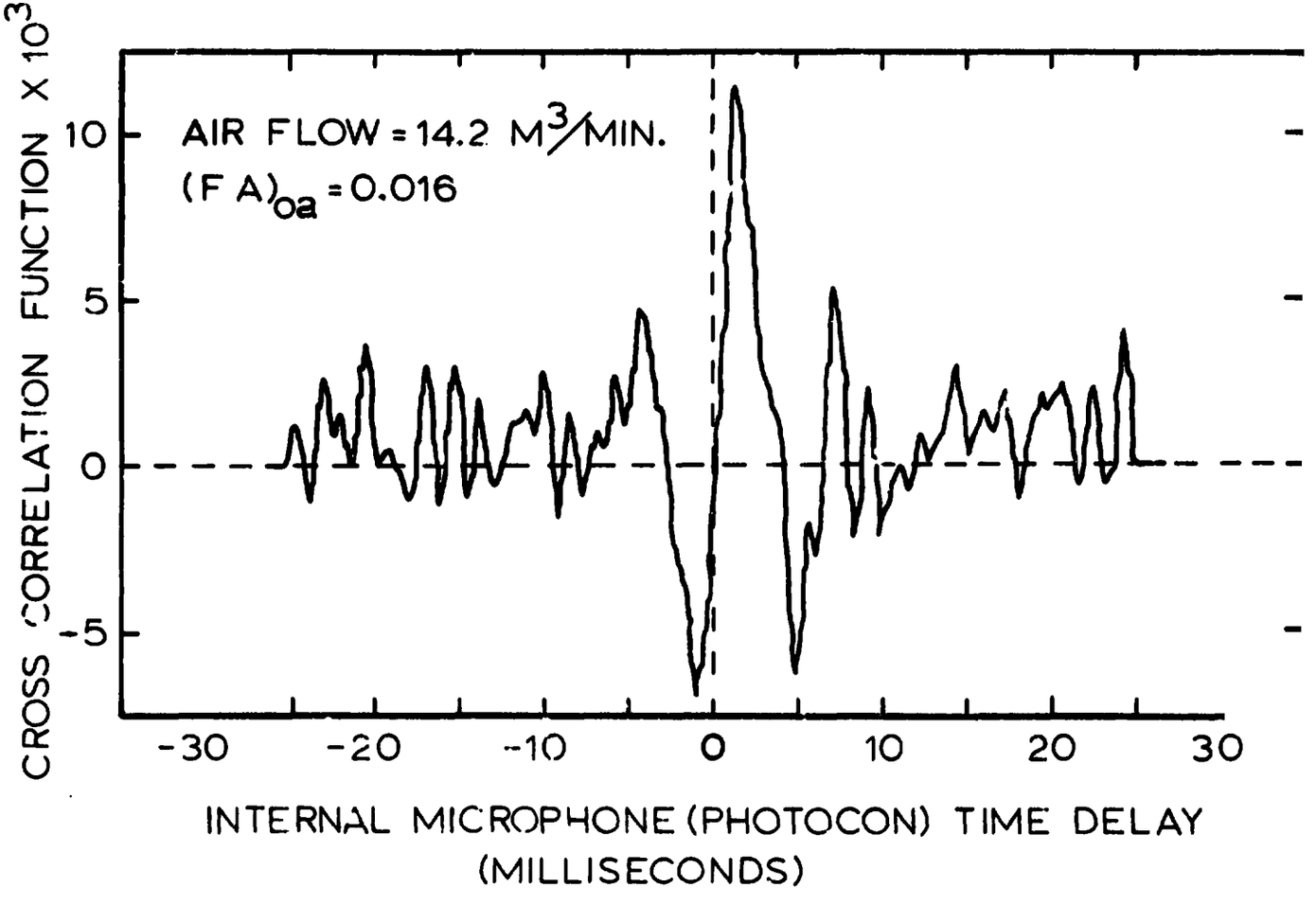


Figure E2. Cross correlation coefficient between an exit plane thermocouple and the interior microphone.

# Appendix F

## Thermocouple Time Constant Measurement by Cross Power Spectra

*Reprinted from* AIAA JOURNAL, Vol. 14, No. 11, November 1976, pp. 1642-1644
Copyright, 1976, by the American Institute of Aeronautics and Astronautics, and reprinted by permission of the copyright owner

# Thermocouple Time Constant Measurement by Cross Power Spectra

Warren C. Strahle* and M. Muthukrishnan†
*Georgia Institute of Technology, Atlanta, Ga.*

## Introduction

THE measurement of fluctuating temperatures downstream of the combustor in turbopropulsion systems is required to quantify the importance of entropy noise generation in these systems.[1-3] It is well known, however, that most thermocouples suitable for use in such a hostile environment have response times considerably longer than required for flat response in the audible frequency range. Consequently, they must be compensated. Central to the compensation problem is the problem of measuring the response time of a given thermocouple, because it must be measured in the environment which it will see in use. This is so because the

Received July 19, 1976. This work was supported by NASA under grant no. NSG 3015.
Index categories: Aircraft Noise, Powerplant, Airbreathing Engine Testing, Combustion in Gases.
*Regents' Professor. Associate Fellow AIAA.
†Graduate Research Assistant.

response time depends upon the convective and radiative environment in which the thermocouple is located.[4] Methods previously developed for measurement of the time constant have usually relied on measurement of the impulse response by quickly inserting the thermocouple into the environment, switching a gas stream from cold to hot, or by turning off an initial current through the wire and watching the temperature decay to the temperature of the environment.[5] Mechanical methods are adequate for time constants of the order of 100 msec or longer. However, for "fast" response thermocouples (< 10 msec), the mechanical switching methods are not usually fast enough to provide a true step input temperature change. Electrical methods, since they involve heating of the wire above the environment temperature, are not satisfactory if the thermocouple is operating near its limit of survivability. The purpose of this note is to show a new method of thermocouple time constant measurement, which at the same time is *nonintrusive upon the thermocouple*.

## Analysis

The fundamental assumptions are the equation for the AC output of the thermocouple, $y$, which is proportional to the apparent temperature fluctuation about the mean temperature, is given by $y=\bar{y}+z$, where $\bar{y}$ is the portion of the signal truly proportional to the temperature flucturations, and $z$ is the background electronic noise. $\bar{y}$ obeys the linear differential equation

$$\frac{d\bar{y}}{dt}=\frac{1}{\tau}(\eta x-\bar{y}) \tag{1}$$

Here $\tau$ is the time constant, $x$ is the true temperature fluctuation, and $t$ is time. $\eta$ is a factor, usually very near unity, which may be calculated from known radiation and conduction correction factors.[4] $\eta$ is the ratio of the equilibrium thermocouple reading to the reading it would give if it were at the true temperature. The method of measurement of $\tau$ is the issue. In the method outlined here, two thermocouples, denoted by 1 and 2, of differing time constants are required to be placed in the flow as closely as possible to one another so as to see the same temperature history. Any separation of the two thermocouples will yield some error, the exact nature of which is discussed later.

The method assumes the availability of equipment which will readily process the signals by Fourier analysis. Taking the finite Fourier transform of Eq. (1),

$$\bar{Y}(1+i\omega\tau)=\eta X$$

and by definition

$$Y=\bar{Y}+Z=\frac{\eta X}{1+i\omega\tau}+Z \tag{2}$$

Here capital letters stand for the Fourier transform of the small letter quantities. The cross power spectrum and the auto power spectra are‡

$$S_{12}=Y_1Y_2^* \qquad S_{11}=Y_1Y_1^*$$

$$S_{22}=Y_2Y_2^*$$

which yield from Eq. (2)

$$S_{12}=\left(\frac{\eta X}{1+i\omega\tau_1}+Z_1\right)\left(\frac{\eta X^*}{1-i\omega\tau_2}+Z_2^*\right)$$

$$S_{11}=\left(\frac{\eta X}{1+i\omega\tau_1}+Z_1\right)\left(\frac{\eta X^*}{1-i\omega\tau_1}+Z_1^*\right) \tag{3}$$

‡Here, because they will cancel out later, proportionality constants in the spectral functions involving the sampling time have been omitted

where a * denotes the complex conjugate. If the spurious noise is *incoherent* with the signal then an ensemble average, denoted by a bar superscript, will yield

$$\bar{S}_{12}=\frac{\eta^2\overline{XX^*}}{1+\omega^2\tau_1\tau_2+i\omega(\tau_1-\tau_2)}$$

$$\bar{S}_{11}=\frac{\eta^2\overline{XX^*}}{(1+\omega^2\tau_1^2)}+\overline{Z_1Z_1^*} \tag{4}$$

provided that $z_1$ is incoherent with $z_2$. In what follows it is presumed that the spurious noise for signal 1 is sufficiently small that $Z_1Z_1^*$ may be neglected in comparison with the first term in $\bar{S}_{11}$. Now constructing the ratio of $\bar{S}_{11}$ to $\bar{S}_{12}$,

$$R\equiv\bar{S}_{11}/\bar{S}_{12}=\frac{1+\omega^2\tau_1\tau_2+i\omega(\tau_1-\tau_2)}{1+\omega^2\tau_1^2} \tag{5}$$

Consider then

$$\lim_{\omega\to\infty}R=R_r=\tau_2/\tau_1 \tag{6}$$

which directly gives the time constant ratio. More importantly, consider the imaginary part of $R$, $R_i$.

$$R_i=\frac{\omega(\tau_1-\tau_2)}{1+\omega^2\tau_1^2}$$

Differentiating, and finding an extremum in this function,

$$\frac{\tau_1-\tau_2}{1+\omega_e^2\tau_1^2}-\frac{2\omega_e^2(\tau_1-\tau_2)\tau_1^2}{(1+\omega_e^2\tau_1^2)^2}=0$$

where the $e$ subscript denotes an extremum value of $\omega$. For $\tau_1\neq\tau_2$, which is the reason for using two different thermocouples, there is a single extremum at

$$\omega_e=1/\tau_1 \tag{7}$$

Thus, $\tau_1$ may be found directly if a plot of $R_i$ is available. The primary restrictions here are that both thermocouples are seeing the same $x$ and that the noise does not mask the signal in the vicinity of $\omega_e$.

The quality of the data can be assured by constructing the coherence function.[6] This is

$$\gamma^2\equiv\frac{\bar{S}_{12}\bar{S}_{12}^*}{\bar{S}_{11}\bar{S}_{22}}=\frac{1}{1+b}$$

$$b=\frac{Z_1Z_1^*[1+(\omega\tau_2)^2]}{\eta^2XX^*}+\frac{Z_2Z_2^*[1+(\omega\tau_1)^2]}{\eta^2XX^*}$$

$$+\frac{Z_1Z_1^*Z_2Z_2^*(\omega\tau_1)^2][1+(\omega\tau_2)^2]}{\eta^4XX^*}$$

All the terms in $b$ are positive, real quantities. A *sufficient* condition, therefore for Eq. (7) to be valid is one of $\gamma^2$ being close to unity in the vicinity of $\omega_e$. This condition furthermore assures that $X$ at position 1 is the same as $X$ at position 2 since the effect of any difference is to insert a spurious noise into one signal that is not seen at the other. This coherence condition of unity is not a necessary one, however. All that are necessary are the conditions leading to Eq. (5), in the vicinity of $\omega_e$. The reason the coherence condition is introduced is that there is commercially available equipment that will readily compute $\gamma^2$.

Finally, Eq. (6) is not useful as Eq. (7) because it requires a large value of frequency. Since both signals will be falling off

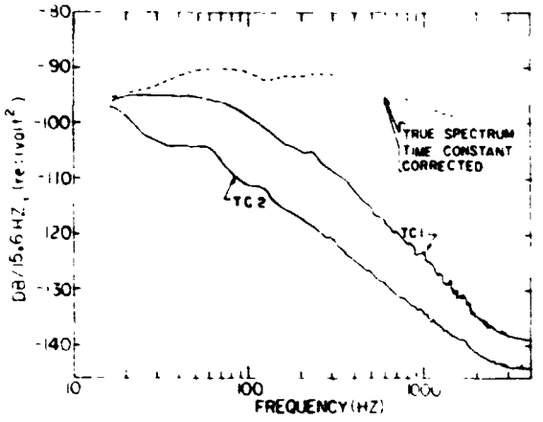


**Fig. 1 Thermocouple spectra for two different thermocouples placed on the centerline at the exhaust plane of a gas turbine combustor.**

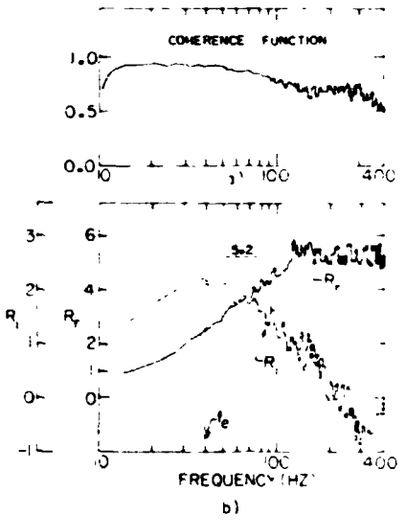


b)

**Fig. 2 Coherence a) between the two thermocouples and b) time constant determination for the thermocouples.**

markedly at high frequency there is much more danger of dropping into the background noise at high frequency as compared with $\omega_c$.

## Experiment

To illustrate the procedure two commercial Chromel-Alumel thermocouples of wire diameters 0.001 in. (TC1) and 0.003 in. (TC2) were mounted less than 1/8 in. apart in the exhaust of a gas turbine combustor. Fixed bandwidth spectra (15.6 Hz) of the AC component of temperature are shown in Fig. 1. Also shown in Fig. 1 is the true temperature spectrum ($\eta^2 X_1 X_1^*$) after correction, knowing the thermocouple time constant. Since the time constant goes roughly as $D^{1.5}$, where $D$ is the wire diameter, TC2 has a poorer response, which is also shown in Fig. 1. In this example the ratio of the time constant, $\tau_2/\tau_1$, should be roughly $3^{1.5} = 5.2$.

The time constant for TC1 was expected to lie between 1 and 10 msec, so finer bandwidth filtering (3.1 Hz), and a narrower frequency range (0-400 Hz) was chosen for time constant analysis in Fig. 2. In Fig. 2a, the coherence function is seen to be adequate within the band 10-400 Hz. In Fig. 2b are shown $R_r$ and $R_i$. $R_r$ shows the expected behavior of monotonically going from unity to $\tau_2/\tau_1$ as $\omega$ goes from zero to values much greater than $1/\tau_1$. $R_i$ shows the expected behavior of a maximum at 40 $Hz$, corresponding to $\tau_1 = 1/(2\pi 40) = 4$ msec.

Some problems with this method are a) the AC component of temperature is usually substantially lower than the DC component so that high systems gains are needed and higher than desired background noise is usually evident, especially for the larger thermocouple, and b) the maximum is somewhat broad in $R_i$ so that, in this example, about 25% error in $\tau$ may be expected. Problem a) is minimized by using thermocouples of nearly equivalent (but not equal) time constants. However, it appears that problem b) must be accepted as a limitation of the method.

## References

[1] Zukoski, E., "Temperature Distortion Effect on Turbine and Afterburner Noise," ASME Paper No. 75-61-40, 1975.

[2] Cumpsty, N. A., "Excess Noise from Gas Turbine Exhausts," ASME Paper No. 75-6T-61, 1975.

[3] Pickett, G. F., "Core Engine Noise due to Temperature Fluctuations Convecting through Turbine Blade Rows," AIAA Paper 75-528, Hampton, Va., 1975.

[4] Scadron, M. D. and Warshawsky, S., "Experimental Determination of Time Constants and Nusselt Numbers for Bare-Wire Thermocouples in High Velocity Air Streams and Analytic Approximation of Conduction and Radiation Error," NACA TN 2599, 1952.

[5] Carbon, M. W., Kutsch, H. J., and Hawkins, G. A., "The Response of Thermocouples to Rapid Gas Temperature Changes," *ASME Transactions*, July 1950, pp. 655-657.

[6] Bendat, J. S. and Piersol, A. G., *Random Data: Analysis and Measurement Procedures*, Wiley-Interscience, N. Y., 1975, p. 32.

## Appendix G

### Liner Hole Size Variation Investigation

The special manufacture of different liners was described in Appendix A. These were tested in the nozzle-off configuration to determine spectral shifts in the combustion noise due to liner hole size modifications. Only the near field microphone was used, it being the one to sense primarily combustion noise.

The results of the near field spectra for several runs are shown in Figs. G1 - G3. The raw spectra show little, if any, change in frequency content with a change in liner hole size. To put this on a more precise basis, the spectra for the 14.2 $m^3$/min air flow, 0.02 fuel/air ratio cases were integrated over the range 0-2000 Hz. The results are presented in Fig. G4; from this plot the "half-power" frequency may be seen, above and below which half of the cumulative noise exists. There is virtually no shift in frequency with liner hole size. If anything, there is a mild shift to higher frequency with an increase in hole size, contrary to physical expectation.

To put the results on an even more fundamental basis, the technique of Appendix C is applied to extract the heat release spectrum for a set of three liners at fixed fuel/air and mass flow. Shown in Figs. G5 - G7 are the heat release, hydrodynamic noise, and interior microphone spectra as well as the integrated (or cumulative) spectrum of the heat release function. The heat release spectrum is virtually unchanged with a change in liner hole size.

The results were surprising, since a previous combustion noise study[G1] showed a correlation of frequency content with turbulence properties, including turbulence length scale. The hole size variation was specifically carried out to modify turbulence length scale. Previous results[G2] have shown that virtually no flow, heat release, or combustion rate property

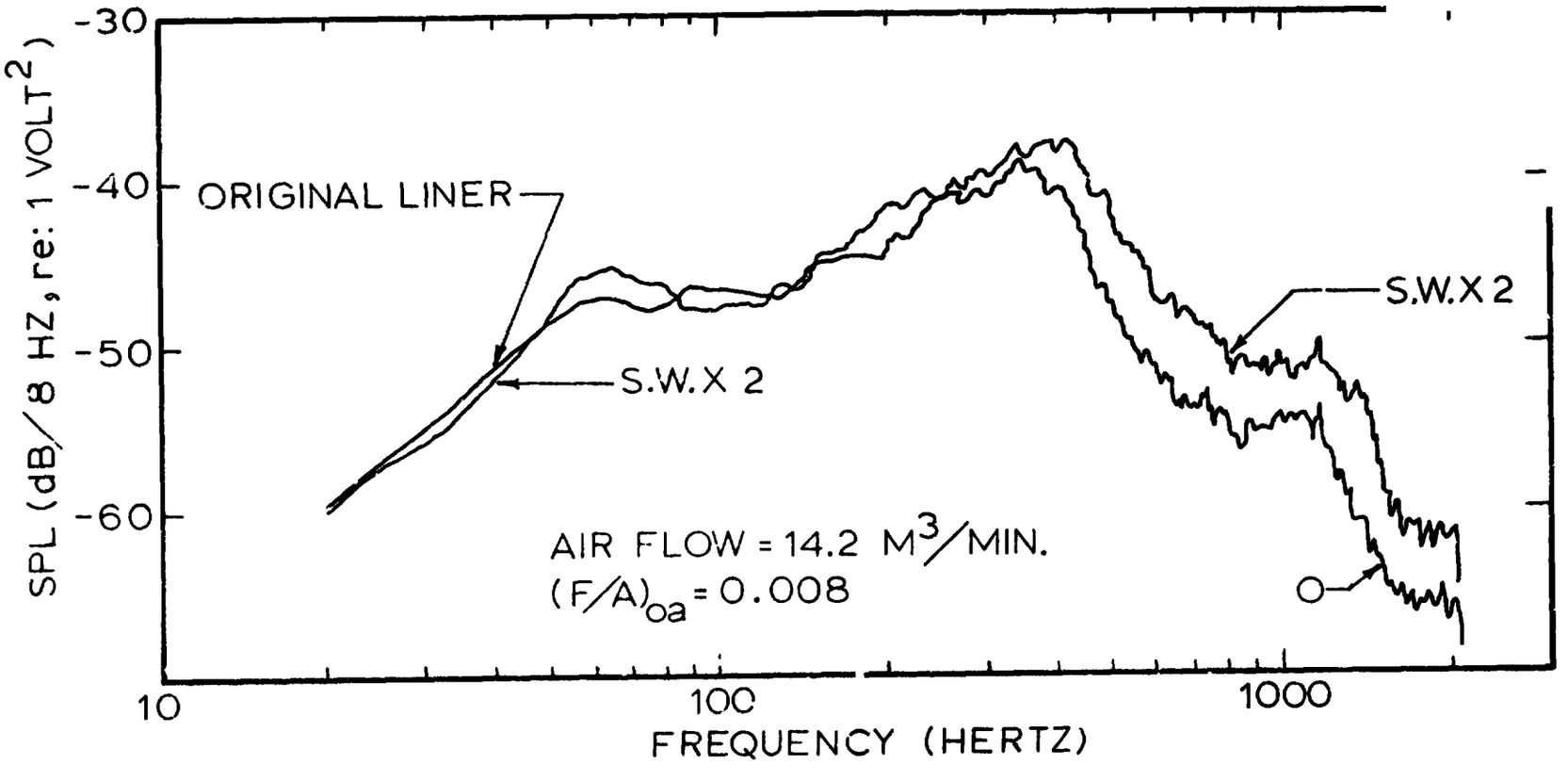


Figure G1. Near field spectra for two different liners.

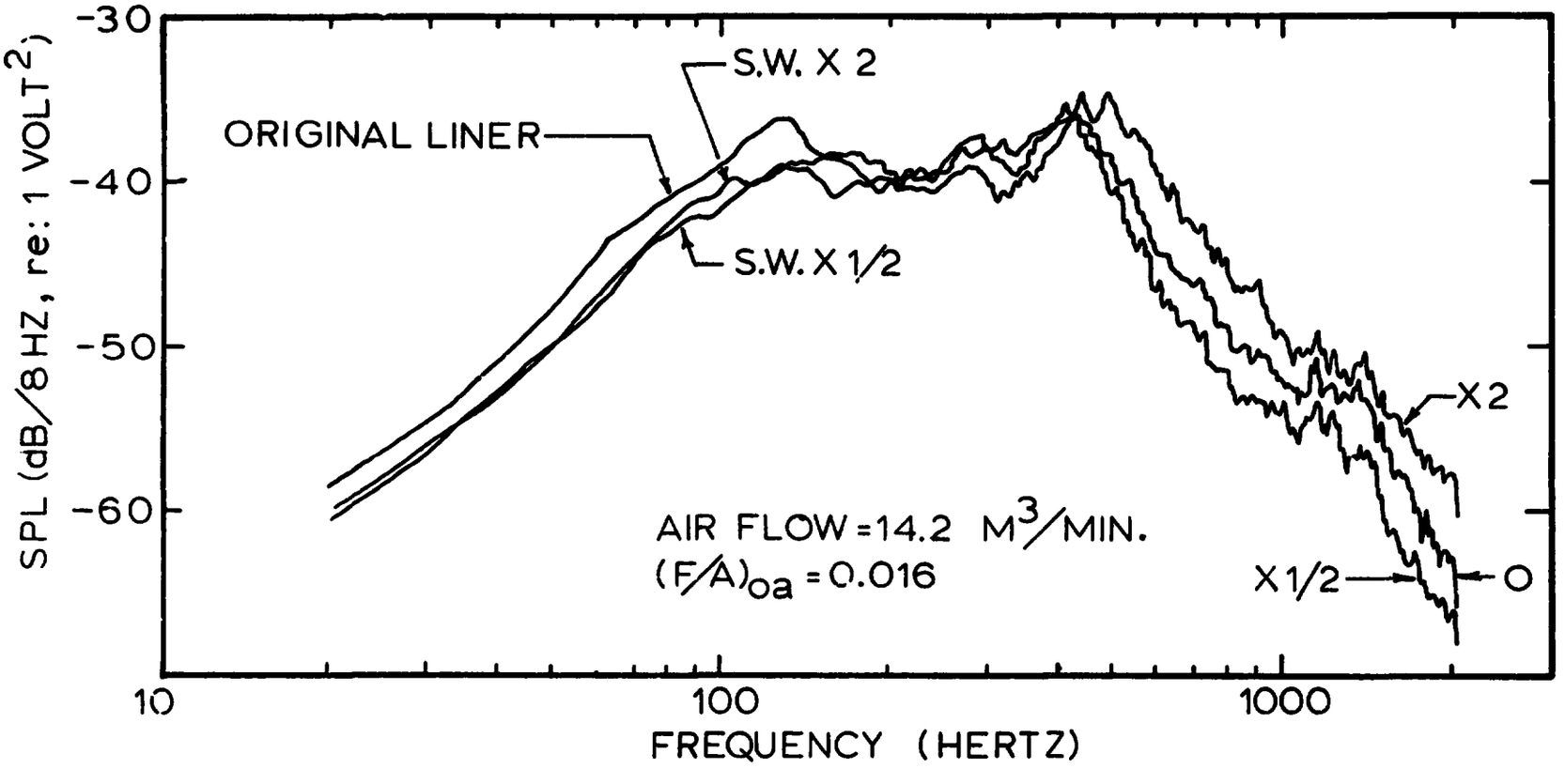


Figure G2. Near field spectra for three different liners.

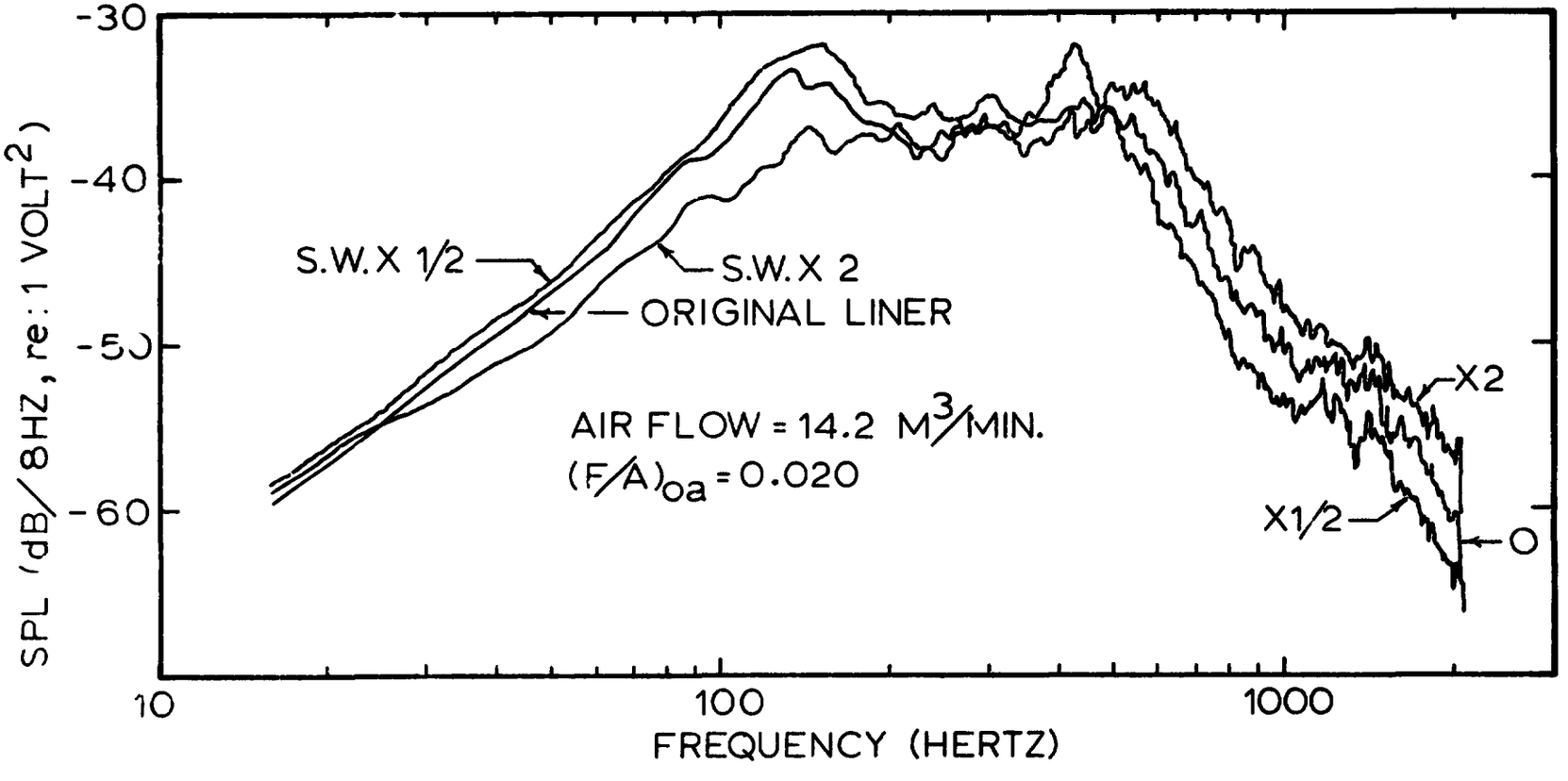


Figure G3. Near field spectra for three different liners.

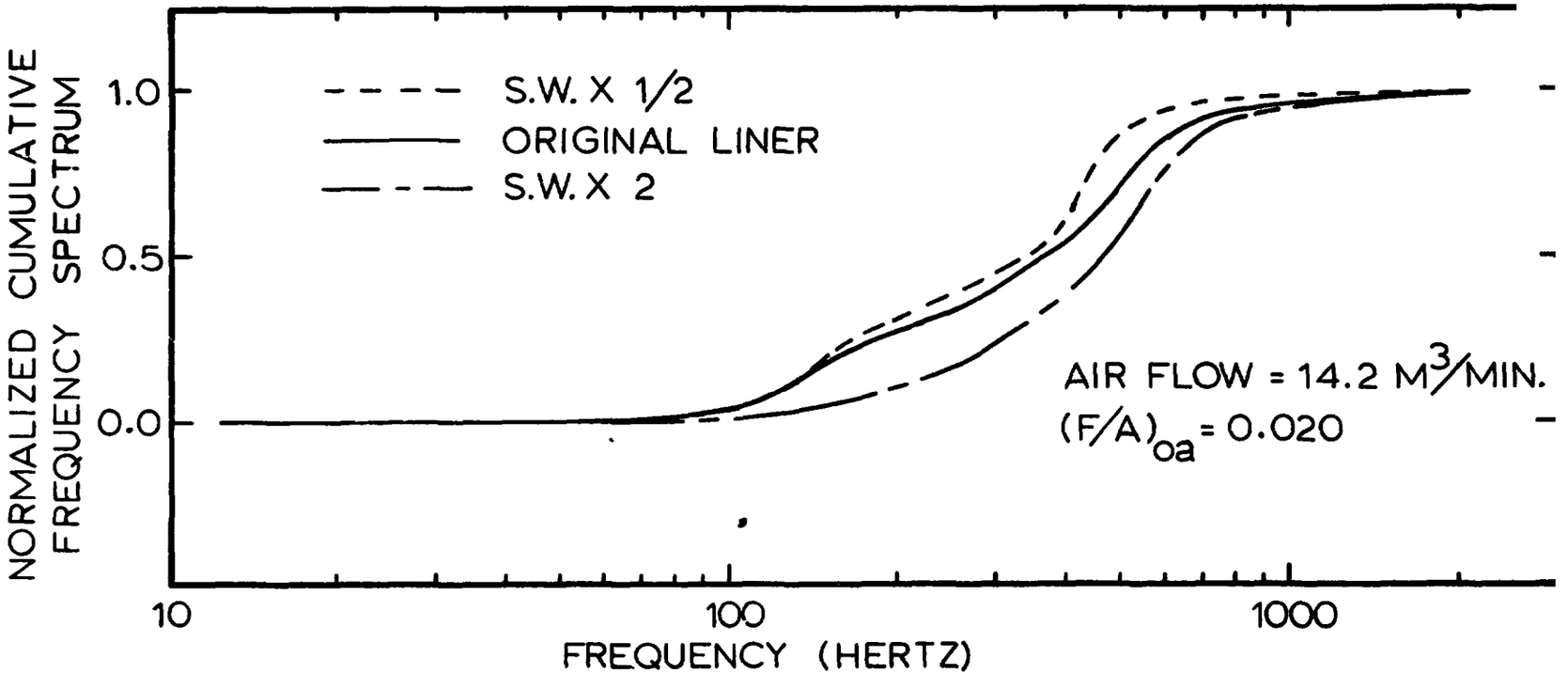


Figure G4. Cumulative sound pressure level as a function of frequency for three different liners.

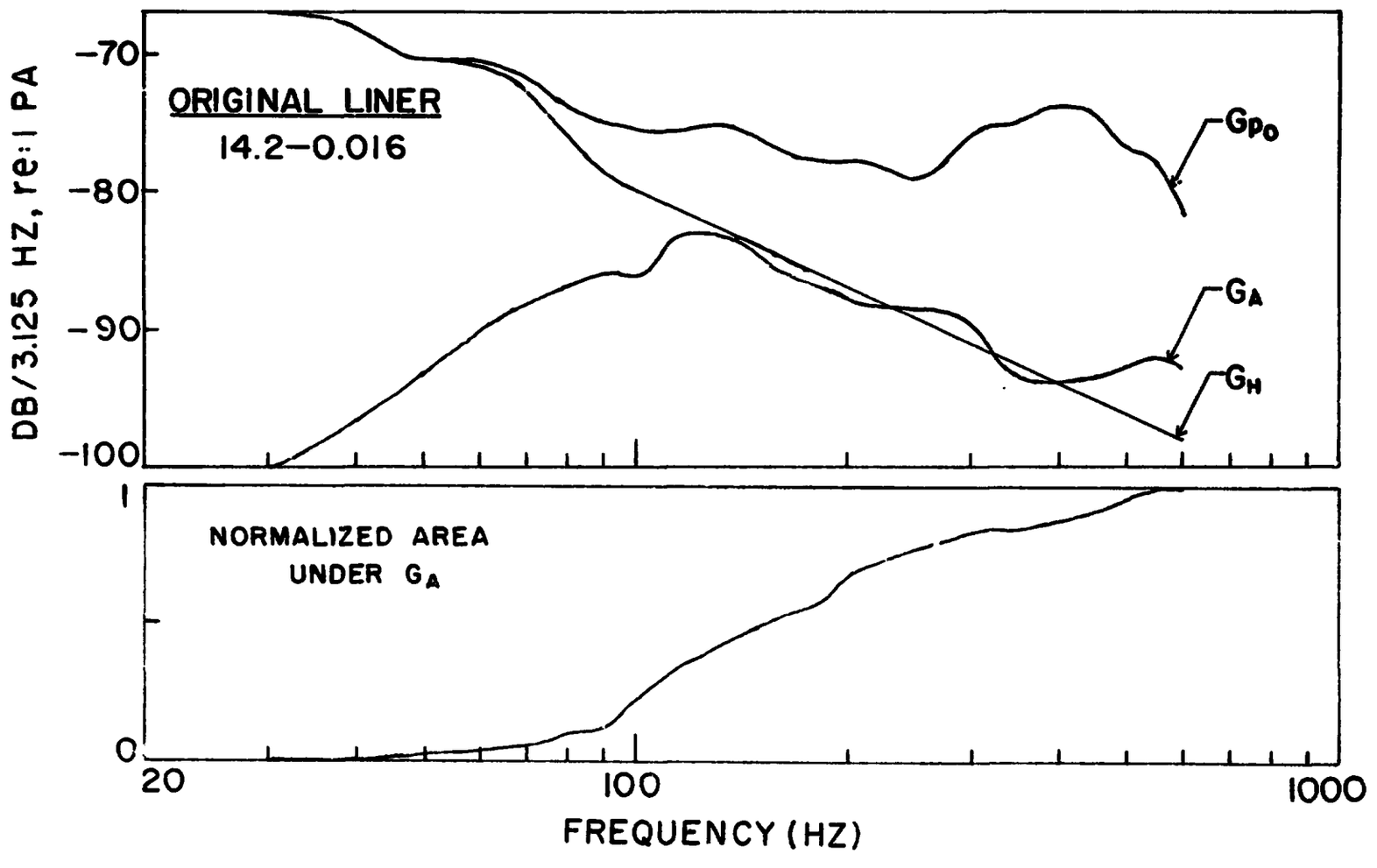


Figure G5. Deduced spectra of the heat release function, integrated spectra and deduced hydrodynamic noise for the original liner.

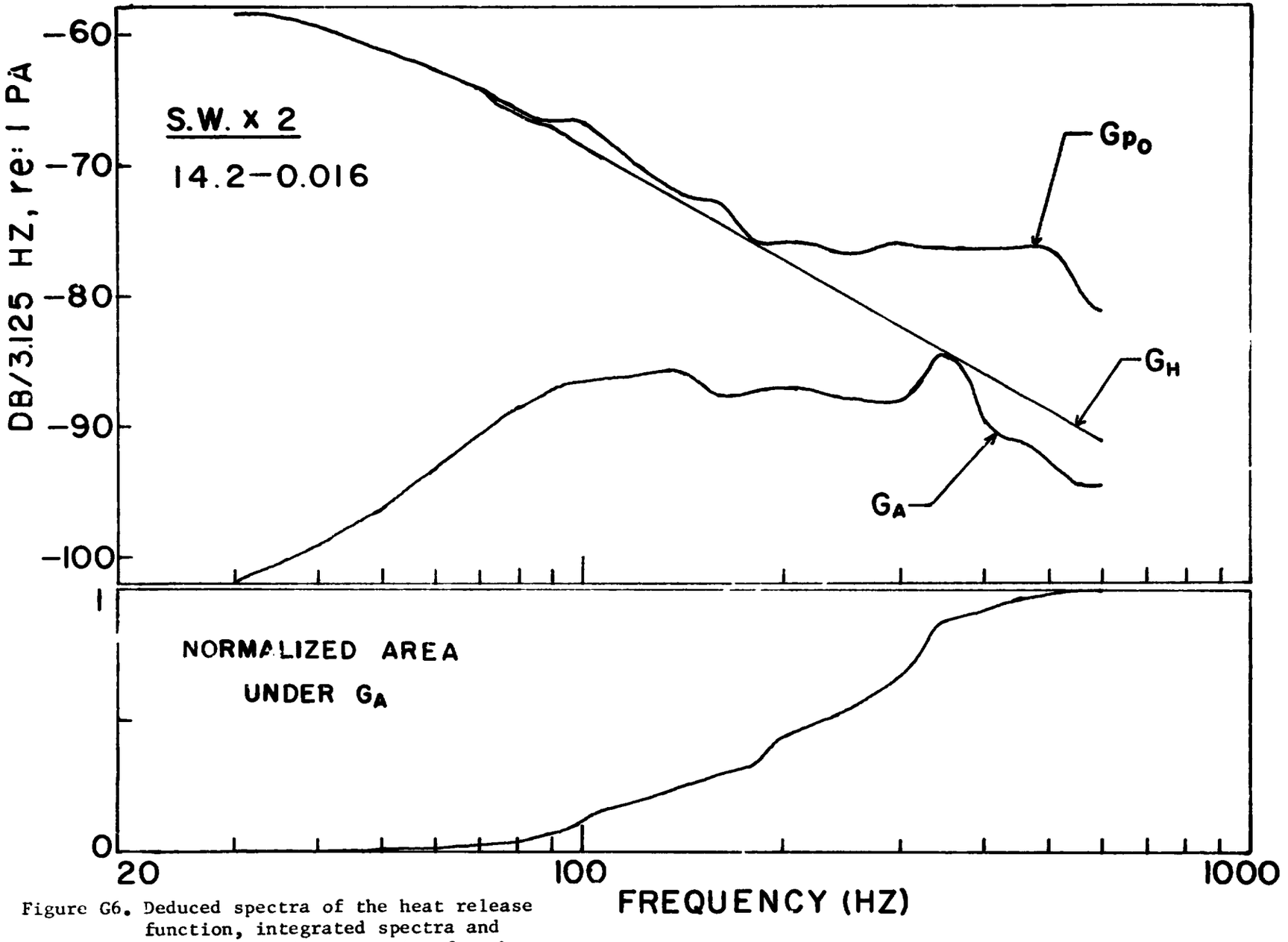


Figure G6. Deduced spectra of the heat release function, integrated spectra and deduced hydrodynamic noise for the SW x 2 liner.

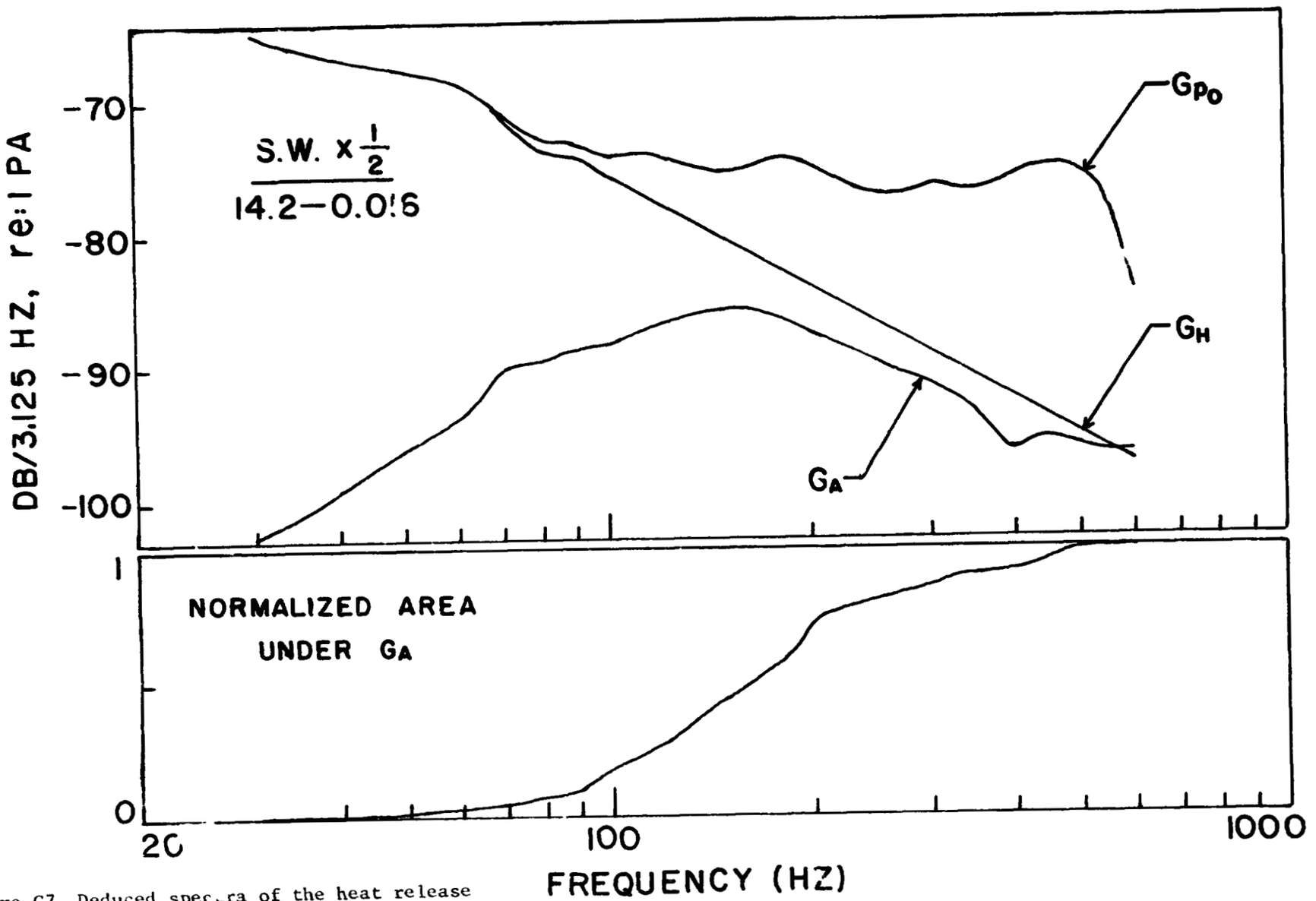


Figure G7. Deduced spectra of the heat release function, integrated spectra and deduced hydrodynamic noise for the SW x 1/2 liner.

affects the frequency content. This is an untenable situation. In the experiments of Ref. (G2), however, the fuel reactivity was only varied over a factor of about 2:1, and the more sophisticated analysis used here was not applied to those results. It is believed a more corrected effort with a wide range of fuel reactivity should be carried out to determine if fuel reactivity is the determinant of frequency content.

References

G1. Strahle, W. C. and Shivashankara, B. N., "A Rational Correlation of Combustion Noise Results from Open Turbulent Premixed Flames," Fifteenth Symposium (International) on Combustion, The Combustion Institute, Pittsburgh (1974) pp. 1379-1385.

G2. Strahle, W. C. and Shivashankara, B. N., "Combustion Generated Noise in Gas Turbine Combustors" NASA CR-134843, August, 1974.